REVIEWS OF MODERN PHYSICS VOLUME 44, NUMBER 2 APRIL 1972

The Properties of Defects in Magnetic Insulators

R. A. COWLEY, *University of Edinburgh, Scotland*

W. J. L. BUYERS, *Atomic Energy of Canada Limited, Chalk River, Ontario, Canada*

The introduction of a low concentration of defects into a magnetic insulator modifies the spectrum of the magnetic excitations. In general the spectrum consists of a set of impurity modes associated with the defect and its immediate neighbors. Impurity modes that occur outside the band of host excitations are localized in the neighborhood of the defect and at the same time perturb the host band, while modes lying within the band lead to resonant behavior of the excitations of the host. In recent years, optical, neutron scattering, and nuclear magnetic resonance techniques have been used to study mixed crystals of antiferromagnetic transition metal fluorides. Many of the features may be understood by using the molecular field or Ising model for the excitations. An improvement on this form of the theory is to use a cluster model to describe the excitations near to the defect. Some features may however be described only when the excitations of the host are treated adequately; this requires the use of Green's function theories that have been developed for antiferromagnets containing defects. A detailed comparison is presented of the predictions of the various theories with the experimental results. Although the theory is fairly satisfactory for a low concentration of defects and low temperatures, considerable complexities arise in extending it to higher temperatures and large concentrations.

CONTENTS

I. INTRODUCTION

The introduction of substitutional defects into crystals modifies the spectrum of the elementary excitations. It is the purpose of this review to discuss the experimental and theoretical results which have been obtained for the modifications in the magnetic excitations which occur when one transition metal fluoride is mixed with another. A large body of work has now been performed which has established at least the qualitative features of the changes in the spectrum as a result of the introduction of a few defects. In some cases, the introduction of defects gives rise to the possibility of excitations whose characteristic frequencies lie outside the band of the excitation frequencies of the host crystal and whose wave functions are localized in the neighborhood of the defect. These are the localized defect modes. In other cases, the frequencies of the excitations lie within the band of the excitation frequencies of the host crystal: these excitations are not localized but give rise to a "resonant" perturbation of the excitations of the host crystal.

The theory of these effects is very similar for different types of systems as demonstrated in the review by Izyumov (1965) for electrons, phonons, and magnons. The effects of both the localized modes and the resonant perturbations have been observed in many different systems. In the phonon case, the localized modes have been observed by optical techniques (Schäfer, 1960) and by neutron scattering techniques (Nicklow *et al.*, 1968), while resonant modes have been studied by thermal conductivity (for example, Baumann *et al.*, 1967), optical techniques (Kirby *et al.*, 1968) and neutron scattering (Svensson *et al.*, 1965).

In view of these successes, one may well question the usefulness of pursuing a similar study for magnetic systems. First, there is the obvious requirement to confirm the theory for a very different system. Second, we obtain information about the exchange constants between different ions. These provide a test of the theory of exchange constants which is quite different from that provided by measurements on pure crystals. A more important reason, however, is that it is possible to make a more detailed comparison of theory and experiment for magnetic systems than is possible to make for either the phonon or electron systems. The introduction of a defect atom of very different mass into a crystal inevitably produces changes in the neighboring force constants and also considerable local strain. It is difficult to allow for these features adequately in theoretical calculations. In the magnetic case, however, atoms which have very similar masses and very similar chemical properties may have quite different magnetic properties. As we shall see below, Mn^{2+} and Fe^{2+} are very different magnetically but the substitution of one for the other in a crystal produces a minimum of mechanical strain. In practice, theoretical calculations therefore depend on fewer arbitrary parameters and thus permit a direct quantitative check of the theory.

In the case of electrons, a detailed comparison of experiment and theory is impossible because existing observational techniques do not provide sufficiently detailed information about the electronic excitation spectrum. For magnons and phonons on the other hand, the excitations can be studied by optical and neutron spectroscopy.

A further feature of this similarity in the chemical properties is that it permits the preparation of specimens with a very large number of defects. For example, MnF_2 and CoF_2 are soluble for all concentrations, even though their magnetic properties are very different,

but crystals containing large concentrations of atoms of very different mass are frequently impossible to produce. Either the constituents are insoluble except for very low concentrations or else the atoms order so as to give rise to a new crystal structure. The magnetic systems therefore would seem to be the most suitable ones to test the recent theories on very concentrated systems for which even the qualitative features of the excitation spectrum are uncertain (Anderson, 1958; Mott, 1967; Ziman, 1968a, b; and Lloyd, 1969).

In this review, we shall restrict attention to the magnetic systems formed by mixing the transition metal (Mn^{2+}, Fe^{2+}, Co^{2+}, Ni^{2+}, Zn^{2+}) fluorides of the rutile and perovskite structures, Fig. 1. Since we are concerned with as close a comparison between theory and experiment as possible, we begin the review with a discussion of the magnetic properties of these different ions, and of the magnetic excitations in the pure materials.

Most of the review is concerned with those aspects which are well understood: the excitations at low temperatures in materials which have a small concentration of defects. In Sec. III the excitations in these systems are described by initially using the single-ion Ising approximation and then extending it to incorporate the interactions between the neighboring cluster of ions.

The properties of these materials have been investigated by a large number of different experimental techniques. In particular, there have been detailed optical measurements using far-infrared spectroscopy, Raman scattering, and fluorescence, as well as neutron scattering and nuclear magnetic resonance measurements. In Sec. IV we review the information which may be obtained with the aid of these different techniques.

Although the molecular field and cluster models are able to give a remarkably good account of the results, some features can only be obtained by the use of more complex theories. The usefulness of applying Green's functions to defect problems has been apparent since the work of Lifshitz (1943) on the analogous phonon problem. Similar techniques were applied to ferromagnets by Wolfram and Callaway (1963), and by Takeno (1963). It has been only relatively recently (Tonegawa and Kanamori, 1966) that similar theories have been used for antiferromagnets because of the greater complexity involved. In Sec. V we describe the application of these techniques to antiferromagnets, by extending the work of Tonegawa (1968, 1969) and Lovesey (1968) for isolated defects to obtain results which are correct to terms linear in the concentration of defects, analogous to the work of Elliott and Taylor (1967) for the phonon problem. In Sec. VI, the predictions of the Ising, cluster, and Green's function theories are compared with experimental results. A remarkably consistent account of the experimental results is obtained.

The excellent agreement between theory and experiment obtained in Sec. VI for the dilute alloys enables us to go forward to discuss two aspects which are far less well understood theoretically and which as yet have been less studied experimentally. In Sec. VII are described the difficulties encountered in extending the theory to high temperatures. Despite these difficulties, many of the experimental results may be understood. On the other hand, extending the theory to large concentrations is even more difficult, and as explained in Sec. VIII, it is by no means certain which features are the most important.

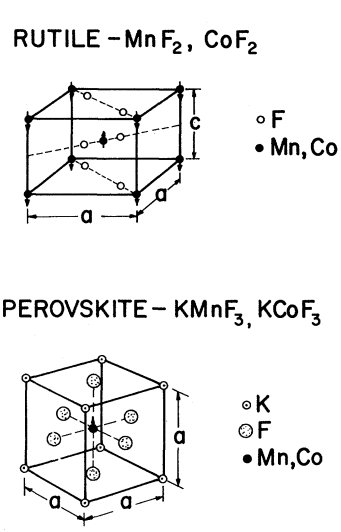

FIG. 1. The rutile and perovskite crystal structures. Other transition metal fluorides have similar chemical structures apart from certain small distortions, and most, but not all, have the same spin structure.

II. THE PURE MATERIALS

1. Crystal Field Theory

It is impossible to discuss the magnetic properties of the transition metal ions without first describing the effect of the crystal fields on these ions. There are many excellent accounts of crystal field theory available (for example, Low, 1960; Hutchings, 1964), and we may restrict our discussion to a presentation of the relevant results

Mn^{2+}

The crystal field theory of the ions is summarized in Fig. 2. The ground state of the free Mn^{2+} ion has orbital angular momentum $L=0$ and spin angular momentum $S=\frac{5}{2}$. It is therefore not influenced to a good approximation by either its crystal field environment or by the spin–orbit interaction. It is adequately described in both the rutile and perovskite structures by a spin Hamiltonian with an effective spin equal to the actual spin $S=\frac{5}{2}$ and with negligible single ion anisotropy. The anisotropy in MnF_2 arises largely from the magnetic dipolar interactions.

Fe^{2+}

The atomic ground state of the free Fe^{2+} ion has $L=2$ and $S=2$. In the octahedral cubic crystal field this is

TABLE 1. The effective spin, S', and its relationship to the true spin, S, and orbital angular momentum for the different ions. Proportionality factor between L and l is α_L.

	$\mathbf{S}=+\beta_S\mathbf{S}'$		$\mathbf{L}=+\beta_L\mathbf{S}'$		
	Mn^{2+}	Fe^{2+}	Co^{2+}	Ni^{2+}	Zn^{2+}
		Perovskite structure			
S'	5/2	1	1/2	1	0
β_S	1	5/3	5/3	1	0
β_L	0	$-(1/2)\alpha_L$	$-(2/3)\alpha_L$	0	0
		Rutile structure			
S'	5/2	2	1/2	1	0
β_S	1	1		1	0
β_L	0	0		0	0

Co^{2+} β is not isotropic and has values

Model	β_S^+	β_S^-	β_S^z	β_L^+	β_L^-	β_L^z	Ref.
A	0.39	1.44	2.05	$-0.31\alpha_L$	$-0.36\alpha_L$	$-0.31\alpha_L$	a
B	0.51	1.56	1.78	$-0.42\alpha_L$	$-0.41\alpha_L$	$-0.26\alpha_L$	b

[a] Gladney (1966).

[b] Martel, Cowley, Buyers, and Stevenson (private communication).

split into a doublet, E, and a triplet, T_2, with a separation in frequency of 300 THz. Throughout this paper, frequencies are quoted in these units (1THz=33 cm^{-1}=48°K). The orbital angular momentum within the lowest tripet state may be described by an effective angular momentum $l=1$, and the matrix elements of L within the T_2 manifold are minus those of l (Griffith, 1961). In the perovskite structure, the spin-orbit interaction splits the 15-fold degenerate state into a triplet, quintet, and septet. Within the ground triplet state the transitions may be described by an effective spin $S'=1$, and the relationships between the matrix elements of the real L and S and those of the effective S' are listed in Table 1. These relationships will, however, be changed in practice because the exchange field is large enough to cause appreciable mixing between the lowest $S=1$ triplet and the excited states which lie only 4 THz higher in frequency.

In the rutile crystal structure, the T_2 orbital state is split by the orthorhombic distortion to give three orbital singlets. The separation between the lowest two states is 33 THz (Stout *et al.*, 1968). The ground state then has an effective spin equal to the real spin $S=2$, but the spin–orbit interaction is sufficiently large to give rise to a single ion anisotropy by mixing the A_1 state with the B_1 and B_2 states. The form of the anisotropy is

$$H_{AN}(i)=-DS_z(i)^2+E[S_x(i)^2-S_y(i)^2], \quad (2.1)$$

where $D=0.21$ (Tinkham, 1956; Hutchings *et al.*, 1970a), while $E\approx 0.10$.

Co^{2+}

The free Co^{2+} ion has seven d electrons so that $L=3$ and $S=\frac{3}{2}$. The octahedral crystal field gives a T_1 triplet lowest within which the matrix elements of L may be described in terms of those of an effective orbital angular momentum $l=1$. The proportionality constant $L\rightarrow\alpha_L l$ is -1.5 when the mixing with an upper state is neglected, and is estimated by Gladney (1966) to be -1.42 in practice. In the perovskite structure the spin–

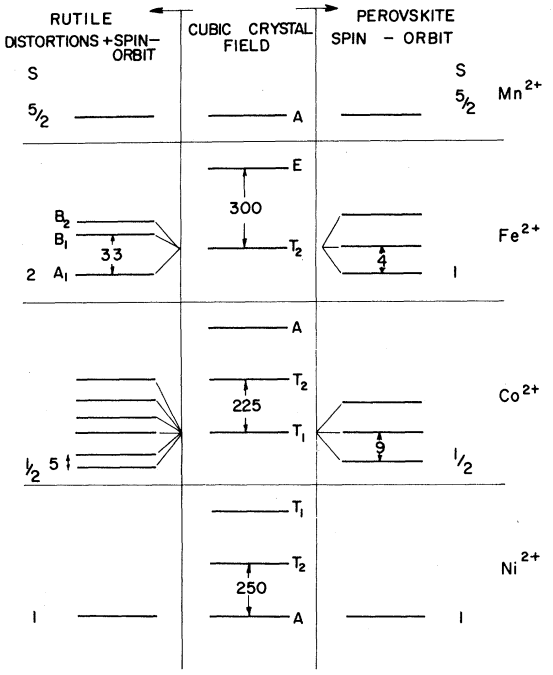

FIG. 2. Energy levels of transition metal ions in the rutile and perovskite structures. The lowest energies are shown in units of THz, and S is the effective spin of the ground multiplet.

orbit interaction gives a doublet state, $S'=\frac{1}{2}$, lowest. The matrix elements of S and L in terms of those of S' are listed in Table 1. Exchange fields are, however, frequently large enough to give rise to appreciable mixing of this ground state with the upper states (Buyers *et al.*, 1971a).

The orthorhombic crystal field and the spin–orbit interaction in the rutile structure give rise to six Kramers doublets. The lowest state is described by an effective spin $S'=\frac{1}{2}$. For ions other than Co, the proportionality constants between the matrix elements of the effective spin operators, S', and the spin, S, and angular momentum, L, operators have been determined by symmetry. For cobalt, they are dependent on the parameters of the crystal field interaction which are not well known. In Table 1 we list two different sets of constants, one derived from the crystal field parameters of Gladney (1966) and the other from those of Martel, Cowley, Buyers, and Stevenson (private communication). Once again exchange interactions may give rise to appreciable mixing of the lowest two doublets.

Ni^{2+}

The atomic ground state of Ni^{2+} has $L=3$ and $S=1$. The cubic field gives a singlet state A as the lowest state giving rise to an effective spin equal to the real spin $S=1$ in both structures. In the rutile structure there are sufficient crystal field distortions that mixing of the states gives rise to single ion anisotropy. Its form is the same as that given by Eq. (2.1), but with $D=0.13$ and $E=0.05$ (Peter and Moch, 1960; Hutchings *et al.*, 1970b).

Zn^{2+}

The Zn^{2+} ion is nonmagnetic.

2. The Spin Waves in the Pure Materials

The exchange interactions between the ions in the pure materials cause the magnetic moments to align antiferromagnetically at low temperatures and give rise to the spin wave spectrum. Measurements of the spin waves have been made by optical, anti-ferromagnetic resonance and neutron scattering techniques. In all cases, the results at low temperatures for the excitations of lowest frequency may be interpreted in terms of an effective spin Hamiltonian which may be written

$$H=-\sum_i S_z(i)H_A P_i+\tfrac{1}{2}\sum_{ij} I(ij)\mathbf{S}(i)\cdot\mathbf{S}(j), \quad (2.2)$$

where P_i is $+1$ and -1 for up and down sites, and where H_A is the sum of the single ion anisotropy and the magnetic dipole–dipole interactions which are approximately independent of wave vector. When the exchange is not isotropic as in CoF_2, the transverse part is included in $I(ij)$ and H_A then contains a term proportional to the difference between the longitudinal and transverse parts of the exchange constant. We omit the prime on the effective spins. If we neglect the small corrections due to spin–wave interactions (Oguchi, 1960) the spin–wave frequency for wave vector $\mathbf{q}$ may be written for all the materials except NiF_2 as (Kittel, 1963)

$$\omega(\mathbf{q})=[A(\mathbf{q})^2-B(\mathbf{q})^2]^{1/2}, \quad (2.3)$$

where

$$A(\mathbf{q})=H_A+S\sum_{j=L} I(ij)\{\exp[i\mathbf{q}\cdot\mathbf{R}(ij)]-1\}+S\sum_{j=A} I(ij), \quad (2.4)$$

$$B(\mathbf{q})=S\sum_{j=A} I(ij)\exp[i\mathbf{q}\cdot\mathbf{R}(ij)], \quad (2.5)$$

and H_A represents the effect of both the single ion and dipole–dipole anisotropy, $\mathbf{R}(ij)$ is the distance between the ions i and j, while $\sum_{j=L}$ and $\sum_{j=A}$ represent summations over like and antiferromagnetic neighbors respectively.

In Table 2 are listed the best sets of parameters for the anisotropy fields, H_A, and for the exchange constants $I(1)$, $I(2)$, and $I(3)$ between the three nearest neighbor pairs of ions. In the rutile structure, the nearest neighbors are ferromagnetically aligned, and the second nearest neighbors have the strong antiferromagnetic coupling. Throughout the paper we quote exchange and anisotropy constants in THz.

In the case of NiF_2, the magnetic structure is more complex than are those of the other fluorides. The spins do not align along the c axis but align in the a/b plane with a slight canting. There are then two branches of the dispersion relation but this can be described by the single ion anisotropy Eq. (2.1) and isotropic exchange interactions which are tabulated in Table 2.

The authors are unaware of any direct measurements of the spin wave spectrum of $KFeF_3$.

The effective exchange constants listed in Table 2 are identical with the exchange constants between real spins except for the two Co salts. Likewise, except for the Co salts, the size of the anisotropy is consistent with the anisotropy arising from the single ion anisotropy, Eq. (2.1), and the dipole–dipole anisotropy. In principle, for the Co salts, it is possible to work back from the effective exchange constants to the exchange between real spins with the aid of Table 1. In practice, this is not satisfactory because of the mixing between the levels but the true exchange constants with due allowance made for the mixing are listed in Table 2. In $KCoF_3$ the exchange is found to be between nearest neighbors with negligible anisotropy. In CoF_2 (Martel *et al.*, 1968) there is appreciable nearest and next nearest-neighbor exchange. The latter has been assumed to be anisotropic (Martel, Cowley, Buyers, and Stevenson, private communication) to account for the anisotropy in CoF_2.

III. CLUSTER MODELS OF A DEFECT

1. Ising Approximation

In the preceding section the spin–wave spectrum was obtained for a pure material with an effective spin, S,

TABLE 2. The anisotropy and exchange constants in THz which describe the pure crystal spin waves within the effective spin approximation. The Co parameters are also shown treating the ions in terms of "true" spins. The anisotropy for the canted antiferromagnet NiF_2 is not given since it is more complex in form.

	Perovskite structure		
	$KMnF_3$	$KCoF_3$	$KNiF_3$
S'	2.5	0.5	1.0
H_A	0.00097	0.07	0.052
$I(1)$	0.151	2.34	2.125
$I(2)$	0.0	0.04	···
Ref.	a	b	c

	Rutile structure			
	MnF_2	FeF_2	CoF_2	NiF_2
S'	2.5	2.0	0.5	1.0
H_A	0.0222	0.603	0.376	···
$I(1)$	0.0132	−0.0015	−0.060	−0.006
$I(2)$	0.0744	0.1092	0.370	0.416
$I(3)$	0.0018	0.0057	···	0.024
Ref.	d	e	f	g

	Cobalt salts			
	$J(1)$	$J_{xx}(2)$	$J_{zz}(2)$	Ref.
CoF_2	−0.018	0.151	0.115	h
$KCoF_3$	0.622	···	···	b

[a] Pickart *et al.* (1966) with the anisotropy modified so as to give agreement with resonance measurements of Heeger *et al.* (1961) which are consistent with the neutron scattering measurements of the magnons near the zone centre made by Coombs, Svensson, Holden, and Buyers (private communication).
[b] Buyers *et al.* (1971a).
[c] Chinn *et al.* (1970) and Richards (1963).
[d] Okazaki *et al.* (1964) and Nikotin *et al.* (1969).
[e] Hutchings *et al.* (1970a).
[f] Martel *et al.* (1968).
[g] Hutchings *et al.* (1970b).
[h] Martel, Cowley, Buyers, and Stevenson (private communication).

and effective exchange constants, $I(ij)$. If a single defect is introduced at the origin, up site, with an effective spin S', and exchange interaction $I(0j)$, the spin-wave modes will be modified in the neighborhood of the defect. In all the cases considered here, the spin direction of the impurity atom is the same as that of the host atom if it was at the same site. The simplest approximation with which to discuss the modes is the Ising approximation in which the transverse parts of the exchange interaction are neglected. The full Ising Hamiltonian is

$$H_0=-\sum_{i\neq 0} H_A S_z(i)P_i - H_A' S_z'(0)P_0 + \tfrac{1}{2}\sum_{i,j\neq 0} I(ij)S_z(i)S_z(j) + \sum_{j\neq 0} I'(0j)S_z'(0)S_z(j), \quad (3.1)$$

where P_i is $+1$ for i on up sites, and -1 for i on down-sites. The magnetic excitations are now localized on particular sites, and for the site 0 the excitation frequency is

$$\omega_D = H_A' - \sum_j I'(0j)\langle S_z(j)\rangle,$$

where $\langle S_z(j)\rangle$ is the expectation value of the spin on the jth site. If we take the ground state to be the Néel state, the frequencies of the excitations in the perovskite structure are for the defect

$$\omega_D = H_A' + 6SI'(1), \quad (3.2)$$

and for the neighbors of a defect

$$\omega_N = H_A + 5SI(1) + S'I'(1). \quad (3.3)$$

The neglect of interactions beyond nearest neighbors is a good approximation for perovskites.

In the rutile structure, the results neglecting interactions between neighbors more distant than second are

$$\omega_D = H_A' - 2SI'(1) + 8SI'(2), \quad (3.4)$$

$$\omega_{N1} = H_A - SI(1) - S'I'(1) + 8SI(2), \quad (3.5)$$

$$\omega_{N2} = H_A - 2SI(1) + 7SI(2) + S'I'(2). \quad (3.6)$$

These results show that if the introduction of a defect alters the spin or exchange interactions, then the excitation frequencies of its neighbors are also altered. A change of spin is therefore analogous to a change of force constant in the phonon problem.

If these frequencies [Eqs. (3.2)–(3.6)] lie outside the band of the spin-wave frequencies of the host crystal, then local modes associated with either the defect or its neighbors may result.

2. Symmetry

When the transverse part of the exchange interactions is added to the Hamiltonian Eq. (3.1), the magnetic excitations are no longer confined to single sites. It is therefore useful to classify the modes in the neighborhood of the defect by their symmetry. If we restrict attention to the cluster of atoms around each defect and the form of interactions which were discussed above, the classification may be performed directly with the aid of standard group theoretical techniques (Heine, 1960). The Hamiltonian is invariant under a space group, G. This group is the space part of the spin–space group introduced by Brinkman and Elliott (1966), and its elements operate only on the lattice and not on the spins. For the perovskite structure, the seven excitations associated with the defect and its six neighbors may be classified by the irreducible representations of the group $m3m$ as

$$2A_{1g} + E_g + T_{1u}. \quad (3.7)$$

The two A_{1g} modes correspond to excitations that are partly on the defect and partly distributed equally on all the neighbors. The doubly degenerate E_g modes and triply degenerate T_{1u} modes describe excitations on the neighbors. Other authors (Takeno, 1963; Tonegawa,

1968; Lovesey, 1968) have labeled these modes as s, d, and p modes, respectively, using s_0 and s_1 for the A_{1g} modes that are mainly on the defect $A_{1g}(D)$, and mainly on the neighbors $A_{1g}(N)$, respectively.

In the rutile structure, we consider two nearest neighbors and eight second nearest neighbors around each defect. The group is $4/mmm$ and the corresponding irreducible representations are

$$3A_{1g}+2A_{2u}+B_{1u}+B_{2g}+E_g+E_u. \tag{3.8}$$

The three A_{1g} modes correspond to excitations on the defect and to excitations on the neighbors and next nearest neighbors. The A_{2u} modes are excitations on the nearest and next nearest neighbors, while the B_{1u}, B_{2g}, and the doubly degenerate E_g and E_u modes are entirely associated with the next nearest neighbors of the defect. Lovesey (1968) denotes the A_{1g} mode localized mainly on the defect as s_0, while that localized mainly on the next nearest neighbors is s_1. The A_{2u} and E_u modes are denoted as p_z and the doubly degenerate p_x and p_y, while E_g and B_{2g} are d modes labeled by (xz), (yz), and (xy), respectively, and B_{1u} is denoted as an f mode.

3. Excitations in a Cluster Model

The transverse part of the exchange interaction is

$$H_T=\tfrac{1}{4}\sum_{ij}J(ij)[S_+(i)S_-(j)+S_-(i)S_+(j)], \tag{3.9}$$

where $J(ij)$ is equivalent to the longitudinal effective exchange constant, $I(ij)$, for all pairs of ions except when one of the ions is a Co^{2+} ion as discussed in Sec. II. The excitations of the cluster may be calculated in a way analogous to the spin–waves of a pure crystal. The spin operators on the "up sites" are unchanged but the operators on the "down sites" are reversed by a canonical transformation which leaves the commutation relations unchanged; for the down sites we make the replacements

$$S_z\rightarrow -S_z, \qquad S_+\rightarrow S_-, \qquad S_-\rightarrow S_+. \tag{3.10}$$

The Hamiltonian for a nearest-neighbor cluster in the perovskite lattice may now be written in terms of the defect–host exchange constants I' and J' and the transformed operators as

$$\begin{aligned}H_D=&-H_A'S_z'(0)-\sum_{i=1}^{6}[H_A+5SI(1)]S_z(i)\\&-I'(1)\sum_{i=1}^{6}S_z'(0)S_z(i)\\&+\tfrac{1}{2}J'(1)\sum_{i=1}^{6}[S_+'(0)S_+(i)+S_-'(0)S_-(i)].\end{aligned} \tag{3.11}$$

Since we have included the transverse part of the interaction only between the defect and its neighbors, the interactions within the cluster are treated exactly thus far, while the remaining interactions are approximated by the Ising theory.

The equations of motion for the spin operators give

$$\begin{aligned}-id&S_+'(0)/dt=[H_D, S_+'(0)]\\&=-H_A'S_+'(0)-I'(1)S_+'(0)\sum_i S_z(i)\\&\quad -J'(1)S_z'(0)\sum_i S_-(i),\\-id&S_-(i)/dt=[H_D, S_-(i)]\\&=[H_A+5SI(1)]S_-(i)\\&\quad +I'(1)S_-(i)S_z'(0)+J'(1)S_z(i)S_+'(0).\end{aligned} \tag{3.12}$$

These equations are solved by replacing $S_z'(0)$ and $S_z(i)$ by their expectations in the ground state, which are S' and S since the Néel state is assumed. These approximate equations are then linear in the operators $S_+'(0)$ and $S_-(i)$ and can be solved by an extension of the methods described by Walker (1963). Pseudoboson creation operators for the spin excitations (n) are written as either

$$\alpha_n^+=(2S')^{-1/2}C_n(0)S_-'(0)+(2S)^{-1/2}\sum_i C_n(i)S_+(i), \tag{3.13}$$

or alternatively

$$\alpha_n^+=(2S')^{-1/2}C_n(0)S_+'(0)+(2S)^{-1/2}\sum_i C_n(i)S_-(i), \tag{3.14}$$

where the appropriate choice between Eqs. (3.13) and (3.14) will be made later, and the equations for the annihilation operators are identical except for an interchange of the S_+ and S_- operators.

The nth eigenvector is assumed to have a time dependence $\exp[i\omega(n)t]$, and the annihilation operator to be $\exp[-i\omega(n)t]$, so that the $\omega(n)$ are eigenvalues and the $C_n(i)$ eigenvectors, which may be obtained from the matrix of coefficients on the right-hand side of Eqs. (3.12). The choice between the eigenvectors (3.13) and (3.14) is made on the basis of normalization. If the $\alpha^+(n)$ and $\alpha(n)$ obey the normal commutation relations and the spin operators do so likewise, then the coefficients in Eq. (3.13) must satisfy

$$C_n(0)^2-\sum_i C_n(i)^2=-1, \tag{3.15}$$

whereas if Eq. (3.14) is appropriate then the requirement is

$$C_n(0)^2-\sum_i C_n(i)^2=1. \tag{3.16}$$

The right-hand side of Eq. (3.12) is then written in matrix form as

$$\begin{pmatrix} -\omega_D & -J'S' & -I'S' & -I'S' & -J'S' & -J'S' & -J'S' \\ +J'S' & +\omega_N & 0 & 0 & 0 & 0 & 0 \\ +J'S & 0 & +\omega_N & 0 & 0 & 0 & 0 \\ +J'S & 0 & 0 & +\omega_N & 0 & 0 & 0 \\ +J'S & 0 & 0 & 0 & +\omega_N & 0 & 0 \\ +J'S & 0 & 0 & 0 & 0 & +\omega_N & 0 \\ +J'S & 0 & 0 & 0 & 0 & 0 & +\omega_N \end{pmatrix}.$$

The matrix is diagonalized and the eigenvectors examined. If they satisfy Eq. (3.15) then Eq. (3.13) is the correct choice for the creation operator and the eigenvalue is associated with $\omega(n)$. If on the other hand the eigenvectors satisfy Eq. (3.16), then Eq. (3.14) gives the creation operator and its eigenvalue is associated with $-\omega(n)$. In a stable system, $\omega(n)$ must be positive.

When this theory is applied to the perovskite lattice and the eigenvectors are classified by their irreducible representations the results are

$$\omega(E)=\omega(T_1)=\omega_N, \tag{3.17}$$

while the frequencies of the two A_1 modes are given by

$$\omega(A_1)=\left|\tfrac{1}{2}(\omega_D-\omega_N)\pm\tfrac{1}{4}[(\omega_D+\omega_N)^2-6SS'J'(1)^2]^{1/2}\right|, \tag{3.18}$$

where ω_N and ω_D are given by Eqs. (3.2) and (3.3). The degeneracy of the E and T_1 modes occurs because of the extra symmetry inherent in our simple model.

The results for the rutile structure are more complex, in part because of the lower symmetry, but also because the cluster involves both nearest and next nearest neighbors. The results have however been obtained by the same techniques and are

$$\omega(E)=\omega(B_2)=\omega_{N2}+SJ(1), \tag{3.19}$$

$$\omega(B_1)=\omega_{N2}-SJ(1), \tag{3.20}$$

$$\omega(A_2)=\left|\tfrac{1}{2}(\omega_{N2}-\omega_{N1})\pm\{\tfrac{1}{4}(\omega_{N2}+\omega_{N1})^2-4[SJ(2)]^2\}^{1/2}\right|, \tag{3.21}$$

while the frequencies of the A_1 modes are given by the modulus of the three eigenvalues of the matrix

$$\begin{pmatrix} \omega_D & (8SS')^{1/2}J'(2) & (2SS')^{1/2}J'(1) \\ -(8SS')^{1/2}J'(2) & -[\omega_{N2}+SJ(1)] & -2SJ(2) \\ (2SS')^{1/2}J'(1) & 2SJ(2) & \omega_{N1} \end{pmatrix}. \tag{3.22}$$

In addition to the frequencies of the modes, it is also possible to deduce the coefficients C_n, explicitly. For example, in the perovskite structure the A_{1g} mode localized mainly on the defect has an approximate probability amplitude,

$$C_{A_{1g}}(1)/C_{A_{1g}}(0)=-[J'(1)S'/(\omega_D+\omega_N)],$$

of being on any one neighbor of the defect. A similar result is obtained for the A_{1g} mode in the rutile structure and results may also be obtained for the other modes but will not be listed explicitly.

4. Perturbation Theory

An alternative approach to the calculation of the frequencies of the excitations of the cluster is to use the eigenstates of the Ising Hamiltonian, Eq. (3.1), as a basis and then to treat the transverse part of the Hamiltonian, Eq. (3.9), as a perturbation. As before, we label the longitudinal exchange I to distinguish it from the transverse part J. This approach, which will be most successful if $J\ll I$ or H_A, has the advantage that the frequencies are obtained without the use of the pseudoboson technique. Results of perturbation theory have been used by Dietz *et al.*, (1970) and we give the basis of the method here. Initially we consider the influence of the perturbation on the ground state of the cluster, treating the interaction of the neighbors of the defect with their neighbors within the Ising approximation. The perturbation, Eq. (3.9), mixes into the ground state excited states containing pairs of excitations, one of which is on the defect and the other of which is on its neighbors. The frequency within the Ising approximation of this state is $\omega_D+\omega_N-I'(1)$, where ω_D and ω_N are given by Eqs. (3.2) and (3.3). The ground-state energy may now be obtained by second-order perturbation theory as

$$E_G=-30S^2I(1)-6SS'I'(1)-6SH_A-S'H_A' \\ -6SS'J'(1)^2/[\omega_D+\omega_N-I'(1)]. \tag{3.23}$$

In a similar manner the effect of the perturbation on the excited states may be calculated. If the spin at the

defect is excited, the perturbation mixes this state with one in which there are two excitations on the defect and one on a neighbor. If $S'=\frac{1}{2}$, then no more than one excitation is permitted on the defect and the perturbation is not able to alter the energy of the excited state. The energy of this excited state for all values of S' is

$$E_D=-30S^2I(1)-6SS'I'(1)-6SH_A-S'H_A+\omega_D$$
$$-6S(2S'-1)J'(1)^2/[\omega_D+\omega_N-2I'(1)]. \quad (3.24)$$

The excitation frequency E_D-E_G is then given by (3.24–3.23)

$$\omega[A_1(D)]=\omega_D-6SJ'(1)^2$$
$$\times\left(\frac{2S'-1}{\omega_D+\omega_N-2I'(1)}-\frac{S'}{\omega_D+\omega_N-I'(1)}\right). \quad (3.25)$$

The perturbation theory may also be applied to the excitations on the neighbors. The results are

$$\omega(E)=\omega(T_1)=\omega_N-S'J'(1)^2$$
$$\times\left(\frac{6S-1}{\omega_D+\omega_N-2I'(1)}-\frac{6S}{\omega_D+\omega_N-I'(1)}\right), \quad (3.26)$$

and

$$\omega[A_1(N)]=\omega_N-S'I'(1)^2$$
$$\times\left(\frac{12S-1}{\omega_D+\omega_N-2I'(1)}-\frac{6S}{\omega_D+\omega_N-I'(1)}\right). \quad (3.27)$$

Similar results may be derived for the rutile structure; we shall not present them, however, as they are very cumbersome because of the necessity of including both sets of neighbors.

It is of interest to compare these results with Eqs. (3.17) and (3.18) obtained by the pseudoboson techniques. Even in the limit $J\ll I$ these results differ. Since the perturbation theory is then correct, we must conclude that the pseudoboson technique is in error in this limit. If we consider the mode associated with the defect, Eq. (3.18) predicts that its frequency is given when $J\ll I$, by

$$\omega[A_1(D)]=\omega_D-6SS'J'(1)^2/(\omega_D+\omega_N)$$

which is the same as Eq. (3.25) if S and S' are infinite. In fact if $S'=\frac{1}{2}$, Eq. (3.25) shows that the frequency $\omega[A_1(D)]$ is increased by the perturbation. The error of the boson technique is not limited to $J\ll I$ as pointed out by Thorpe (1970). Consider a system of two spins, S_1 and S_2, interacting antiferromagnetically with the Heisenberg interaction $J\mathbf{S}_1\cdot\mathbf{S}_2$. The lowest two states of this system are separated in frequency by $J(S_2-S_1+1)$ if $S_1<S_2$. The boson technique does not give this result. The frequencies of the excited states are 0 and $J(S_2-S_1)$, from the aligned ground state. We may therefore conclude that the boson technique underestimates excitation frequencies for all ratios of I and J. This difficulty arises because the ground state is not the Néel state as assumed by the boson technique and because the boson technique permits an arbitrarily large number of excitations on each site.

5. Pair Excitations

(*a*) *The Ising Model*

Optical measurements of the properties of defects frequently give the frequencies of pairs of excitations as well as the frequency of single excitations. The reason for this will be discussed in detail in Sec. IV. If the excitations were strictly independent of one another the frequency of the pair would be the sum of the frequencies of the individual excitations. The excitations are not, however, independent and the frequencies differ from the sum of the frequencies by an amount δ. In this section, we calculate δ by various different techniques.

In the Ising approximation pairs of excitations localized on the same atom are permitted provided that the effective spin is greater than $\frac{1}{2}$. Furthermore, they do not interact with one another so that we have

$$\delta_{D+D}=\delta_{N+N}=0, \quad (3.28)$$

where we have assumed that the anisotropy energy is described adequately by $-H_AS_z$. (Later we shall discuss Ni in MnF_2 where this is not a good approximation.)

If one excitation is situated on the neighbors and another on the defect there will however be an interaction which for perovskites is

$$\delta_{D+N}=-I'(1). \quad (3.29)$$

In the rutile structure the results are more complex because of the nature of the cluster. There is an interaction between excitations on the defect and its nearest neighbors,

$$\delta_{D+N1}=-I'(1),$$

and its next nearest neighbors,

$$\delta_{D+N2}=-I'(2),$$

while there are further interactions between neighbors separated by $(\pm a/2, \pm a/2, \pm c/2)$ of

$$\delta_{N1+N2}=-I(2)$$

and between neighbors separated by $(0, 0, \pm c)$ of

$$\delta_{N2+N2}=-I(1).$$

There results show that the pair excitations involving antiferromagnetic coupling are reduced in frequency by the interaction. The effect is similar to that of magnon–magnon interaction in pure antiferromagnets in that it modifies the two-magnon spectrum as discussed by Elliott *et al.* (1968) and demonstrated by Fleury (1968)

(*b*) *Perturbation Theory*

The results of the previous section may be improved by inclusion of the effect of the transverse part of the

exchange Hamiltonian, Eq. (3.9). The calculation of the energy of a pair of excitations proceeds in a similar manner to that already described for the single excitations. If two modes are localized on the defect, the energy is

$$E_{D+D}=-30S^2I(1)-6S(S'-2)I'(1)-6SH_A$$
$$-(S'-2)H_A'-18J'(1)^2S(S'-1)L(3), \qquad S'>\tfrac{1}{2},$$

where the function $L(n)$ is

$$L(n)=1/[\omega_D+\omega_N-nI'(1)].$$

The interaction energy between two modes on the defect is then

$$\delta_{D+D}=E_{D+D}-E_G-2\omega(D),$$

where $\omega(D)$ is given in Eq. (3.25) and is the perturbed single excitation. The result is then

$$\delta_{D+D}=6SJ'(1)^2[-S'L(1)+(4S'-2)L(2)$$
$$-(3S'-3)L(3)]. \qquad S'>\tfrac{1}{2}. \quad (3.30)$$

If we neglect the difference between the different $L(n)$ functions, this result shows that δ_{D+D} is positive or that the interaction between two modes on the defect is repulsive.

In calculations for the other pairs of modes the only cases of importance are those in which one of the excitations is localized mainly on the defect. In the perovskite structure we find

$$\delta_{D+E}=\delta_{D+T_1}=-I'(1)+J'(1)^2[-(6S-1)(2S'-1)L(3)$$
$$-(-18SS'+6S+S')L(2)-6SS'L(1)], \quad (3.31)$$

while

$$\delta_{D+A_1}=-I'(1)+J'(1)^2[6SS'L(-1)$$
$$-(12S-1)(2S'-1)L(3)$$
$$+(24SS'-6S-S')L(2)-6SS'L(1)]. \quad (3.32)$$

The calculations may also be evaluated for the rutile structure but are not listed here as they give rise to very lengthy expressions.

(c) *Spin-Wave Approximation*

It is more difficult to calculate the interaction between the modes in the spin-wave approximation, and in general this problem has not been solved. Thorpe (1970) has developed a simple prescription which appears to be successful for combination modes when one of the modes is highly localized on the defect. The prescription is that we neglect the extent to which the defect mode spreads onto its neighbors. The frequency of the pair of modes is then calculated by initially exciting the defect mode and then calculating the energy needed to excite the additional mode in the presence of the defect mode. The operators $S_z'(0)$ in the equations of motion for the spin operators, (3.12), are then replaced by $(S'-1)$. The frequencies of excitation of the modes in the presence of a defect mode are then given by Eqs. (3.17) to (3.22) but with S' replaced by $(S'-1)$.

The differences in the frequencies between the excitation of a pair of modes and the excitation of two single modes are then, for the perovskite structure,

$$\delta_{D+D}=6SJ'(1)^2L(1), \quad (3.33)$$

$$\delta_{D+E}=\delta_{D+T_1}=-I'(1), \quad (3.34)$$

$$\delta_{D+A_1}=-I'(1)+6SJ'(1)^2L(1), \quad (3.35)$$

where we have expanded the results in powers $J'(1)/\omega_D$. It is readily seen that the expression for δ_{D+D} is identical with the results obtained by the cluster model Eq. (3.30), if the difference between the $L(n)$ factors is ignored. This is the result to be expected for a spin-wave theory. On the other hand, the expressions for δ_{D+E} and δ_{D+A_1} are not the same in this limit. Because the defect mode spreads onto its neighbors to order $J'(1)/\omega_D$, the δ will be reduced by this effect to order $J'(1)^2/\omega_D$. Allowing for this effect by perturbation theory replaces $I'(1)$ in Eqs. (3.34) and (3.35) by

$$I'(1)[1-6J'(1)^2SS'L(0)^2],$$

which, on neglecting H_A' and ω_N with respect to ω_D, reduces to

$$I'(1)-S'J'(1)^2/\omega_D.$$

When this is substituted into Eqs. (3.34) and (3.35) for $I'(1)$, they are seen to become identical with the perturbation theory results [Eqs. (3.31) and (3.32)] when the differences between the $L(n)$ and $1/\omega_D$ are ignored.

IV. EXPERIMENTAL TECHNIQUES

1. Optical Techniques

There are a number of different optical techniques which may be used to study magnetic defects. The two most useful approaches are far infrared spectroscopy in which the absorption of radiation by the crystal is measured as a function of its frequency, and Raman scattering in which the inelastic scattering of the radiation by the specimen is observed. Unfortunately, the detailed theory of the interaction between radiation and magnetic excitations is still not well understood. The simplest process is the infrared absorption by a single excitation. This is believed to arise from a coupling of the magnetic field of the electromagnetic wave, $\mathbf{H}^R$, to the spins through the Hamiltonian,

$$H_{\mathrm{INT}}=-\mu_B\sum_{\alpha\beta}\sum_i H_\alpha^R S_\beta(i)g_{\alpha\beta}(i), \quad (4.1)$$

where $g_{\alpha\beta}(i)$ is the "g" factor of the atom at the ith site, and μ_B is the Bohr magneton. Since the electromagnetic wave has a wavelength much greater than the interatomic spacing, it is permissible for most purposes to omit the wave vector dependence of the interaction from Eq. (4.1).

It is convenient to rewrite Eq. (4.1) in terms of the magnetic dipole moment operator of the crystal, $\mathbf{M}$, when

$$H_{\mathrm{INT}}=-\sum_\alpha H_\alpha^R M_\alpha, \quad (4.2)$$

where

$$M_\alpha = \sum_\beta \sum_i \mu_B g_{\alpha\beta}(i) S_\beta(i). \tag{4.3}$$

The susceptibility of the crystal at frequency ω may then be calculated by conventional second-order perturbation theory as

$$\chi_{\alpha\beta}(\omega) = (Nv)^{-1} \sum_{nm} \frac{\rho_n \omega_{mn} \langle n \mid M_\alpha \mid m \rangle \langle m \mid M_\beta \mid n \rangle}{\hbar(\omega_{mn}^2 - \omega^2)}, \tag{4.4}$$

where v is the volume of the unit cell, N the number of unit cells, the initial state of the crystal is n with probability ρ_n, and m is the final state, while ω_{mn} is the difference between the energies of the excited and initial states.

We now wish to apply this formalism to the cluster model developed in Sec. III. When the eigenvectors of the excitation of the cluster model are substituted into the matrix element $\langle n \mid M_\alpha \mid m \rangle$ of Eq. (4.4), it is found that the only nonzero terms are those arising from the modes of A_{1g} symmetry. The same result follows from group theory.

In addition to the absorption by single excitations, there is also a strong absorption in antiferromagnets by pairs of excitations. This is believed to arise as shown schematically in Fig. 3(1). The electric field of the incident radiation induces a virtual transition in one atom which then interacts with its neighbors through an exchange interaction (Tanabe *et al.*, 1965). In practice the interaction may be written (Elliott and Thorpe, 1969) in terms of the electric dipole moment as

$$M_\alpha = \sum_{\beta\gamma} \sum_{ij} A_{\alpha\beta\gamma} S_\beta(i) S_\gamma(j),$$

where the coefficients $A_{\alpha\beta\gamma}$ depend on i and j. Since exchange interactions are usually of short range, it seems reasonable to restrict the summation over i and j to nearest neighbors. Even with this restriction however there are seven arbitrary constants needed to specify the A's for the nearest-neighbor interaction around a defect in the perovskite structure. It is therefore usual to further assume that the exchange interaction is of the Heisenberg form, and to write

$$M_\alpha = A \sum_{ij} \hat{R}_\alpha(ij) \mathbf{S}(i) \cdot \mathbf{S}(j), \tag{4.5}$$

where $\hat{\mathbf{R}}(ij)$ is a unit vector specifying the direction between the ions i and j, and the interaction is restricted to nearest neighbors. In the perovskite structure the defect modes which give rise to absorption are then $A_{1g}+T_{1u}$, and E_g+T_{1u}. In practice, however, not all of these pairs are observed. Since the interaction couples most strongly ions that are nearest antiferromagnetic neighbors the impurity absorption arises from pairs of modes one of which is normally localized mainly on the defect, and the other of which is localized on the neighbor. The only such pair in the perovskite structure is $A_{1g}(D)+T_{1u}$, where $A_{1g}(D)$ denotes the A_{1g} mode, localized mainly on the defect. In the rutile structure these pairs are $A_{1g}(D)+E_u$ and $A_{1g}(D)+B_{1u}$. Far-infrared absorption therefore permits measurement of the frequencies of some of the modes associated with the defects, and also of some of the pair modes. In both of these experiments, identification of the magnetic character of the mode and the value of its g factor is obtained by applying a magnetic field and observing the splittings of the lines.

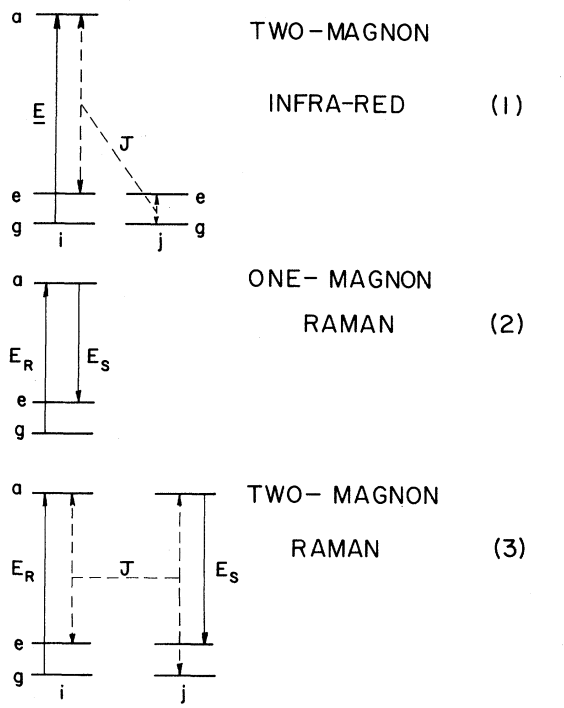

FIG. 3. Schematic diagram of processes occurring in absorption and scattering of light which take the crystal from its ground state, g, to excited states, e, on one or more sites, i, j, via a virtual state, a. The interactions inducing the virtual transition involve either E, the electric vector of the light and/or J, the exchange.

In Raman scattering experiments, light is inelastically scattered by the magnons. The theory of the Raman scattering in pure crystals has been reviewed in detail by Fleury and Loudon (1968). We shall merely take over the main points of their argument to crystals containing defects. The one-magnon Raman scattering arises as shown in Fig. 3(2). The electric field of incident light $\mathbf{E}^R$ excites a virtual electronic transition which then decays to a state with a different spin from the original state by the emission of light described by the electric field $\mathbf{E}^S$. The Hamiltonian for the interaction between the light and the S_x component of the spins is then found to be

$$H_{\mathrm{INT}} = \sum_i \Gamma(i)(E_z^R E_x^S - E_x^R E_z^S) S_x(i),$$

from which it is convenient to define a polarizability of the crystal so that

$$H_{\mathrm{INT}} = \sum_{\alpha\beta} P_{\alpha\beta} E_\alpha^R E_\beta^S,$$

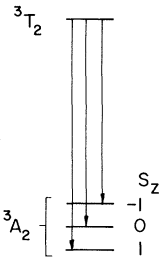

FIG. 4. Principle of fluorescence measurements illustrated for Ni^{2+} in $KMnF_3$. The ratio of the main electronic transition to the ground state splitting is reduced in the drawing for clarity. The states with $S_z=0$ and -1 are the states containing one and two A_{1g} excitations on the defect (after Johnson *et al.*, 1966).

when

$$P_{\alpha\beta}=\sum_i \Gamma(i)[S_\beta(i)\delta_{\alpha z}-S_\alpha(i)\delta_{\beta z}]. \quad (4.6)$$

The scattering cross section for Raman scattering is then defined by the Raman tensor (Born and Huang, 1954) in terms of the initial, n, and final states, m, as

$$I_{\alpha\beta\gamma\delta}=\sum_{nm}\rho_n\langle n\mid P_{\alpha\beta}\mid m\rangle\langle m\mid P_{\gamma\delta}\mid n\rangle\delta(\omega-\omega_{mn}). \quad (4.7)$$

By substituting the eigenvectors for the cluster models into the matrix elements for the polarizability, we can readily see that only modes of A_{1g} symmetry give rise to single excitation Raman scattering.

Two-magnon Raman scattering occurs with the aid of the process, shown in Fig. 3(3), which is closely similar to that giving rise to two-magnon infrared absorption. The polarizability is

$$P_{\alpha\beta}=\sum_{\gamma\delta}\sum_{ij}B_{\alpha\beta\gamma\delta}S_\gamma(i)S_\delta(j),$$

which even for very symmetric structures contains a large number of parameters. It is usual to approximate $P_{\alpha\beta}$ by assuming only nearest-neighbor interactions and further to assume that the S's enter with a Heisenberg form. The polarizability is then, for the perovskite structure,

$$P_{\alpha\beta}=\sum_{ij}\Gamma_{ij}\mathbf{S}(i)\cdot\mathbf{S}(j),$$

where

$$\Gamma_{ij}=B_1\hat{R}_\alpha(ij)\hat{R}_\beta(ij)+(B_2-\tfrac{1}{3}B_1)\delta_{\alpha\beta}. \quad (4.8)$$

Terms in B_1 and B_2 belong to particular representations (Elliott *et al.*, 1968). This gives rise to scattering by pairs of modes one of which is localized on the defect, for the same reasons as already described for the far infared absorption. The possible pairs in the perovskite structure are $A_{1g}(D)+A_{1g}(N)$, and $A_{1g}(D)+E_g$. These pairs can be distinguished because the scattering of the former is isotropic while that of the latter is anisotropic.

In the rutile structure, the possible pairs of modes are $A_{1g}(D)+A_{1g}(N)$, $A_{1g}(D)+B_{2g}$, and $A_{1g}(D)+E_g$, which can all be distinguished by polarization studies. Raman scattering may therefore be used to measure the frequencies of the modes localized on the defects and also of pairs of modes. Infrared and Raman studies together provide particularly detailed information about the frequencies of localized modes and also of pairs of modes, one of which is localized mainly on the defect while the other is mainly associated with its neighbors. Further information about the g factors of the modes may be found by applying a magnetic field to the crystal while the optical measurement is in progress.

Two other optical techniques have been used to study modes around defects. One of these is the fluorescence which occurs when the impurity ion is excited to a new state and then decays by emission of a photon to either the ground state or one of the low-lying excited states. The process is shown schematically for Ni^{2+} in $KMnF_3$ in Fig. 4. The technique has the advantage that whereas the other techniques, infrared spectroscopy and Raman spectroscopy, can be used to study modes where the change in spin S at any site is ±1 from its value in the ground state, no such restriction occurs in the case of fluorescence. The spin state of the excited state may be quite different. The disadvantages of the technique are twofold. First, the basic mechanism of fluorescence is uncertain so that it is difficult to make a detailed comparison between experiment and theory, and second, the excited state must be well localized, which implies that there must not be excited states of the host with energies close to those of the excited states of the defect. The technique is therefore very good for studying the localized modes of ions where excited states lie within an energy gap of the host material. In practice, the technique has been mainly used for Ni^{2+} in various Mn^{2+} hosts (Johnson *et al.*, 1966).

It is also possible to study localized modes by studying the sidebands on optical transitions. The process is essentially that of fluorescence in reverse except for the fact that both the exciton and localized mode are created simultaneously. The localized mode is localized predominantly on the defect. The disadvantage of this technique is that there will be an interaction between the localized mode and the exciton in an analogous way to the occurrence of an interaction between the pairs of defect modes discussed in Sec. III. Since this interaction is usually unknown it is difficult to disentangle information about the pure-defect mode from that obtained about the pair of exciton and defect modes.

2. Neutron Scattering

The magnetic scattering cross section of slow unpolarized neutrons for a wave vector transfer $\mathbf{Q}$, and frequency transfer ω, is given for magnetic system by

$$\frac{d^2\sigma}{d\omega d\Omega}=\left(\frac{2ge^2}{m_ec^2}\right)^2\left|\frac{\mathbf{k}'}{\mathbf{k}_0}\right|F(\mathbf{Q})^2\sum_{\alpha\beta}\left(\delta_{\alpha\beta}-\frac{Q_\alpha Q_\beta}{|\mathbf{Q}|^2}\right)S_{\alpha\beta}(\mathbf{Q},\omega), \quad (4.9)$$

where e and m_e are the electronic charge and mass, g is the neutron gyromagnetic ratio, and $\mathbf{k}'$ and $\mathbf{k}_0$ are the wave vectors of the scattered and incident neutrons, respectively. The form factor of the ions $F(\mathbf{Q})$ is assumed to be the same for all ions, and for a system at

absolute zero in the small Q approximation (Schwinger, 1937),

$$S_{\alpha\beta}(\mathbf{Q},\omega)=\sum_{nm}\rho_n\langle n\mid\sum_i[S_\alpha(i)+\tfrac{1}{2}L_\alpha(i)]\times\exp[i\mathbf{Q}\cdot\mathbf{R}(i)]\mid m\rangle\langle m\mid\sum_i[S_\beta(i)+\tfrac{1}{2}L_\beta(i)]\times\exp[-i\mathbf{Q}\cdot\mathbf{R}(i)]\mid n\rangle\delta(\omega-\omega_{mn}),\quad(4.10)$$

where $\mid m\rangle$ is the excited state of the system, and ω_{mn} the excitation frequency of that state from the initial state $\mid n\rangle$.

It is usually possible to rewrite the spin and orbital angular momentum variables in terms of the effective spin operators S',

$$S_\alpha+\tfrac{1}{2}L_\alpha=b_\alpha S_\alpha',$$

where the coefficients b_α may be found from Table I. The intensity of the scattering from a particular excitation, m, of a cluster may then be expressed in terms of a reduced structure factor at low temperatures so that

$$S_{\alpha\beta}(\mathbf{Q},\omega)=\sum_m F_\alpha(\mathbf{Q}/m)F_\beta(\mathbf{Q}/m)^*\delta(\omega-\omega_m),$$

in which

$$F_\alpha(\mathbf{Q}/m)=\langle 0\mid\sum_i b_\alpha(i)S_\alpha(i)\exp[i\mathbf{Q}\cdot\mathbf{R}(i)]\mid m\rangle,\quad(4.11)$$

where $\mid 0\rangle$ is the ground state, and we have again neglected the prime on the effective spin variable. From these results it is clear that inelastic neutron scattering enables the frequencies of the modes of a cluster to be determined. In addition, there is a variation of the intensity with wave vector transfer Q, as illustrated in Fig. 5, where $\mid F_x(\mathbf{Q}/m)\mid^2$ is shown for the different modes of the nearest-neighbor cluster in the perovskite lattice. The behavior of the intensity is clearly quite different for the A_{1g}, E_g, and T_{1u}, modes and in principle allows each to be identified experimentally.

In principle, two-excitation scattering may be observed through the $S_{zz}(\mathbf{Q},\omega)$ part of the cross section. This arises because it is possible to excite two A_{1g} modes; one mode predominantly localized on the defect and the other localized on its neighbors, without altering the total spin of the crystal. Since however the cross section for this process is very weak, it has not been observed, and is unlikely to be of much practical use.

Neutron scattering may therefore be used to determine the frequencies and to identify the modes around defects. It has less frequency resolution than the optical techniques. It has, however, the advantage that by measuring the wave vector dependence of the intensity it is possible to obtain not only the symmetry of the mode but also, as shown in Fig. 5, the eigenvectors of the modes when these are not entirely determined by symmetry. This latter information cannot be directly determined by optical techniques. In the sense that the mode form factors allow the transverse exchange $J'(1)$ to be deduced, the information is similar to that which is obtained by studying the two excitation processes optically. The other main advantage of the neutron technique is that it may be used to determine the host magnons. It is not possible to discuss the effect of the defects on the magnons of the host within the cluster model and so we shall therefore postpone its discussion until Sec. V is reached.

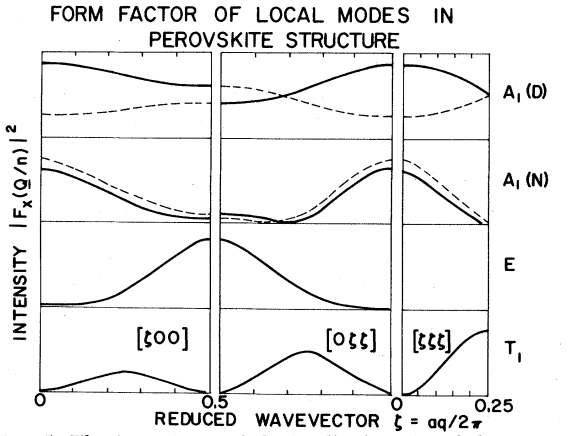

FIG. 5. The form factor of the localized modes of the nearest neighbor cluster in the perovskite structure for wavevector transfer Q along three symmetry directions. The results for the four modes, n, whose group theoretic labels appear on the right, are given for both magnetic (solid lines) and nuclear (dashed lines) zones.

3. Other Techniques

There are a number of other techniques which may in principle be used to give further information about magnetic defects. Measurements of the NMR frequency of both the defect, its nearest neighbors, and the host give information about the behavior of the magnetization at each of these sites as a function of temperature. This may then be analyzed to give information about the exchange constants between the defect and the host (Butler *et al.*, 1970). Unfortunately, the theory is very difficult (see Sec. VII) and furthermore is uncertain because there is no reliable theory for the temperature dependence of the magnetization of pure materials.

Mössbauer measurements may also be used to determine the magnetization of, particularly, Fe^{2+} ions as a function of temperature (see Wertheim *et al.*, 1969).

V. THEORY OF DEFECTS USING GREEN'S FUNCTIONS

1. Formalism and the Perfect Crystal

One of the most powerful theoretical methods which has been applied to the problem of defects is that of Green's functions. Unlike the cluster model, the theory

enables us to treat the host crystal exactly and further to solve the problem for isolated defects in great detail. One of the advantages in using Green's functions lies in the way in which they are very directly related to experimental measurements. In Sec. IV, we found that the physical properties of systems can frequently be expressed in terms of correlation functions of pairs of operators of the form

$$F(AB,\omega)=\sum_{nm}\rho_n\langle n\mid A\mid m\rangle\langle m\mid B\mid n\rangle\delta(\omega-\omega_{mn}),$$

where ρ_n is the probability of the system being in a state $\mid n\rangle$, and ω_{mn} is the energy of excitation to the state $\mid m\rangle$. Zubarev (1960) shows that this correlation function is related to a Green's function, G, which is analytic over the whole complex frequency, ω, plane.

$$[G(\omega+i\epsilon)-G(\omega-i\epsilon)][n(\omega)+1]=-2\pi iF(\omega), \quad (5.1)$$

where $n(\omega)$ is the Bose occupation number

$$n(\omega)=1/[\exp(\omega/k_\beta T)-1]$$

and we are putting $\hbar=1$ throughout.

In the upper half of the complex ω plane, G is the Fourier transform of the retarded Green's function

$$G_R(AB,t)=i\theta(t)\langle[A(t),B(0)]\rangle,$$

where

$$\theta(t)=1 \qquad t>0$$
$$=0 \qquad t<0,$$

and in the lower half ω plane it is the Fourier transform of the advanced Green's function

$$G_A(AB,t)=-i\theta(-t)\langle[A(t),B(0)]\rangle.$$

The properties of G can, for our purposes, be obtained from the equation

$$\omega G(AB,\omega)=\delta(t)\langle[A(t),B(0)]\rangle+G([A,H]B,\omega). \quad (5.2)$$

Initially, we introduce the canonical transformation of the spin operators on the down sublattice already described by Eq. (3.10). The perfect crystal Hamiltonian is then [cf. Eq. (2.2)] unchanged for the intra sublattice interactions L

$$H_1=-\sum_i H_A S_z(i)+\tfrac{1}{2}\sum_{ij}^{L} I(ij)\mathbf{S}(i)\cdot\mathbf{S}(j),$$

but for the inter sublattice terms A, becomes for isotropic exchange

$$H_2=\tfrac{1}{2}\sum_{ij}^{A} I(ij)[\tfrac{1}{2}(S_+(i)S_+(j)+S_-(i)S_-(j))-S_z(i)S_z(j)],$$

where the total Hamiltonian is $H=H_1+H_2$.

In applying this formalism to the antiferromagnet, we shall follow the work of Lines (1964), but rewrite his results in a form which is more amenable to the defect calculations later. We introduce four Green's functions for the perfect crystal

$$P_1(ij,\omega)=(2S)^{-1}G(S_+(i)S_-(j),\omega),$$
$$P_2(ij,\omega)=(2S)^{-1}G(S_-(i)S_-(j),\omega),$$
$$P_3(ij,\omega)=(2S)^{-1}G(S_+(i)S_+(j),\omega),$$
$$P_4(ij,\omega)=(2S)^{-1}G(S_-(i)S_+(j),\omega),$$

where, provided that we are not discussing Co^{++} ions in the rutile structure, P_1 and P_4 are nonzero only if i and j belong to the same sublattice, while for P_2 and P_3 i and j belong to different sublattices.

The equations of motion can be written using Eq. (5.2); for example

$$\omega P_1(ij,\omega)=S^{-1}\langle S_z(i)\rangle\delta_{ij}+(2S)^{-1}\sum_{k=L}I(ik)[G(S_+(k)S_z(i),S_-(j);\omega)-G(S_z(k)S_+(i),S_-(j);\omega)]+(2S)^{-1}\sum_{k=A}I(ik)[G(S_-(k)S_z(i),S_-(j);\omega)+G(S_z(k)S_+(i),S_-(j);\omega)]+H_AP_1(ij,\omega).$$

These equations of motion are solved at low temperatures by making use of the decoupling procedure of Tyablikov (1959)

$$(2S)^{-1}G[S_+(k)S_z(i),S_-(j);\omega]=\langle S_z(i)\rangle P_1(kj,\omega)$$

and

$$\langle S_z(i)\rangle=S.$$

The equations of motion may then be written in a matrix form

$$\sum_k[\omega\mathsf{I}\delta_{ik}-\mathsf{D}(ik)]\mathsf{P}(kj,\omega)=\delta_{ij}\mathsf{K}, \quad (5.3)$$

where

$$\mathsf{I}=\begin{pmatrix}1&0\\0&1\end{pmatrix},\qquad \mathsf{K}=\begin{pmatrix}1&0\\0&-1\end{pmatrix},$$

$$\mathsf{P}=\begin{pmatrix}P_1&P_3\\P_2&P_4\end{pmatrix},$$

and

$$\mathsf{D}=\begin{pmatrix}D_1&D_2\\-D_2&-D_1\end{pmatrix},$$

where

$$D_1(ik)=SI(ik),\ k\neq i \text{ but on the same lattice,}$$

and

$$D_1(ii)=-S\sum_{k=L}I(ik)+S\sum_{k=A}I(ik)+H_A,$$

while

$D_2(ik)=SI(ik)$ if k and i are on different lattices.

These equations are solved by introducing Fourier transforms

$$P(\mathbf{q},\omega)=\sum_i P(ij,\omega)\exp[i\mathbf{q}\cdot\mathbf{R}(ij)], \quad (5.4)$$

where the summation is over a single sublattice.

The equation of motion (5.3) then becomes

$$[\omega\mathsf{I}-\mathsf{D}(\mathbf{q})]\mathsf{P}(\mathbf{q},\omega)=\mathsf{K}, \quad (5.5)$$

where, in the notation of Sec. II, Eqs. (2.4) and (2.5),

$$D(\mathbf{q})=\begin{pmatrix} A(\mathbf{q}) & B(\mathbf{q}) \\ -B(\mathbf{q}) & -A(\mathbf{q}) \end{pmatrix}.$$

Using these results we can obtain detailed expressions for $P_1(\mathbf{q},\omega)$ and $P_2(\mathbf{q},\omega)$ as

$$P_1(\mathbf{q},\omega)=[\omega+A(\mathbf{q})]/[\omega^2-\omega(\mathbf{q})^2], \quad (5.6)$$

while

$$P_2(\mathbf{q},\omega)=-B(\mathbf{q})/[\omega^2-\omega(\mathbf{q})^2] \quad (5.7)$$

where $\omega(\mathbf{q})$ is the frequency of the magnon of wave vector $\mathbf{q}$, Eq. (2.3).

We shall need the limits of these expressions as $\omega\to\omega+i\epsilon$ in order to calculate the scattering properties. These are given by

$$\mathrm{Re}[P_1(\mathbf{q},\omega)]=[2\omega(\mathbf{q})]^{-1}\times\left(\frac{\omega(\mathbf{q})+A(\mathbf{q})}{[\omega-\omega(\mathbf{q})]_p}+\frac{\omega(\mathbf{q})-A(\mathbf{q})}{[\omega+\omega(\mathbf{q})]_p}\right)$$

$$\mathrm{Im}[P_1(\mathbf{q},\omega)]=[-\pi/2\omega(\mathbf{q})]\{[\omega(\mathbf{q})+A(\mathbf{q})]\times\delta[\omega-\omega(\mathbf{q})]+[\omega(\mathbf{q})-A(\mathbf{q})]\delta[\omega-\omega(\mathbf{q})]\},$$

while

$$\mathrm{Re}[P_2(\mathbf{q},\omega)]=-[B(\mathbf{q})/2\omega(\mathbf{q})]\times\{[\omega-\omega(\mathbf{q})]_p^{-1}-[\omega+\omega(\mathbf{q})]_p^{-1}\}$$

$$\mathrm{Im}[P_2(\mathbf{q},\omega)]=+[B(\mathbf{q})\pi/2\omega(\mathbf{q})]\times\{\delta[\omega-\omega(\mathbf{q})]-\delta[\omega+\omega(\mathbf{q})]\}. \quad (5.8)$$

We can also show from these results that

$$P_3(\mathbf{q},\omega)=P_2(\mathbf{q},-\omega)$$

and

$$P_4(\mathbf{q},\omega)=P_1(\mathbf{q},-\omega).$$

The original Green's functions in real space $[P(ij,\omega)]$ can be obtained from these by the inverse transformation to Eq. (5.4)

$$P(ij,\omega)=N^{-1}\sum_{\mathbf{q}} P(\mathbf{q},\omega)\exp[-i\mathbf{q}\cdot\mathbf{R}(ij)].$$

These functions have then both real and imaginary parts: the imaginary parts being finite over the range of frequencies ω lying within the band of the host frequencies and zero outside.

2. The Green's Functions for an Isolated Defect

Suppose that a defect is introduced into the lattice at the site labeled 0. As already discussed in Sec. III, this may give rise to changes in the effective spins, exchange, and anisotropy constants. Although in practice these may all be of importance, we neglect the changes in the anisotropy constants, and the possibility of more complex exchange constants than anisotropy along the z axis. Although the theory may be readily extended to include these features, it adds considerably to the complexity of the equations. The terms in the Hamiltonian which involve the defect are then

$$\sum_{j=L}\{J'(0j)[S_x'(0)S_x(j)+S_y'(0)S_y(j)]+I'(0j)S_z'(0)S_z(j)\}+\sum_{j=A}\{J'(0j)[\tfrac{1}{2}S_+'(0)S_+(j)+\tfrac{1}{2}S_-'(0)S(j)]-I'(0j)S_z'(0)S_z(j)\}.$$

With these terms in the Hamiltonian, the equations of motion for the Green's functions are modified. As with the pure crystal, it is useful to define four Green's functions. For example, we have

$$G_1(ij,\omega)=\tfrac{1}{2}[S(i)S(j)]^{-1/2}G[S_+(i)S_-(j),\omega],$$

where

$$S(i)=S \text{ if } i\neq 0, \text{ and } S' \text{ if } i=0.$$

The equations of motions for these Green's functions may then be obtained in a way similar to those for the pure crystal. The result analogous to Eq. (5.3) is

$$\sum_k[\omega\mathsf{I}\delta_{ik}-\mathsf{D}(ik)]\mathsf{G}(kj,\omega)=\delta_{ij}\mathsf{K}+\sum_k\mathsf{C}(ik)\mathsf{G}(kj,\omega), \quad (5.9)$$

where

$$\mathsf{C}=\begin{pmatrix} C_1 & C_2 \\ -C_2 & -C_1 \end{pmatrix}$$

with

$$C_1(0j)=(S'S)^{1/2}J'(0j)-(S^3/S')^{1/2}I(0j) \qquad j=L$$

$$C_1(j0)=(S'S)^{1/2}[J'(j0)-I(j0)] \qquad j=L$$

$$C_1(00)=-S\sum_{j=L}I'(0j)+S\sum_{k=A}I'(0k)-H_A+S\sum_{j=L}I(0j)-S\sum_{k=A}I(0k)$$

$$C_1(jj)=\pm S'I'(0j)\mp SI(0j)$$

upper, lower j sign for $j=A, L$

$$C_2(0j)=(SS')^{1/2}J'(0j)-(S^3/S')^{1/2}I(0j) \qquad j=A$$

and

$$C_2(j0)=(S'S)^{1/2}[J'(j0)-I(j0)], \qquad j=A$$

where the index j refers to a neighbor of the defect.

In Eq. (5.9), the left-hand side and the first term on the right-hand side are identical with those of Eq. (5.3) for the pure crystal. The second term of the right-hand side represents the perturbation introduced into the crystal by the presence of a single defect. The equation can be solved by making use of the solutions of the pure crystal problem found in the preceding section. Using Eq. (5.3) to give the inverse matrix to $[\omega \mathsf{I}\delta_{ik}-\mathsf{D}(ik)]$ gives

$$\mathsf{G}(ij,\omega)=\mathsf{P}(ij,\omega)+\sum_{k_1k_2}\mathsf{P}(ik_1,\omega)\mathsf{KC}(k_1k_2)\mathsf{G}(k_2j,\omega). \tag{5.10}$$

This equation gives the exact solution to the single impurity problem. Since the k indices are restricted to the defect or the relatively few neighbors with which it directly interacts, the solution is quite tractable. The presence of the G on the right-hand side shows that the exact solution includes multiple scattering of the spin excitations by the defect. If this G is replaced by an unperturbed Green's function P, then the solution gives only the effect of the defect in first order perturbation theory. The complete solution may be rewritten as

$$\mathsf{G}(ij,\omega)=\mathsf{P}(ij,\omega)+\sum_{k_1k_2}\mathsf{P}(ik,\omega)\mathsf{X}(k_1k_2,\omega)\mathsf{P}(k_2j,\omega), \tag{5.11}$$

where

$$\mathsf{X}(k_1k_2,\omega)=\sum_{k_3}\mathsf{KC}(k_1k_3)\mathsf{M}^{-1}(k_3k_2,\omega), \tag{5.12}$$

where

$$\mathsf{M}(ij,\omega)=\mathsf{I}\delta_{ij}-\sum_{k}\mathsf{P}(ik,\omega)\mathsf{KC}(kj). \tag{5.13}$$

This solution is now a complete description of the formalism. The matrix $\mathsf{M}(ij,\omega)$ is of size $2(n+1)\times 2(n+1)$ where n is the number of neighbors with which the defect interacts directly. In the perovskite structure it may reasonably be taken to be a 14×14 matrix. The unperturbed Green's functions and therefore the matrix have real and imaginary parts.

There will clearly be a large perturbation of the Green's functions if the matrix X is large. This will occur when the M matrix is singular or nearly singular. Since for ω within the band of host excitation frequencies the matrix has both real and imaginary parts, there is no difficulty in performing the inverse for all frequencies ω lying within the band of the host spin wave frequencies. We expect X will be large, however, for those frequencies for which the Re$[\mathsf{M}]$ is singular. These frequencies are known as resonant frequencies. Outside the band of host frequencies, there is no imaginary part to M and singularities in M must be treated more carefully. These frequencies correspond to the frequencies of the localized modes. In Sec. V.4, we shall discuss how the matrix X may then be inverted to calculate the scattering from the localized modes.

We may see from this discussion, however, that the frequencies at which the Re$[\mathsf{M}]$ is singular play an essential role in the theory of magnetic defects. They may be quite directly compared with the excitation frequencies given by the cluster models of Sec. II. In the present case, these frequencies have been calculated incorporating the host in a far more satisfactory way than was achieved by a cluster model. The approximations made in these calculations for the form of the ground state are equivalent to those of the pseudoboson technique described for the cluster models in Sec. III. The results are not, therefore, necessarily better than those of the cluster models. In fact, we may expect the perturbation treatment (III.4) to work best[1] for systems with small spin and for frequencies well away from the band of frequencies of the host crystal. Conversely, if we are interested in effects with frequencies lying within or close to those of the pure crystal, we expect the Green's function treatment to give superior results.

The matrix $\mathsf{M}(ij,\omega)$ is of very similar structure to the self-energy matrix of the cluster models. In particular, it is possible and frequently advantageous to make use of symmetry to block diagonalize the matrix in a way similar to that used for the cluster models. When this is done the expressions become particularly simple for the E_g and T_{1u} modes of the perovskite structure. For the E modes, the matrix $\mathsf{M}(ij,\omega)$ reduces to

$$[S'I'(0j)-SI(0j)]N^{-1}$$
$$\times\sum_{\mathbf{q}}\{[\cos(q_xa)-\cos(q_ya)](\omega+A(\mathbf{q}))/[\omega^2-\omega(\mathbf{q})^2]\}-1,$$

and for the T_{1g} modes, it reduces to

$$[S'I'(0j)-SI(0j)]N^{-1}$$
$$\times\sum_{\mathbf{q}}\{2\sin^2(q_xa)[\omega+A(\mathbf{q})]/[\omega^2-\omega(\mathbf{q})^2]\}-1.$$

The frequencies of the E_g and T_{1u} modes are given by the frequencies ω for which these expressions are zero. Similar expressions may be written for the A_{1g} modes and for all the different modes of the perovskite structure, but several of them are considerably more complex and will not be given in detail.

It is of interest to compare these results with those obtained in Sec. III. If we make Ising model approximation

$$A(\mathbf{q})=\omega(\mathbf{q})=6SI(1)+H_A,$$

the both of the above results give zero when $\omega=\omega_N$ [Eq. (3.3)].

The frequencies at which the matrix $\mathsf{M}(ij,\omega)$ is singular have been calculated for various different sets of parameters by a number of authors. Parkinson (1969)

[1] Cluster models work well for highly localized modes and the difference between the perturbation and quasiboson technique is greatest for small spin.

has discussed the perovskite structure. He assumes that all the exchange interactions are of the Heisenberg type between nearest neighbors, $I'=J'$, and that the anisotropy of the host is negligible. His results for the frequencies of the E_g and T_{1u} local modes are shown in Fig. 6 for increasing values of the parameter

$$\rho=(S'I'/SI)-1,$$

and compared with the predictions of the Ising model. He also calculates the frequencies of the A_g, E_g, and T_{1u} modes for $S'/S=1.2$ and various values of I'/I.

The rutile structure has been considered by Lovesey (1968), Tonegawa (1968), Shiles and Hone (1970) and Walker[2] (private communication). Lovesey and Tonegawa discuss the rutile structure with Heisenberg exchange interactions only between nearest neighbors of opposite magnetic moment.

In Fig. 7 we show Lovesey's results for the frequency of the A_{1g} mode localized predominantly on the defect atom as a function of the exchange I'/I. The anisotropy was taken to be that appropriate for MnF_2. The Ising model predictions are essentially identical to those for $S'/S=0.1$. Lovesey and Tonegawa present calculations of these modes for a variety of different parameters. Shiles and Hone extend the calculations to include firstly the effects of nonzero exchange between the ferromagnetic neighbors at $\pm(00c)$ and secondly to allow for anisotropic exchange. The parameters in their calculations are chosen to be appropriate for Fe^{2+} and Ni^{2+} in MnF_2.

3. The Self-Energy of the Excitations

The analysis of the preceding section was applicable when only a single defect was present in the crystal. In practice, experiments are performed with a large number of defects, which we shall denote by a concentration c. In this and the next two sections we shall assume

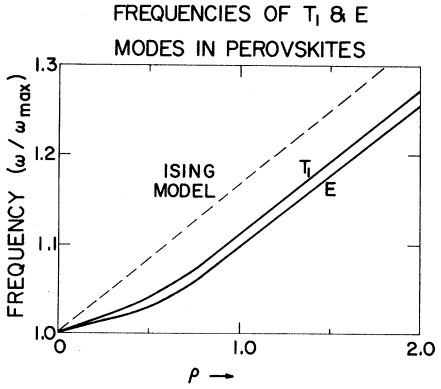

FIG. 6. Dependence of T_{1u} and E_g modes in perovskites (Parkinson, 1969) according to Ising theory (broken line) and Green's function theory. The fractional increase in the interaction, IS, between defect and host is denoted by ρ and ω_{max} is the maximum frequency of the host spin-wave band.

[2] Calculations have been done for Zn, Fe, and Ni in MnF_2.

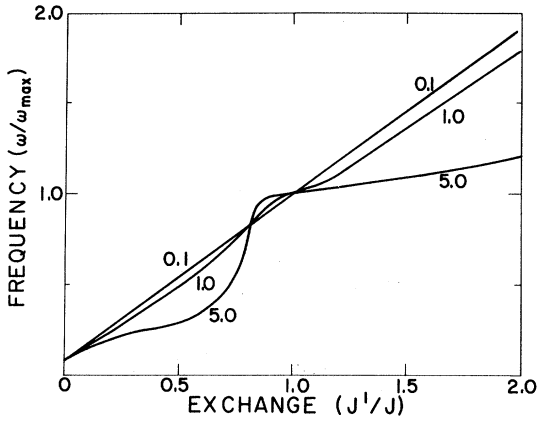

FIG. 7. The frequency of the A_{1g} mode localised principally on the defect as calculated by Lovesay (1968) for the rutile lattice as a function of the Heisenberg exchange ($J=1$). Different values of S'/S are indicated on the curves. ω_{max} is the maximum frequency of the host spin-wave band.

that the concentration is small enough that we may neglect the interference between different defects, or, alternatively, in the sense of Sec. VIII, we shall expand the results in powers of the concentration of defects and keep only those terms which are linear in the concentration.

Initially, Eq. (5.10) must be extended to include the effects of many defects at the site labelled by d. The equation may then be written schematically as

$$\mathbf{G}=\mathbf{P}+\sum_d \mathbf{PKC}(d)\mathbf{G}, \tag{5.14}$$

where the summation is over all the cN defects. In the preceding section, we have seen that the solution to the one defect problem incorporates the multiple scattering of the spin excitations at the defect. We therefore look for a solution to the above equation which includes all the multiple scattering at a single defect but the scattering at different defects only correct to terms linear in the concentration of defects. This then leads us to rewrite the equation in the approximate form

$$\mathbf{G}=\mathbf{P}+\sum_d \mathbf{PX}(d)\mathbf{G}. \tag{5.15}$$

This equation differs from Eq. (5.11) in that it permits scattering in succession at different defects, but it is approximate because the multiple scattering at a single defect d_1 is included in $\mathbf{X}(d_1)$ and hence the next scattering can occur not at any defect but only at defects other than d_1: Equation (5.15) therefore overcounts the scattering. This subject will be further discussed in Sec. VIII and until then it is sufficient to note that the error in Eq. (5.15) is only of order c^2.

Equation (5.15) may now be averaged over the randomly distributed defects. The terms in the equation are then translationally invariant so that the averaged Green's function becomes

$$\bar{\mathbf{G}}(\mathbf{q},\omega)=\mathbf{P}(\mathbf{q},\omega)+c\mathbf{P}(\mathbf{q},\omega)\mathbf{X}(\mathbf{q},\omega)\bar{\mathbf{G}}(\mathbf{q},\omega), \tag{5.16}$$

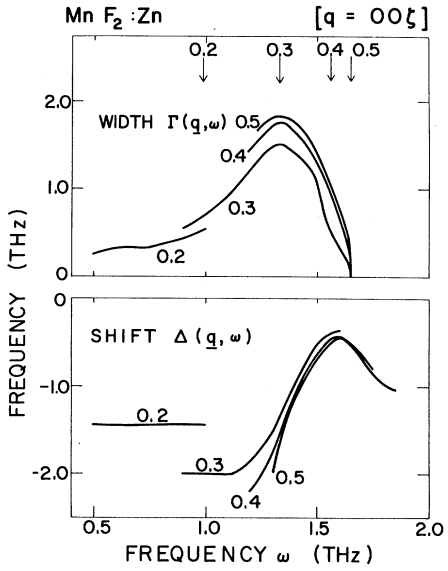

FIG. 8. The width shift functions of band magnons with wave vectors of the form $\mathbf{q}=(00\zeta)2\pi/c$ in MnF_2 containing Zn^{2+} impurities. The value of ζ is shown beside each curve and also beside the arrows which give the frequencies of unperturbed modes in pure MnF_2.

where

$$\mathbf{X}(\mathbf{q},\omega)=\sum_{ij}\mathbf{X}(ij,\omega)\exp\{i\mathbf{q}\cdot[\mathbf{R}(i)-\mathbf{R}(j)]\}.$$

This equation may be rewritten to give

$$[\omega\mathbf{I}-\mathbf{D}(\mathbf{q})-c\boldsymbol{\Sigma}(\mathbf{q},\omega)]\bar{\mathbf{G}}(\mathbf{q},\omega)=\mathbf{K} \qquad (5.17)$$

where the self-energy matrix is given by

$$\boldsymbol{\Sigma}(\mathbf{q},\omega)=\mathbf{K}\mathbf{X}(\mathbf{q},\omega)$$

and may be shown to be of the form

$$\boldsymbol{\Sigma}(\mathbf{q},\omega)=\begin{pmatrix}\Sigma_1(\omega) & \Sigma_2(\omega)\\ -\Sigma_2(-\omega) & -\Sigma_1(-\omega)\end{pmatrix}.$$

Equation (5.17) is the basic equation for the Green's functions of the spin excitations in an antiferromagnet containing a few defects. It plays an essential role in the theory through the remainder of this section.

If we assume that the self-energy is small compared with the unperturbed energies of the spin excitations, then the energy denominators in the Green's functions may be written ($\omega\to\omega+i\epsilon$) by analogy with Eq. (5.8) in the form

$$\omega\pm[\omega(\mathbf{q})+c\Delta(\mathbf{q},\omega)+ic\Gamma(\mathbf{q},\omega)], \qquad (5.18)$$

where the shift in frequency $\Delta(\mathbf{q},\omega)$ is the real part, and $\Gamma(\mathbf{q},\omega)$ the imaginary part of

$$[1/2\omega(\mathbf{q})]\{[A(\mathbf{q})+\omega]\Sigma_1(\mathbf{q},\omega)+[A(\mathbf{q})-\omega]\Sigma_1(\mathbf{q},-\omega)+B(\mathbf{q})[\Sigma_2(\mathbf{q},\omega)+\Sigma_2(\mathbf{q},-\omega)]\}. \qquad (5.19)$$

In Fig. 8 we show calculations of the shift and width functions $\Delta(\mathbf{q},\omega)$ and $\Gamma(\mathbf{q},\omega)$ for zinc impurities in MnF_2. The results are shown only for those values of ω close to the frequencies of the spin excitations $\omega(\mathbf{q})$ of pure MnF_2. The width functions have a peak at about 1.3 THz corresponding to several resonant modes of various symmetries at about this frequency. There is a corresponding marked change in the shift functions at about the same frequency. Provided that the concentration of defects is small, so that $c\Delta$ and $c\Gamma$ are considerably smaller than $\omega(\mathbf{q})$, it is frequently permissible to represent the functions by constants, $\Delta[\mathbf{q},\bar{\omega}(\mathbf{q})]$ and $\Gamma[\mathbf{q},\bar{\omega}(\mathbf{q})]$, where $\bar{\omega}(\mathbf{q})$ is the solution of the equation

$$\bar{\omega}(\mathbf{q})=\omega(\mathbf{q})+c\Delta[\mathbf{q},\bar{\omega}(\mathbf{q})].$$

In this approximation, the imaginary part of the Green's function is represented by a Lorentzian centered about $\bar{\omega}(\mathbf{q})$ and of half-width $c\Gamma[\mathbf{q},\bar{\omega}(\mathbf{q})]$. In Fig. 9, we show the calculated form of the imaginary parts of the Green's functions using the shift and width functions of Fig. 8, and assuming $c=0.05$. The results show that for $\mathbf{q}=(0,0,0.2)(2\pi/c)$, the curve is very close to a Lorentzian in shape but at larger wave vectors there are marked asymmetries which can only be understood on the basis of the full frequency dependent width and shift functions. The nonLorentzian character of the results increases as the concentration of defects increases.

In Fig. 8 it is noticeable that the magnitude of both the shift and the width increase as the wave vector increases. This behavior arises because unlike the single mass defect problem, Δ and Γ depend not only on ω, but also on wave vector $\mathbf{q}$. The increase with increasing wave vector is not always the case as shown by similar curves for Ni^{2+} impurities in MnF_2 in Fig. 10. In this case, the effects are largest for small wave

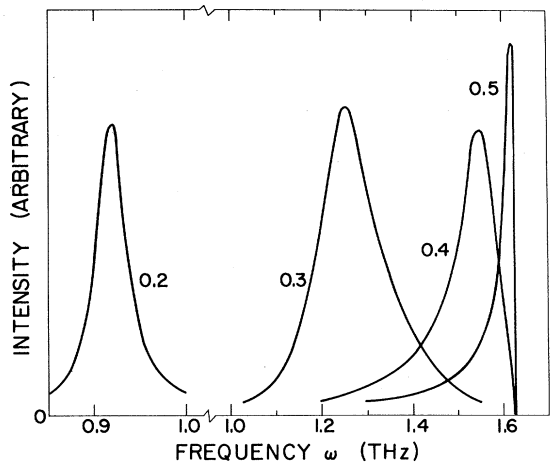

FIG. 9. The imaginary parts of the Green's functions in $Mn_{0.95}Zn_{0.05}F_2$ for different reduced wavevectors $\zeta[\mathbf{q}=(00\zeta)2\pi/c]$ calculated from the frequency dependent width and shift functions.

vectors, and smallest for large wave vectors. The magnitude of the width function is also nearly an order of magnitude less than for a zinc impurity. The origin of these differences lies in the different pattern of the resonant mode frequencies in the two materials. In the zinc case, there are fairly well-defined resonant modes at frequencies of about 1.3 THz, but in the nickel case these resonant modes occur near the peak of the host density of states (1.6 THz). Thus they are not well defined and have little influence on the host modes. The width function is therefore considerably larger for the zinc impurities than for the nickel impurities.

Lastly, we should remark that the expressions for $c\Delta$ and $c\Gamma$ are only valid provided that they are small compared with $\omega(\mathbf{q})$. Close to a localized mode or an exceptionally well-defined resonant mode, the more accurate complete expressions for $\bar{\mathbf{G}}(\mathbf{q},\omega)$ given by Eq. (5.15) are necessary.

4. Neutron Scattering

In Sec. IV.4, the theory of the neutron scattering cross section for a magnetic material was discussed. The cross section for a momentum transfer $\mathbf{Q}$ and frequency transfer ω depends essentially on the functions $S_{\alpha\beta}(\mathbf{Q},\omega)$, Eq. (4.10). This function is of similar form to the spectral function introduced at the beginning of this section

$$S_{\alpha\beta}(\mathbf{Q},\omega)=F(AB,\omega)$$

with the operators given by Eq. (4.11)

$$A=\sum_i b_\alpha(i)S_\alpha(i)\exp[i\mathbf{Q}\cdot\mathbf{R}(i)],$$

where $b_\alpha(i)$ is a proportionality constant, and $B=A^*$. The neutron scattering is then known once the Green's functions, $\mathbf{G}(ij,\omega)$, are known in detail.

Initially, suppose we consider a pure crystal. The constant $b_\alpha(i)$ may be written as b. When the indices α and β are taken as x, using $S_+=S_x+iS_y$ we find

$$S_{xx}(\mathbf{Q},\omega)=-[n(\omega)+1](b^2S/2\pi)\times\sum_{ij}\mathrm{Im}\{[P_1(ij,\omega)+P_4(ij,\omega)+P_2(ij,\omega)+P_3(ij,\omega)]\exp i\mathbf{Q}\cdot[\mathbf{R}(i)-\mathbf{R}(j)]\}.$$

Now performing the summations over i and j and noting that P_1 and P_4 are nonzero only for i and j on the same sublattice, while P_2 and P_3 are nonzero only on different sublattices, we find

$$S_{xx}(\mathbf{Q},\omega)=-[n(\omega)+1](b^2S/\pi)N\times\mathrm{Im}\{P_1(\mathbf{q},\omega)+P_4(\mathbf{q},\omega)+\exp(i\boldsymbol{\tau}\cdot\mathbf{R})[P_2(\mathbf{q},\omega)+P_3(\mathbf{q},\omega)]\}\Delta(\mathbf{Q}-\mathbf{q}),\quad(5.20)$$

where $\boldsymbol{\tau}$ is a reciprocal lattice vector and $\Delta(\mathbf{Q}-\mathbf{q})$ means that

$$\mathbf{Q}=\boldsymbol{\tau}+\mathbf{q},$$

while $\mathbf{R}$ is the vector distance between the two sublattices. Substituting in the equation for P_1, P_2, P_3, and P_4 yields

$$S_{xx}(\mathbf{Q},\omega)=[n(\omega)+1][NS\pi b^2/\omega(\mathbf{q})]\times[A(\mathbf{q})-\exp(i\boldsymbol{\tau}\cdot\mathbf{R})B(\mathbf{q})]\times\{[\delta(\omega-\omega(\mathbf{q})]-\delta[\omega+\omega(\mathbf{q})]\}\Delta(\mathbf{Q}-\mathbf{q}).$$

This is the well-known (Nagai and Yoshimori, 1961) result for the scattering cross section for an antiferromagnet. In order to extend the result to a crystal containing defects, there are two difficulties. In the first place, the dynamics of the spin are altered. This may be incorporated by replacing the $\mathbf{P}$ of Eq. (5.18) by the $\bar{\mathbf{G}}(\mathbf{q},\omega)$ deduced in the preceding section. In the second place, the scattering of the defect is altered so that the coefficients $b_\alpha(i)S_\alpha(i)$ for the defects may be different from those of the host atoms. Suppose the defects have a coefficient $(b+\Delta b)(S/S')^{1/2}$; then the cross section for a defect crystal may be written as the sum of three terms:

$$S_{xx}^{1}(\mathbf{Q},\omega)=\tfrac{1}{2}(b^2S)\sum_i\sum_j\Phi_{ij},\quad(5.21)$$

$$S_{xx}^{2}(\mathbf{Q},\omega)=\tfrac{1}{2}(b\Delta bS)\sum_{i=d}\sum_j\Phi_{ij},\quad(5.22)$$

$$S_{xx}^{3}(\mathbf{Q},\omega)=\tfrac{1}{2}(\Delta b^2S)\sum_{i=d}\sum_{j=d}\Phi_{ij},\quad(5.23)$$

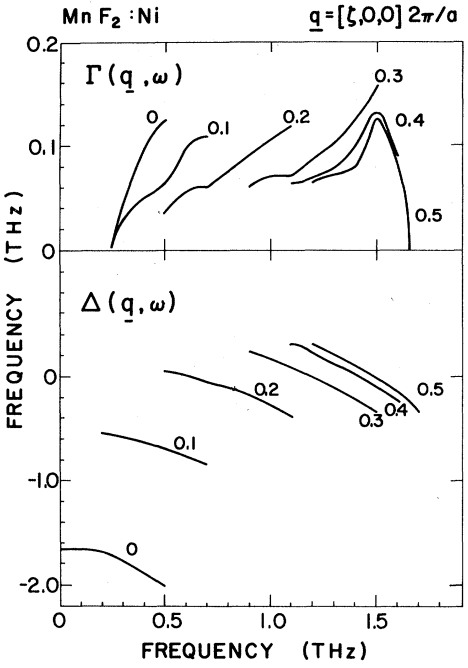

FIG. 10. The width and shift functions of band magnons with $\mathbf{q}=(\zeta,0,0)2\pi/a$ in MnF_2 doped with Ni^{2+} calculated for several values of ζ.

where the function Φ_{ij} is

$$\Phi_{ij}=-(2\pi)^{-1}[n(\omega)+1]\,\mathrm{Im}\,\{[G_1(ij,\omega)+G_2(ij,\omega)+G_3(ij,\omega)+G_4(ij,\omega)]\times\exp\{i\mathbf{Q}\cdot[\mathbf{R}(i)-\mathbf{R}(j)]\}\}.$$

The first of these terms gives the scattering if there is no change in the scattering length. The sums over i and j run over all the atoms of the crystal and may be rewritten in terms of the $\bar{\mathsf{G}}(\mathbf{q},\omega)$ functions obtained in the previous section. By analogy with Eq. (5.18) for the pure crystal, the result is

$$S_{xx}^{1}(\mathbf{Q},\omega)=-[n(\omega)+1](b^2SN/\pi)\,\mathrm{Im}\,\{\bar{G}_1(\mathbf{q},\omega)+\bar{G}_4(\mathbf{q},\omega)+\exp(i\boldsymbol{\tau}\cdot\mathbf{R})[\bar{G}_2(\mathbf{q},\omega)+\bar{G}_3(\mathbf{q},\omega)]\}\times\Delta(\mathbf{Q}-\mathbf{q}). \quad (5.24)$$

The second term arises from the interference between the scattering of the pure crystal and the change in the scattering produced at the defect. The appropriate Green's functions for this scattering are defined by

$$\mathsf{G}^{D}(\mathbf{q},\omega)=N^{-1}\sum_{i=d}\sum_{j}G(ij,\omega)\exp\{i\mathbf{q}\cdot[\mathbf{R}(i)-\mathbf{R}(j)]\}, \quad (5.25)$$

where the summation over i is restricted to only the defect sites. In terms of these Green's functions the scattering function is given by

$$S_{xx}^{2}(\mathbf{q},\omega)=-[n(\omega)+1]2b\Delta bN\times\mathrm{Im}\,\{\bar{G}_1^{D}(\mathbf{q},\omega)+\bar{G}_4^{D}(\mathbf{q},\omega)+\exp(i\boldsymbol{\tau}\cdot\mathbf{R})[\bar{G}_2^{D}(\mathbf{q},\omega)+\bar{G}_3^{D}(\mathbf{q},\omega)]\}\Delta(\mathbf{Q}-\mathbf{q}). \quad (5.26)$$

The calculation of this term in the scattering reduces therefore to the calculation of $\bar{\mathsf{G}}^{D}(\mathbf{q},\omega)$. The basic equation for the Green's functions was written schematically in Eq. (5.14). If we rewrite this equation in more detail, it becomes

$$\mathsf{G}(ij,\omega)=\mathsf{P}(ij,\omega)+\sum_{d}\sum_{k}\mathsf{P}(ik,\omega)\mathsf{KC}(kd)\mathsf{G}(dj,\omega)+\sum_{n}\sum_{k}\mathsf{P}(ik,\omega)\mathsf{KC}(kn)\mathsf{G}(nj,\omega),$$

where d is a suffix which runs over all the defect sites, and n runs over all the neighbors of the defects with which they directly interact. This equation may now be averaged over all configurations of the defects and Fourier transforms taken to obtain

$$\mathsf{G}(\mathbf{q},\omega)=\mathsf{P}(\mathbf{q},\omega)+\mathsf{P}(\mathbf{q},\omega)\mathsf{KC}^{D}(\mathbf{q})\bar{\mathsf{G}}^{D}(\mathbf{q},\omega)+\mathsf{P}(\mathbf{q},\omega)\mathsf{KC}^{N}(\mathbf{q})\bar{\mathsf{G}}^{N}(\mathbf{q},\omega),$$

where

$$\mathsf{C}^{D}(\mathbf{q})=\sum_{k}\mathsf{C}(kd)\exp\{i\mathbf{q}\cdot[\mathbf{R}(k)-\mathbf{R}(d)]\},$$

and C^{N} and G^{N} are defined in a similar manner to C^{D} and G^{D} but with the restricted summations over the neighbors rather than the defects. If this equation is compared with the earlier result we obtained for $\mathsf{G}(\mathbf{q},\omega)$ in Eq. (5.16), then we obtain with the aid of Eq. (5.12) for $\mathsf{X}(\mathbf{q},\omega)$,

$$\bar{\mathsf{G}}^{D}(\mathbf{q},\omega)=c\mathsf{L}^{D}(\mathbf{q},\omega)\bar{\mathsf{G}}(\mathbf{q},\omega), \quad (5.27)$$

where the matrix

$$\mathsf{L}^{D}(\mathbf{q},\omega)=\sum_{i}\mathsf{M}^{-1}(id,\omega)\exp\{i\mathbf{q}\cdot[\mathbf{R}(i)-\mathbf{R}(d)]\},$$

and the matrix M is defined by Eq. (5.13), while M^{-1} denotes its inverse. Collecting the results of Eq. (5.27) and (5.26) then enables us to obtain the contribution to the scattering $S_{xx}^{2}(\mathbf{Q},\omega)$.

The third contribution can be obtained in a similar manner. We introduce Green's functions of the form

$$\mathsf{G}^{DD}(\mathbf{q},\omega)=N^{-1}\sum_{i=d}\sum_{j=d}\mathsf{G}(ij,\omega)\times\exp\{i\mathbf{q}\cdot[\mathbf{R}(i)-\mathbf{R}(j)]\}.$$

Now within the low-concentration approximation, we may neglect the correlations between the defects when this reduces, on averaging over all configurations of defects, to

$$\mathsf{G}^{DD}(\omega)=c\mathsf{G}(dd,\omega) \quad (5.28)$$

which does not depend on the wave vector, $\mathbf{q}$, and furthermore has nonzero components only for G_1^{DD} and G_4^{DD}. The contribution to the scattering is then

$$S_{xx}^{3}(\mathbf{Q},\omega)=(\Delta b)^2S\,\mathrm{Im}\,[G_1^{DD}(\omega)+G_4^{DD}(\omega)] \quad (5.29)$$

which is also independent of the wave vector transfer $\mathbf{Q}$.

The calculation of $\mathsf{G}^{DD}(\omega)$ is most readily performed from Eq. (5.10). Equation (5.10) may be written as

$$\mathsf{G}(id,\omega)=\mathsf{P}(id,\omega)+\sum_{k_1k_2}\mathsf{P}(ik,\omega)\mathsf{KC}(k_1k_2)\mathsf{G}(k_2d,\omega).$$

If we consider the index i to take on values appropriate to the defect and its n neighbors, these equations form a $2(n+1)$ set of coupled equations. The solution is formally

$$\mathsf{G}(id,\omega)=\sum_{k}\mathsf{M}^{-1}(ik,\omega)\mathsf{P}(kd,\omega),$$

where M^{-1} is the matrix inverse of the matrix of Eq. (5.13). The required Green's functions are then obtained from

$$\mathsf{G}(dd,\omega)=\sum_{k}\mathsf{M}^{-1}(dk,\omega)\mathsf{P}(kd,\omega)$$

when the scattering is obtained from Eqs. (5.28–5.29).

Now that the scattering cross section has been obtained formally, let us discuss the form of the scattering in practice. When the scattering occurs within the band of frequencies of the host crystal, the largest contribution arises from the contribution $S_{xx}^{1}(\mathbf{Q},\omega)$ of Eq. (5.24) and is peaked around the frequencies of the host lattice $\omega(\mathbf{q})$. If the shift and width of the peaks are

small, then the expected form of the scattering is a Lorentzian peak centered on $\bar{\omega}(\mathbf{q})=\omega(\mathbf{q})+c\Delta[\mathbf{q},\omega(\mathbf{q})]$ and of half-width $\Gamma[\mathbf{q},\omega(\mathbf{q})]$. In practice this seems to be a very adequate approximation to the scattering of systems containing only a low concentration of defects.

A more accurate representation of the scattering is obtained by using the full frequency dependent self-energy $\boldsymbol{\Sigma}(\mathbf{q},\omega)$ of Eq. (5.17). The peaks in the imaginary parts of the Green's functions G_1, G_2, G_3, and G_4 may not then be of Lorentzian shape and also may be different for each of the different Green's functions. The numerators in the expressions for the individual Green's functions may differ. Furthermore since the scattering, Eq. (5.24), depends on Im $(G_1+G_2+G_3+G_4)$ for a nuclear reciprocal lattice point and

$$\text{Im}\ (G_1+G_4-G_2-G_3)$$

for a magnetic reciprocal lattice point; the detailed shape of the scattering for different wave vector transfers $\mathbf{Q}$, but the same wave vector $\mathbf{q}$, is in principle different. In practice, however, this difference is small as shown by the detailed calculations of Fig. 11 for the scattering function $S_{xx}{}^1(\mathbf{Q},\omega)$ for these two different types of wave vector transfers in MnF_2 containing 5% of Zn. The intensity of the two peaks is different, but their shapes are very similar.

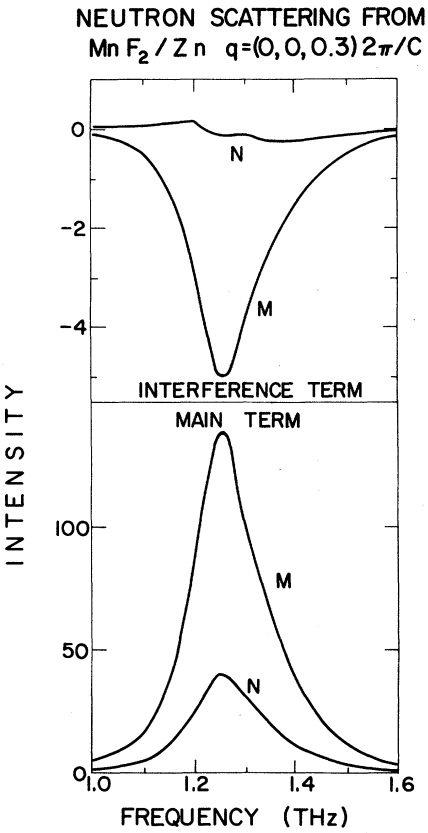

FIG. 11. Neutron scattering from $Mn_{0.95}Zn_{0.05}F_2$ for $\mathbf{q}=(0,0,0.3)2\pi/c$ in nuclear (N) and magnetic (M) zones. The lower part shows the host contribution $S_{xx}{}^1(\mathbf{Q},\omega)$ and the upper part shows the host-defect interference term $S_{xx}{}^2(\mathbf{Q},\omega)$.

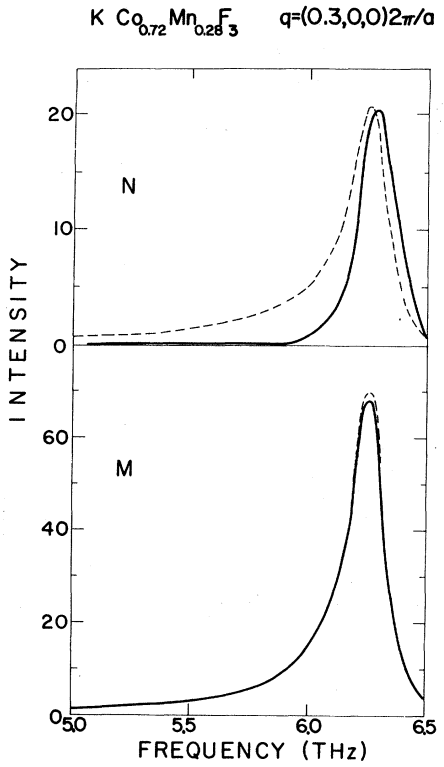

FIG. 12. Neutron scattering from $KCo_{0.72}Mn_{0.28}F_3$ at wave vector $\mathbf{q}=(0.3,0,0)2\pi/a$ in nuclear (N) and magnetic (M) zones. The total scattering (solid lines) differs appreciably from the host contribution $S_{xx}{}^1(\mathbf{Q},\omega)$ (broken lines) only in nuclear zones.

The interference term $S_{xx}{}^2(\mathbf{Q},\omega)$ depends on the Green's functions $\bar{\mathbf{G}}^D(\mathbf{q},\omega)$ through Eq. (5.26). From Eq. (5.27) we have

$$\text{Im}\,[\mathbf{G}^D(\mathbf{q},\omega)]=c\,\text{Re}\,[\mathbf{L}^D(\mathbf{q},\omega)]\,\text{Im}\,[\mathbf{G}(\mathbf{q},\omega)]+c\,\text{Im}\,[\mathbf{L}^D(\mathbf{q},\omega)]\,\text{Re}\,[\mathbf{G}(\mathbf{q},\omega)].$$

This result shows that there will be one contribution proportional to the Re$[G(\mathbf{q},\omega)]$, which is likely to be asymmetric about the frequency $\omega(\mathbf{q})$ at which the imaginary part is a maximum. This latter term will tend to alter the shape of the scattering and more especially tend to alter the frequency at which the scattering cross-section peaks.

In practice these terms appear to be small as shown in Fig. 11. The contribution to the scattering from a particular wave vector $\mathbf{q}=(0,0,0.3)2\pi/c$ for 5% of zinc impurity in MnF_2 is less than 4% of the total scattering. For wave vector transfers close to a magnetic lattice point the contribution is peaked in a manner very similar to that of $S_{xx}{}^1(\mathbf{Q},\omega)$, but near nuclear lattice points it is much smaller in magnitude and tends

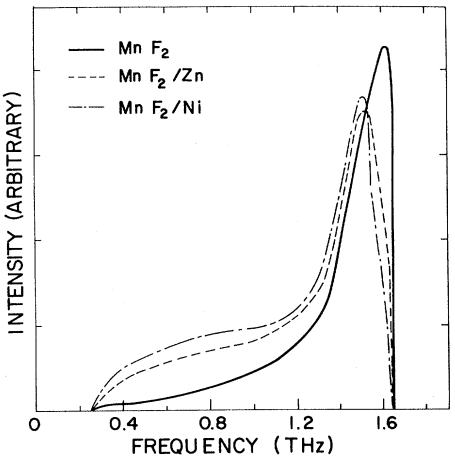

FIG. 13. The defect contribution $S_{xx}^{3}(\mathbf{Q}, \omega)$ to the neutron scattering for Ni^{2+} and Zn^{2+} impurities in MnF_2. Comparison to the density of states curve for the host crystal, Im $[P(dd, \omega)]$, is shown.

to be asymmetric about the peak frequency. In practice however, the effects of these terms on the cross section are negligible. In order to illustrate the effects in more detail Fig. 12 shows S' and the total scattering computed for a crystal of K $Co_{0.72}Mn_{0.28}F_3$. Although the theory is not expected to be valid at these concentrations, the results do show some interesting predictions. Near the magnetic lattice point there is little difference between the total scattering and the contribution $S_{xx}^{1}(\mathbf{Q}, \omega)$. On the other hand, near a nuclear lattice point the total scattering is markedly different from that predicted for scattering near a magnetic lattice point.

The third term in the cross section $S_{xx}^{3}(\mathbf{Q}, \omega)$ is independent of the wave vector $\mathbf{Q}$, and is illustrated in Fig. 13 for both zinc and nickel impurities in MnF_2. If the effect of the defect in the $\mathbf{M}(dk, \omega)$ matrix of Eq. (5.30) is neglected then Im $[G(dd, \omega)]$= Im $[P(dd, \omega)]$; the scattering is independent of the properties of the defect, and represents a density of magnon states of the host crystal. In Fig. 13 we show Im $[P(dd, \omega)]$ as the pure crystal result, and it may be seen that the calculated $S_{xx}^{3}(\mathbf{Q}, \omega)$ are similar in shape but markedly different in detail. The shape of this term in the scattering does therefore depend on the nature of the defect. The magnitude of this term is very small. The calculations for MnF_2 containing zinc impurities predict that the peak in the contribution $S_{xx}^{3}(\mathbf{Q}, \omega)$ is only 0.03% of the height of the peak from the scattering shown by the $S_{xx}^{1}(\mathbf{Q}, \omega)$ curve in Fig. 11.

The expressions for the scattering within the band of host lattice frequencies have shown, for small concentration of defects, that the contributions $S_{xx}^{2}(\mathbf{Q}, \omega)$ and $S_{xx}^{3}(\mathbf{Q}, \omega)$ are in practice small compared with that of $S_{xx}^{1}(\mathbf{Q}, \omega)$. In the case of the scattering from a local mode this is not the cae. A local mode arises when the matrix $\mathbf{M}(ij, \omega)$ is singular at a frequency ω lying outside the band of frequencies of the host spin system. In Fig. 14, we show the qualitative behavior of the eigenvalues of the matrix $M(ij, \omega)$ for Ni defects in a $S=2.5$ perovskite host as a function of ω. The frequencies of the local modes are found by the intercepts of the eigenvalues with the zero line. Near the region of the singularity we assume that the matrix $\mathbf{M}^{-1}(ij, \omega)$ may be written as

$$\mathbf{N}(ij, \omega_L) i\pi\delta(\omega-\omega_L).$$

The matrix $\mathbf{N}(ij, \omega)$ may be found by diagonalizing the matrix $\mathbf{M}(ij, \omega)$ to give eigenvalues $f(\lambda)$ and eigenvectors $\mathbf{e}(\lambda)$. The matrix inverse is then given by

$$\sum_{\lambda}[e_i(\lambda)e_j^{T}(\lambda)/f(\lambda)],$$

where T denotes the transpose operation to a left eigenvalue, since the original matrix $\mathbf{M}$ is not symmetric. If we consider this expression close to the frequency ω_L at which the matrix $\mathbf{M}(ij, \omega)$ is singular, then one or more of the eigenvalues is singular so that $f(\lambda)=\alpha_\lambda(\omega_L-\omega)$. When we permit ω to have a small imaginary part then we have

$$\mathbf{N}(ij, \omega_L)= \sum_{\lambda}'[e_i(\lambda)e_j^{T}(\lambda)/\alpha_\lambda], \qquad (5.30)$$

where the summation is taken over all those modes which are degenerate and singular at $\omega=\omega_L$. The scattering cross section may then be deduced by substituting this expression into the equations for the

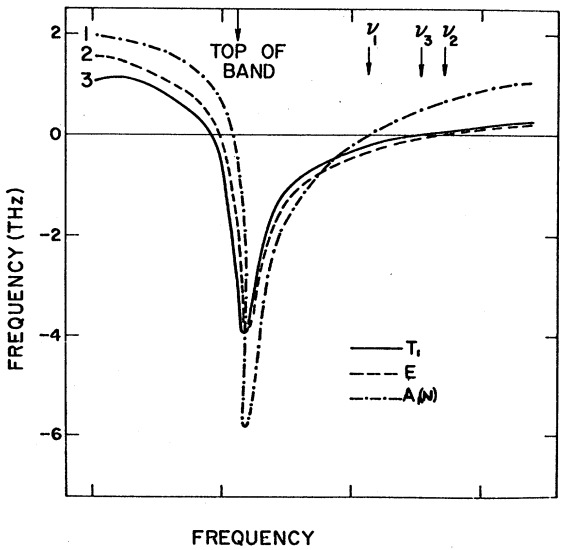

FIG. 14. The eigenvalues $f(\lambda)$ of the defect matrix $M(ij, \omega)$ as a function of frequency for Ni^{2+} in an $S=\frac{5}{2}$ perovskite host (schematic). Strong singularities occur above the band when $\partial f(\lambda)/\partial\omega$ is small and $f(\lambda)$ crosses zero. The $A_1(D)$ mode is not shown as it occurs at a much higher frequency. Numbers 1, 2, 3, give the degeneracies of the modes.

scattering cross section and extracting the parts proportional to $\delta(\omega-\omega_L)$. It is, however, easier to obtain the contributions to $S_{xx}^1(\mathbf{Q},\omega)$ and $S_{xx}^2(\mathbf{Q},\omega)$ directly, by calculating the cross section for a crystal containing a single defect and then multiplying the result by the number of defects. This procedure enables us to use Eq. (5.11) for the Green's function and to write

$$\text{Im}\,[\mathbf{G}(ij,\omega_L)]=\sum_{k_1k_2}\mathbf{P}(ik_1,\omega_L)\pi\mathbf{N}(k_1k_2,\omega_L)\mathbf{P}(k_2j,\omega_L). \tag{5.31}$$

We can then obtain the imaginary part of $\bar{\mathbf{G}}(\mathbf{q},\omega_L)$ by summing over the indices i and j and taking the appropriate Fourier transform, which when averaged over all the defects gives

$$\text{Im}\,[\bar{\mathbf{G}}(\mathbf{q},\omega_L)]=c\pi\mathbf{P}(\mathbf{q},\omega_L)\mathbf{N}(\mathbf{q},\omega_L)\mathbf{P}(-\mathbf{q},\omega_L), \tag{5.32}$$

where

$$\mathbf{N}(\mathbf{q},\omega_L)=\sum_{ij}\mathbf{N}(ij,\omega_L)\exp\{i\mathbf{q}\cdot[\mathbf{R}(i)-\mathbf{R}(j)]\}.$$

The Green's functions required for the interference term are $\mathbf{G}^D(\mathbf{q},\omega_L)$. These can be obtained by taking the index i to be the defect site, summing over all the j sites with appropriate exponentials, and averaging over the different defect configurations to obtain

$$\text{Im}\,[\bar{\mathbf{G}}^D(\mathbf{q},\omega_L)]=c\pi\mathbf{N}^D(\mathbf{q},\omega_L)\mathbf{P}(\mathbf{q},\omega_L), \tag{5.33}$$

where

$$\mathbf{N}^D(\mathbf{q},\omega_L)=\sum_{kj}\mathbf{P}(dk,\omega_L)\mathbf{N}(kj,\omega_L)\times\exp\{i\mathbf{q}\cdot[\mathbf{R}(d)-\mathbf{R}(j)]\}.$$

The third contribution arises from $\bar{\mathbf{G}}^{DD}(\omega)$ and is given by

$$\text{Im}\,[\bar{\mathbf{G}}^{DD}(\omega_L)]=c\pi\sum_k\mathbf{N}(dk,\omega_L)\mathbf{P}(kd,\omega_L). \tag{5.34}$$

When Eqs. (5.32)–(5.34) are substituted into Eqs. (5.24), (5.26), and (5.29), respectively, the total scattering from the localized modes is obtained.

Unlike the case of the scattering at frequencies lying within the band of frequencies of the host crystal, all three contributions are now of comparable size. In Fig. 15 we show the scattering calculated for the local mode produced when Ni impurities are introduced into MnF_2. The curves 1–3 give the three contributions to the scattering at different wave vectors within the magnetic and nuclear Brillouin zones. Contribution 3 is independent of wave vector as expected.

In conclusion it is noted that the scattering depends on $\mathbf{P}(\mathbf{q},\omega_L)$. These terms will be especially large if $\omega_L-\omega(\mathbf{q})$ is small, so that we may expect the scattering to be largest when the local mode and band modes have similar frequencies.

We have suggested that it is permissible to neglect all the scattering except the $S_{xx}^1(\mathbf{Q},\omega)$ contribution

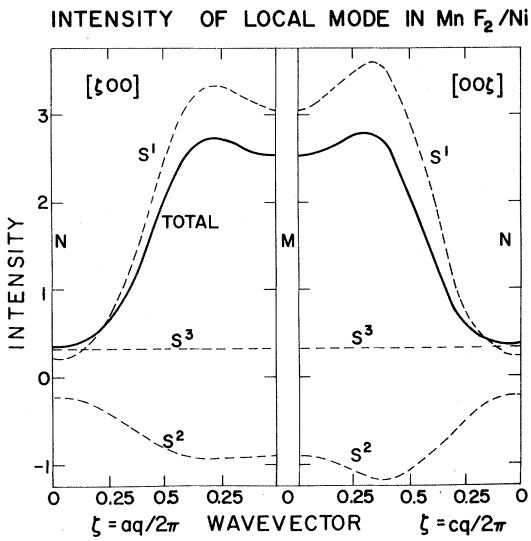

FIG. 15. The intensity of the local mode in MnF_2 containing Ni^{2+} impurities. Results for wave vectors in magnetic (M) and nuclear (N) zones are shown, and the contributions to the scattering are the host scattering, S^1, the host defect interference term, S^2, and the defect scattering, S^3.

within the band of host frequencies but not for the local mode scattering. This approximation might well fail if a resonant mode occurred at a frequency where the density of states of the host lattice is very small. The effect of the S^2 and S^3 contributions to the scattering would then be relatively enhanced at those frequencies.

5. Infrared and Raman Scattering

(a) *The Single Excitations*

The form of the interaction between the incident electromagnetic waves and the spin excitations of a crystal was discussed in Sec. IV. The Green's function theory of the interaction with the single excitations is very similar to that already presented for the neutron scattering. The expression for the susceptibility of the crystal, Eq. (4.4), may be rewritten in terms of the Green's function

$$\chi_{\alpha\beta}(\omega)=(1/Nv)G(M_\alpha M_\beta,\omega), \tag{5.35}$$

where the dipole moment operators are defined in Sec. IV, Eq. (4.3), as

$$M_\alpha=\mu_B\sum_i\sum_\beta g_{\alpha\beta}(i)S_\beta(i),$$

and v is the volume of the unit cell. The "g" factor may be taken as a scalar for all ions other than Co^{2+}, and hence we shall neglect these complexities. Thus the susceptibility may be written in terms of the Green's

functions as

$$\chi_{xx}(\omega)=(\mu_B^2/2Nv)\sum_{ij}S(i)^{1/2}g(i)S(j)^{1/2}g(j)\times\sum_{k=1}^{4}G_k(ij,\omega). \quad (5.36)$$

For a crystal containing defects this may be written in terms of the Green's functions G, G^D, and G^{DD} to give

$$\chi_{xx}(\omega)=(Sg^2/v)\sum_k\tilde{G}_k(\mathbf{0},\omega)+(2Sg\Delta g/v)\sum_k\tilde{G}_k{}^D(\mathbf{0},\omega)+S(\Delta g)^2\sum_k\tilde{G}_k{}^{DD}(\mathbf{0},\omega). \quad (5.37)$$

The g factor of the host crystal is written as g, and for the defect the g factor is $(g+\Delta g)(S/S')^{1/2}$. Similar expressions for the Co^{2+} ion are more complex in form but not in physical content.

The Raman scattering may also be expressed in terms of these Green's functions. The expression for the Raman tensor, Eq. (4.7), for suitable geometry is equivalent to a function $F(PP^+,\omega)$ where the operator P is defined by Eq. (4.6).

The Raman tensor for one magnon scattering then becomes

$$I_{zxzx}(\omega)=-[n(\omega)+1/\pi]N\times\mathrm{Im}\,[S\Gamma^2\sum_k\tilde{G}_k(\mathbf{0},\omega)+2S\Gamma\Delta\Gamma\sum_k\tilde{G}_k{}^D(\mathbf{0},\omega)+S\Delta\Gamma^2\sum_k\tilde{\mathbf{G}}_k{}^{DD}(\mathbf{0},\omega)], \quad (5.38)$$

where Γ is the Raman scattering coupling coefficient for the host and $(\Gamma+\Delta\Gamma)(S/S')^{1/2}$ is the coefficient for the defect.

These results show that the predicted forms of the infrared absorption and of the one-magnon Raman scattering cross section are very similar to those predicted for the neutron scattering. In many cases, however, the two magnon Raman cross section, which has a different form, dominates the spectrum. The optical results are limited in that measurements may only be performed for $Q=0$, but have the advantage of greater resolution and sensitivity.

The main features of the observed spectrum are the band modes with a shift in frequency and increase in width over those of the pure crystal, and an interference term which modulates the scattering particularly in the neighborhood of the band modes. This modulation depends on the ratios of $\Delta g/g$, $\Delta\Gamma/\Gamma$, and $\Delta b/b$ for the different experiments. The detailed shapes of the susceptibility or cross sections will therefore be different. All three cross sections may show localized modes, but for certain symmetries of localized modes the cross sections are zero for the optical experiments. At frequencies well away from the frequencies of band or localized modes, the cross section is dominated by the $G^{DD}(0,\omega)$. No measurements of this type of scattering have as yet been reported.

(b) *Two-Excitation Processes*

In Sec. IV on the experimental techniques, it was shown that optical measurements provide information about the energy needed to excite pairs of excitations. The electromagnetic field then couples with pairs of spin deviation operators on neighboring sites. In principle the contributions to the susceptibility or Raman scattering from these processes may be calculated by use of the Green's-function techniques. The results depend not on the Green's functions already obtained such as $G(S_+(i)S_-(j),\omega)$ but on Green's functions of the form $G(S_+(i)S_-(i'),S_+(j)S_-(j'),\omega)$, where i and i' and j and j' are neighboring sites. Although in principle the technique that may be used to calculate these Green's functions is similar to that described for the simpler ones obtained above, in practice it is by no means so easy. Difficulties arise in the choice of a decoupling scheme for the higher order Green's functions which arise in the equations of motion, and no attempt to solve this difficulty has been reported.

Thorpe (1969, 1970) has used a very convenient approximate way to calculate these Green's functions. Initially he notes that the pair modes of most importance experimentally are those consisting of an excitation which is very much localized on the defect together with an excitation which is almost entirely localized on the neighbors of the defect. His calculation of the pair Green's function then proceeds by assuming that the excitation localized on the defect has a frequency ω_D and is entirely localized at the defect site. He then calculates the Green's function $G(S_+(i)S_-(j),\omega)$ assuming that the aforementioned localized excitation is already present in the crystal. In other words he then uses the same techniques for calculating the Green's function as already described except that in the decoupling procedure $\langle S_z(i)\rangle$ is written as S when i is a host atom but as $S'-1$ when i is a defect. The only difference in the equations for the Green's function then arises in the matrix $\mathbf{C}$, Eq. (5.9), where the elements $C_1(jj)$ become

$$C_1(jj)=\pm(S'-1)I'(0j)\pm SI(0j)\quad\text{with upper, lower signs for } j=A,L. \quad (5.39)$$

The frequency transfer in the experiment Ω is then given by $\Omega=\omega+\omega_D$.

Since, within the low-concentration approximation, there is no interference between the defects, the infrared absorption or the Raman scattering from the pair modes is proportional to

$$c\sum_{ij}\Gamma_{Di}\Gamma_{Dj}\,\mathrm{Im}\,\mathbf{G}(ij,\Omega-\omega_D),$$

where the coefficients Γ_{Di}, Γ_{Dj} are the infrared, Eq. (4.5), or Raman scattering, Eq. (4.8), coefficients describing the matrix elements between the defect and its near neighbors i and j. These expressions were evaluated by Thorpe for Ni^{2+} ions in both $KMnF_3$, and

also in MnF_2. The results are shown in Figs. 16 and 17. In Fig. 16 is also shown the difference between the results calculated by Thorpe's modified decoupling scheme and by neglecting the interaction between the excitations.

VI. COMPARISON BETWEEN EXPERIMENT AND THEORY

In this section we are concerned with collecting the available experimental and theoretical work on the various different defect systems. We shall restrict attention to systems containing only a small concentration of defects and to results obtained at low temperatures. Of particular interest is a comparison of the experimental results with the various different theoretical predictions when both are available.

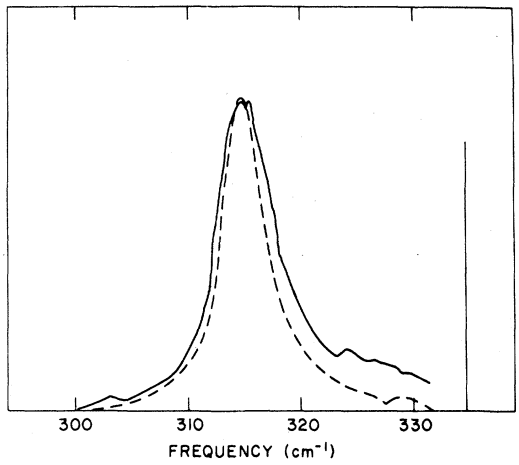

FIG. 16. Raman scattering in Ni:$KMnF_3$ from the $A_1(D)+E$ pair mode. In the absence of interactions the δ-function shown at the sum of the $A_1(D)$ and E mode frequencies is expected. The theory of Thorpe (1970) (broken lines) is compared with unpublished results of Moch *et al.* referred to by Thorpe.

1. $KMnF_3$:Ni

Experimentally this system has been studied by fluorescence measurements (Johnson *et al.*, 1966), by Raman scattering, (Parisot *et al.*, 1971), and by neutron scattering (Holden *et al.*, 1971a). In the fluorescence measurements, Fig. 18, the frequency of the $A_{1g}(D)$ mode and also the frequency of the pair mode $A_{1g}(D)+A_{1g}(D)$ were obtained. The other peaks occurring in the spectrum were assigned as host magnons or phonons from measurements at different temperatures, and from polarization and absorption spectroscopy. The frequency of the pair mode is greater than the sum of the two $A_{1g}(D)$ modes by 0.36 THz. The Raman scattering measurements of Parisot *et al.* (1971) give the frequencies of the $A_{1g}(D)+E_g$ pair modes as shown in Fig. 16.

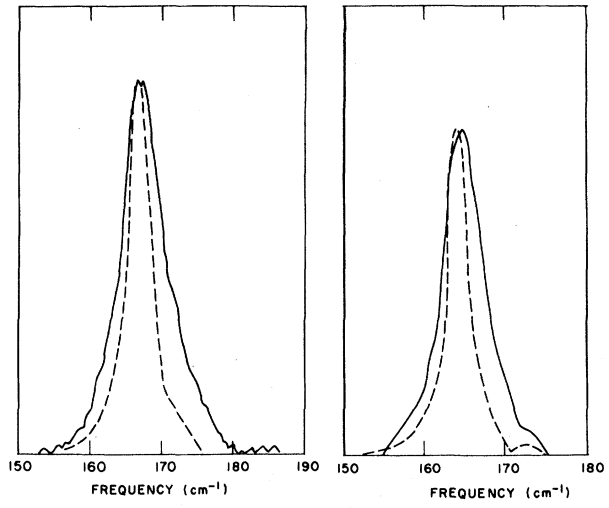

FIG. 17. Raman scattering in Ni:MnF_2 from the $A_{1g}(D)+E_g$ modes (left part), and the $A_{1g}(D)+B_{2g}$ mode (right part). The theory of Thorpe (broken lines) is compared with the Raman results of Moch *et al.* (1968).

The neutron scattering measurements gave the frequency of the $A_{1g}(D)$ mode and approximate values for the $A_{1g}(N)$, E_g, and T_{1u} modes. Unfortunately in the experiment it was not possible to identify these individual modes. In addition the frequencies of the band modes were measured as shown in Fig. 19. The results are collected in Table 3.

Theoretical calculations of Ni^{2+} impurities in $KMnF_3$ were first performed by Misetich and Dietz (1966) who found that a cluster model explained the behavior of the $A_{1g}(D)+A_{1g}(D)$ mode. Cluster models have been further used by Thorpe (1970), whose model is identical

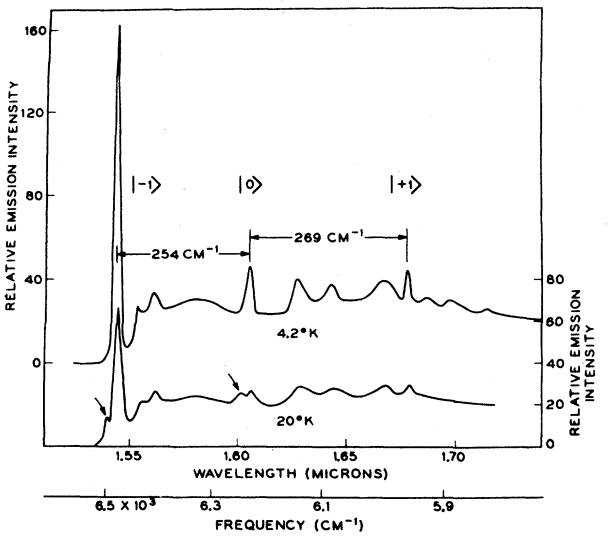

FIG. 18. Fluorescence emission from Ni^{2+} (0.01%) in $KMnF_3$ (Johnson *et al.*, 1966).

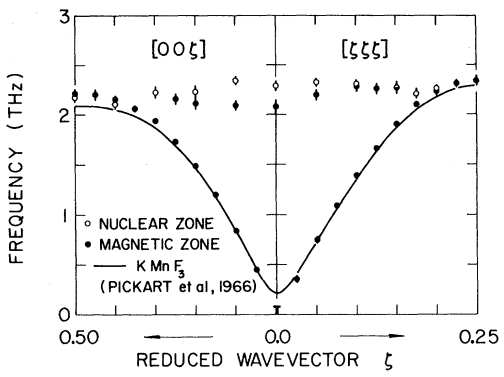

FIG. 19. Band modes and shell modes in $KMn_{0.97}Ni_{0.03}F_3$ measured by neutron scattering (Holden *et al.*, 1971a). In the experiment the local modes occurring near the top of the band were not resolved.

to ours and by Parisot *et al.* (1971a) who took clusters that are somewhat larger and who took account of both nearest and next-nearest neighbor exhange. Thorpe (1970) and Holden *et al.* (1971) have used the Green's function technique (Table 3). In all of the calculations I' was found by fitting the theory to the observed $A_1(D)$ mode, and then that value of I' used to predict the other frequencies. All of the calculations predict that the frequency of the E_g, T_{1u}, and $A_{1g}(N)$ modes lie immediately above the top of the band of pure $KMnF_3$, 2.28 THz. They therefore give rise to three localized modes which are presumably the origin of the band observed in the neutron scattering experiment with a frequency of 2.17±0.15 THz. The frequency of this band appears to be slightly less than predicted by the theories.

The effect of finite concentration (3%), on the other hand, should be to raise the shell mode frequencies since $I'S > IS$. Nonetheless, when the possible effects of interaction between the shell modes at 3% concentration are considered, it is possible for a frequency of 2.17 THz to be observed at the zone center and a frequency higher than 2.28 THz to exist at the zone boundary where the shell modes and the host band modes are not resolved. Interaction will be most important in systems such as the present one where the frequencies of the localized shell modes lie so close to the band that they may be expected to spread out over many Mn^{2+} ions around each Ni^{2+} ion.

As explained in the previous section, Thorpe (1970) has calculated the frequencies of the pair modes. When an $A_1(D)$ localized mode is present on the defect the frequency of the other localized modes is reduced to below the top of the $KMnF_3$ band. The Raman scattering from the $A_{1g}(D)+E_g$ pair mode then has a finite width which cannot be accounted for by the Ising and cluster models. Figure 16 shows that Thorpe's calculations account for the width very satisfactorily. The frequencies of the pair modes are also accounted for by the cluster models of Parisot *et al.* (1971).

Green's function calculations have also been performed of the shift and width of the band modes for a 3% nickel sample. The results which are shown in Fig. 20 predict very small shifts and widths which are qualitatively in accord with experiment. Quantitatively the comparison shown in Fig. 20 suggests that the experimentally observed frequencies of the band modes are larger than the theoretical prediction. It should, however, be noted that the neutron groups of the modes with ζ greater than 0.3, 0.2, and 0.15 in the [100], [110], and [111] directions, respectively, contain scattering from the localized modes above the band and hence the center frequency of the groups will not give a reliable estimate of the frequencies of the band modes. No experimental shift is shown for $\zeta=0$ because of the difficulty of measuring a zone center mode of very low frequency.

The intensity of the neutron scattering from the four localized modes is shown in Fig. 21. A comparison of the calculated intensities with those of Fig. 5 for the cluster model shows considerable differences. These differences are largest for the modes of the neighbors and arise largely because these modes spread out to large distances around each defect. Unfortunately the frequency resolution in the neutron experiment is inadequate to separate the intensity from the different localized shell modes, or to separate the intensity of the shell modes near the zone boundaries from that arising from the band modes. It is therefore not possible to make a detailed comparison of theory and experiment at present.

In conclusion, those experimental results that are available for $KMnF_3$/Ni are in accord with the theory. The value of the Mn–Ni exchange parameter differs in the different theoretical treaments by a small amount but in all cases is quite close to the square root of the product of exchange parameters of $KMnF_3$ and $KNiF_3$, 0.566 THz.

TABLE 3. The frequencies (THz) of the modes in $KMnF_3$:Ni obtained from experiment and from calculations on different models.

	$KMnF_3$:Ni			
Mode	Observed	Ising	Cluster	Green's function
$A_{1g}(D)$	7.68±0.01[a]	7.68	7.68	7.68
E_g	2.17±0.15[b]	2.41	2.42	2.37
T_{1u}	2.17±0.15[b]	2.41	2.42	2.36
$A_{1g}(N)$	2.17±0.15[b]	2.41	2.37	2.33
$[A_{1g}(D)+A_{1g}(D)]_{\text{pair}}-2A_{1g}(D)$	0.35±0.02[a]	0.0	0.40	0.42
$A_{1g}(D)+E_g$	9.50[c]	9.58	9.58	9.51
$I'(1)$		0.512	0.513	0.53

[a] Johnson *et al.* (1966).
[b] Holden *et al.* (1971a).
[c] Parisot *et al.* (1971).

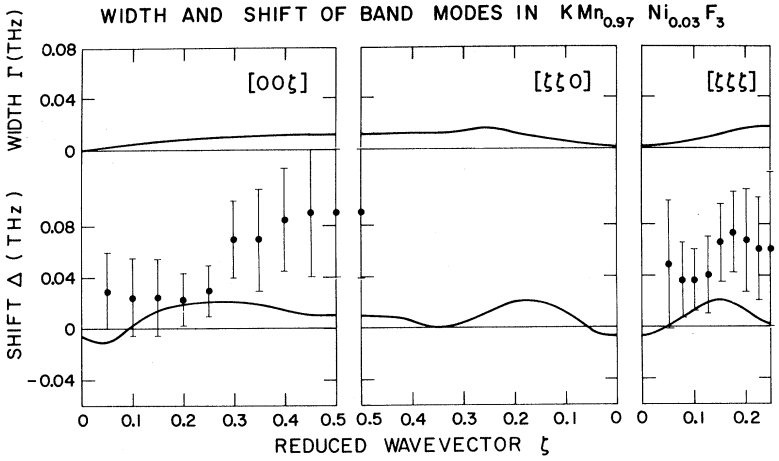

FIG. 20. The width and shift of band modes in $KMn_{0.97}Ni_{0.03}F_3$ as calculated from Green's function theory (solid lines), and as measured by neutron scattering (full circles) (Holden *et al.*, 1971a).

Measurements have been made in the similar system $RbMnF_3$:Ni by Johnson *et al.* (1966) and by Parisot *et al.* (1971). In the latter Raman experiment, the single E mode was not observed although Oseroff *et al.* (1969) claim to have observed this mode at 2.19 THz with different crystals. The results are very similar to the $KMnF_3$ system and the calculations by Parkinson (1969) and Thorpe (1970) are in good agreement with experiment. We shall not therefore discuss these results in detail.

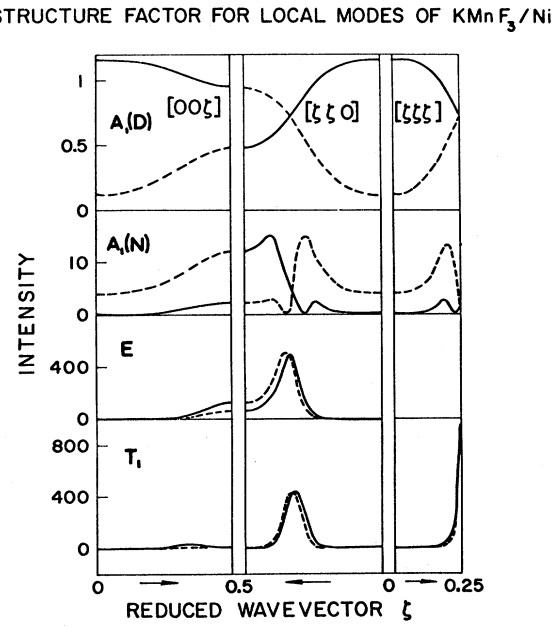

FIG. 21. The structure factor for local modes in Ni:$KMnF_3$ in magnetic (solid lines) and nuclear (broken lines) zones. Note that of the modes that are close to the band, the intensity is largest for modes that are entirely on the neighbors.

2. $KMnF_3$:Fe

No measurements or calculations on this system have as yet been made.

3. $KMnF_3$:Co

This system has been studied with neutron scattering techniques by Svensson *et al.* (1969a). The results showed a localized mode with a frequency of 6.55±0.15 THz, and band modes which were very similar to those of pure $KMnF_3$ as shown in Fig. 22. The latter result was particularly surprising in view of the large concentration, 20%, of cobalt ions present in the specimen.

The interpretation of the results in this system is complicated by the need to allow for the mixing of the cobalt levels by the exchange fields of the surrounding ions. The mixing of the levels has been calculated by the same techniques as those applied to $KCoF_3$ (Buyers *et al.*, 1971), with the molecular field chosen to be that appropriate for Co ions in $KMnF_3$. The results are that the ground state g and first excited state e have the matrix elements:

$$\langle g \mid S_z \mid g\rangle = 1.187, \qquad \langle e \mid S_z \mid e\rangle = -0.24,$$

and

$$\langle e \mid S_- \mid g\rangle = 1.72.$$

It is then straightforward to extend the Ising model to allow for these matrix elements. When this is done it is found that the localized mode $A_1(D)$ gives a nearest-neighbor exchange interaction I' of 0.306±0.020 THz. The large error results primarily from the uncertainties in the matrix elements. The model predicts the frequencies of the other defect modes to be

$$\omega(A_{1g}) = \omega(T_1) = \omega(E) = 2.26 \text{ THz},$$

which is below the top of the $KMnF_3$ band. They do not therefore give rise to additional localized modes as were found in the Ni case, nor were any observed in the experiment.

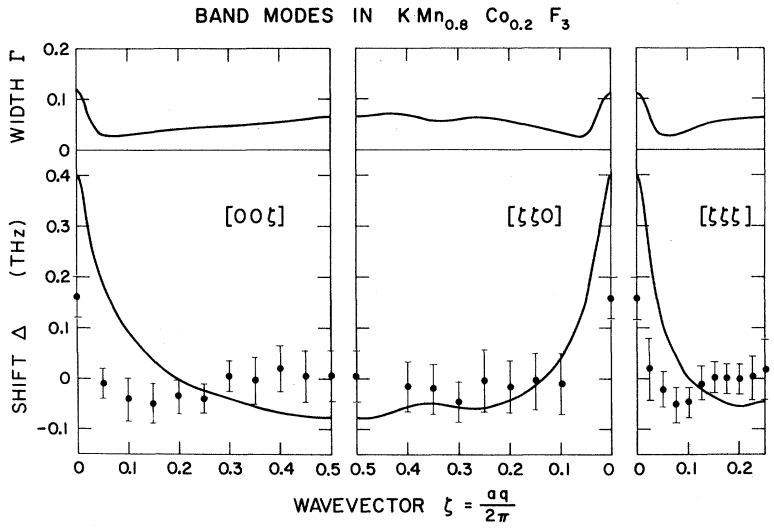

FIG. 22. Shift and width of band modes in $KMn_{0.8}Co_{0.2}F_3$ calculated from Green's function theory (lines) and the experimentally observed shift (Svensson *et al.*, 1969a) all circles).

In order to perform cluster model or Green's function calculations, a form must be assumed for the transverse part of the exchange interaction. Although there is no theoretical justification for a Heisenberg form, neutron measurements of the magnons in $KCoF_3$ (Holden *et al.*, 1971b) are consistent with Heisenberg exchange and we have used it in the calculations. The results of a cluster model calculation are not then significantly different from those of the Ising model except that they do predict the dependence on momentum transfer **Q** of the intensity of the scattering from the localized mode. This is shown in Fig. 23 and corresponds to a probability amplitude for spreading (III.3) of 5% compared with the 8% probability observed.

As usual, the Green's function calculation was performed by fitting the exchange constant to the local mode frequency found by Svensson *et al.* (1969a). This exchange constant was within error the same as that obtained by the Ising model, while the frequencies of the other zeros of the M matrix were very similar to those of the cluster model. The change in the frequency of the band modes was calculated and is shown in Fig. 22. The theory agrees with experiment, in that the changes are very small even for a 20% concentration but they are larger than the experiment near the zone center. The intensity of the scattering from the localized modes was also calculated and is compared in Fig. 23 with that obtained experimentally. The agreement between experiment and both the Green's function and cluster model theories are very satisfactory. This suggests that the assumed Heisenberg form for the exchange interactions is a reasonably good approximation, even though theory suggests that the interaction to be of a more complicated form. Better experimental results may show that a more complicated form is needed.

The square root of the product of the exchange constants for $KCoF_3$ and $KMnF_3$ is 0.31 THz which is only 10% larger than that obtained for the exchange between cobalt and manganese ions.

$RbMnF_3$:Co has been studied by Raman scattering techniques (Moch *et al.*, 1971). They observed a peak at 7.68 THz which they assigned to the $A_{1g}(D)+E_g$ pair mode. Using this assignment they found that $I'(1)$ was approximately the product of the pure $RbMnF_3$ and $RbCoF_3$ exchange constants.

4. $KMnF_3$:Zn

In this system, the zinc forms a vacancy in the magnetic lattice so that there are no adjustable parameters in any calculation. Unfortunately no experiments

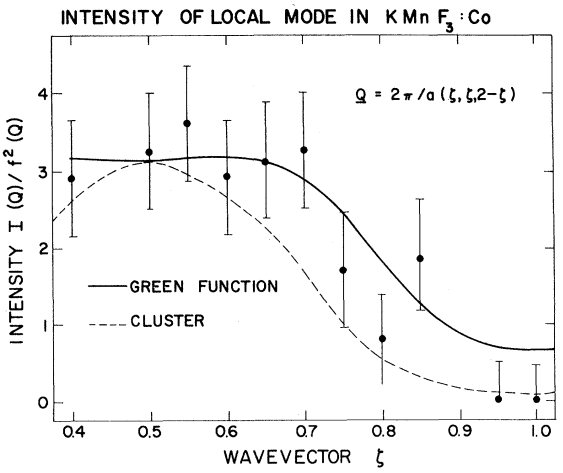

FIG. 23. Intensity of the local $A_1(D)$ mode in $KMn_{0.8}Co_{0.2}F_3$. The experimental results of Svensson *et al.* (1969a) (full circles) are compared with the two theoretical calculations described in the text. The wave vector transfer is **Q**, and the atomic form factor of the magnetic electrons is $f(\mathbf{Q})$.

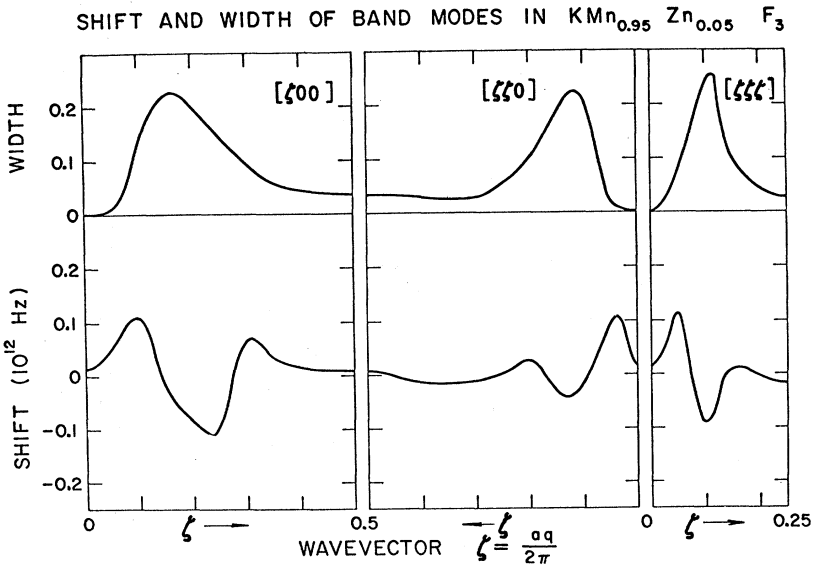

FIG. 24. Width and shift in units THz of the band modes in $KMn_{0.95}Zn_{0.05}F_3$ from Green's function theory.

have as yet been performed on this system. Calculations have however been made using Green's function techniques. No localized modes are predicted but a marked shift and width is predicted for the band modes as shown in Fig. 24 for a crystal containing 5% of Zn. The large width and the anomalous shifts occur when the band modes have frequencies equal to zeros of the M matrix, Eq. (5.13), which correspond to a frequency of about 1.4 THz. An Ising model gives a frequency of 1.9 THz for these modes showing a surprisingly large change in the frequency between the results of an Ising model and the better Green's function calculations.

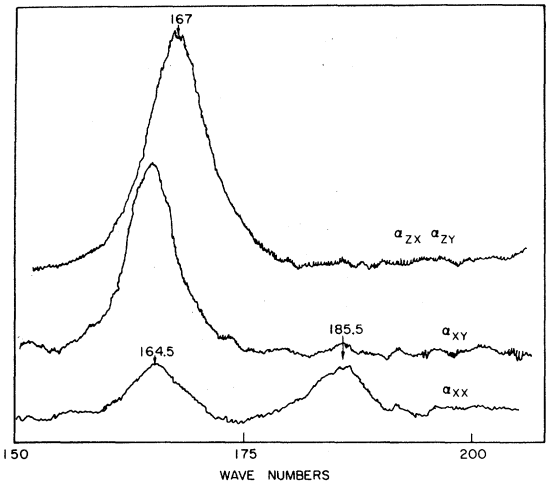

FIG. 25. Raman scattering observed in 1–2% Ni-doped MnF_2 by Moch *et al.* (1968). The line near 167 cm^{-1} is associated with the pair mode $A_{1g}(D)+E_g$, and the 164.5 cm^{-1} line with $A_{1g}(D)+B_{2g}$. The weak scattering at 185.5 cm^{-1} is not understood.

5. MnF_2:Ni

The experiments and the theoretical calculations for the rutile structure matrials are more complex because of the lower symmetry and also because there are two exchange interactions of importance in the pure crystal. Experiments have been performed on Ni impurities in MnF_2 with fluorescence techniques (Johnson *et al.*, 1966), with infrared absorption (Dietz *et al.*, 1970), and with Raman scattering techniques (Moch *et al.*, 1968; Oseroff and Pershan, 1968). The Raman results are shown in Figs. 25 and 26 and the small differences are likely due to different concentrations. The frequencies are listed in Table 4. Fluorescence gives the frequencies of the $A_{1g}(D)$ mode and the $A_{1g}(D)+A_{1g}(D)$ pair mode, Raman scattering gives the frequencies and widths of the pair modes $A_{1g}(D)+E_g$, $A_{1g}(D)+B_{2g}$, and infrared absorption gives the frequency of the $A_{1g}(D)+B_{1u}$ mode. The g values have also been obtained for some of these modes (Dietz *et al.*, 1970).

The theory of Ni in MnF_2 must take account of the change in anisotropy at the impurity. This was discussed in Sec. II and was taken in the calculations to be of the form

$$0.12(S_z'(0)^2-1).$$

In the Ising model calculations of Table 4 we have then used the measured frequency of the $A_{1g}(D)$ mode to calculate exchange constant, I_2', between the nickel and manganese ions assuming that I_1' is zero. The results are in quite good agreement with the experiment. The exchange constant deduced from the product of the square root of the exchange constants in MnF_2 and NiF_2 is 0.176 which is only 5% different from that given by the Ising model. The frequency of the neighbors ω_{N2} on this model is 1.57 THz which is below the top of the band in pure MnF_2 at 1.64 THz.

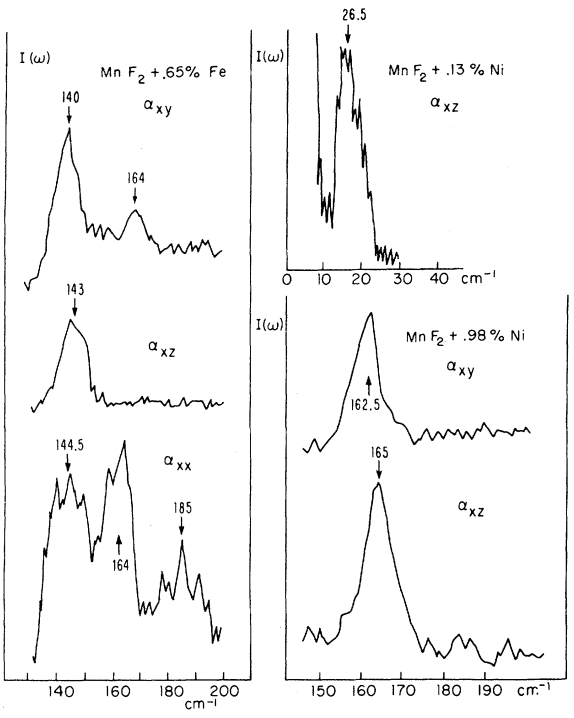

FIG. 26. Raman scattering in Fe: MnF_2 and Ni: MnF_2 measured by Oseroff and Pershan (1968). The orgin of the lines at 185 cm^{-1}, 164 cm^{-1}, and 26.5 cm^{-1} lines is not understood, while the remaining lines are the pair modes $A_{1g}(D)+B_{2g}$ for α_{xy} and $A_{1g}(D)+E_g$ for α_{xz}.

A cluster model was used by Dietz *et al.* (1970). The cluster was larger than that described in Sec. III, taking explicit account of third neighbors of the defects: these results are given in Table 4. They performed a least-squares fit to the experimental data to find the two exchange parameters I_1' and I_2'. Surprisingly, I_1' was quite large and antiferromagnetic. In view of the success of the Ising model with I_1' zero and the approximations inherent in a cluster model, it is by no means certain that this result is physically significant. Somewhat similar results have also been obtained from NMR results as discussed in Sec. VII.

Green's function calculations on the MnF_2/Ni system have been performed by Thorpe (1970) and by Shiles and Hone (1970). Thorpe calculated the frequencies of the pair modes by means of a calculation which depended on the exchange constants only through $\omega(D)$. His results are shown in Fig. 17, and they show both there and in Table 4 good agreement with the experimental results of Dietz *et al.* (1970). Shiles and Hone (1970) have calculated the frequencies of the zeros of the M matrix for a range of parameters of I_1' and I_2'. Unfortunately, since they only have $\omega(D)$ with which to compare their results, I_1' and I_2' cannot be determined independently. We have listed the appropriate value of I_2' assuming I_1' to be zero. Using this value of the parameter, calculations have been performed of the frequencies and widths of the band modes in MnF_2 containing Ni impurities, Fig. 10, and also of the intensity of the scattering from the local mode as a function of wave vector transfer, Fig. 15.

6. MnF_2:Fe

This system has been studied by infrared techniques by Weber (1968) and by Johnson and Weber (1971) to obtain the frequencies of the mode localized on the defect, $A_{1g}(D)$, and also of the $A_{1g}(D)+B_{1u}$ pair mode. The Raman scattering results of Oseroff and Pershan (1968) shown in Fig. 26 gave the frequencies of the $A_{1g}(D)+E_g$ and $A_{1g}(D)+B_{2g}$ pair modes. The results are listed in Table 5 where they are compared with the predictions of the Ising model. The anisotropy of the Fe^{2+} ion was taken as $0.21S_z'(0)^2$ as described in Sec. III. The parameter, I_2', was obtained from the frequency of the $A_{1g}(D)$ mode and used to compute the pair frequencies. The frequency of the modes on the neighbors ω_{N2} is 1.61 THz which, since it is below the top of the MnF_2 band, shows that these modes do not give rise to additional localized modes. The exchange constant obtained in this way is 20% larger than that obtained from the square root of the product of exchange constants for pure MnF_2 and FeF_2.

Unfortunately there has not been much further theoretical work on this system. Thorpe (1970) has calculated the pair spectrum but does not exhibit the results because they are very sensitive to the choice of parameters. Johnson and Weber (1971) suggest that to fit their results exactly a large value of J_1' is required but they also caution that this result is very sensitive to the model and may result from a deficiency in the model calculation. Shiles and Hone (1970) have calculated the single mode frequencies for various values of both I_2' and I_1', but were not able to obtain the values of the exchange constants appropriate to this system.

TABLE 4. The frequencies and exchange constants for MnF_2:Ni as observed experimentally and calculated theoretically. The units are THz.

	MnF_2:Ni			
	Experimental	Ising	Cluster	Green's function
$A_{1g}(D)$	3.61[a]	3.61	3.61	3.61
$A_{1g}(D)+A_{1g}(D)$[b]	0.40[a]	0.12	0.40	
$A_{1g}(D)+E_g$	5.01[c]	5.00	5.00	5.00
$A_{1g}(D)+B_{2g}$	4.94[c]	5.00	4.94	4.93
$A_{1g}(D)+B_{1u}$	5.03[c]	5.00	5.03	5.02
I_1'		0	0.066	0
I_2'		0.185	0.204	0.198

[a] Johnson *et al.* (1966).
[b] The number given is the reduction in frequency of the pair mode by interaction.
[c] Dietz *et al.* (1970).

7. MnF_2:Co

This system has been studied by both optical and neutron scattering techniques. Infrared absorption measurements of the frequency of the mode $A_{1g}(D)$ localized mainly on the defect gave 3.72 THz (Weber, 1969). Raman scattering measurements (Parisot *et al.*, 1970) yielded a similar frequency. Both these experiments were performed with specimens containing about 1% of impurity. Neutron scattering measurements were performed (Buyers *et al.*, 1968) on a specimen containing 5% impurity and gave a somewhat lower frequency 3.57 ± 0.05 THz. This possibly shows a concentration dependence of the frequency. We prefer the optical results as representing the more accurate low concentration frequency as shown in Table 6.

The frequencies of pair modes were obtained by infrared techniques, $A_{1g}(D)+B_{1u}$, (Johnson and Weber, 1971), and also by Raman scattering techniques $A_{1g}(D)+B_{2g}$ and $A_{1g}(D)+E_g$ (Parisot *et al.*, 1970). The results are given in Table 6. The neutron scattering results also yielded measurements of the shift in frequencies of the band modes as shown in Fig. 27 and the variation in the intensity of the scattering from the local mode with wave vector transfer as shown in Fig. 28.

TABLE 5. As for Table 4 but for MnF_2:Fe.

	MnF_2:Fe	
	Experimental	Ising
$A_{1g}(D)$	2.84[a]	2.84
$A_{1g}(D)+E_g$	4.29[b]	4.23
$A_{1g}(D)+B_{2g}$	4.20[b]	4.23
$A_{1g}(D)+B_{1u}$	4.35[c]	4.23
I_2'		0.111

[a] Weber (1968).
[b] Oseroff and Pershan (1969).
[c] Johnson and Weber (1971).

Theoretical calculations for the Co^{2+} ion in the rutile structure are difficult because of the uncertainties in the wavefunctions of the Co ions. In Sec. II we discussed this difficulty and also pointed out that in practice the wavefunctions are further complicated by the mixing of the ground-state doublet and higher excited states by the molecular field acting on the ions. We have obtained the wavefunctions of the lowest two levels of a Co ion in the rutile structure for the molecular field appropriate to a Co ion in MnF_2. This has been done for two different sets of the crystal field parameters, those deduced by Gladney (1966) and those deduced by Martel, Cowley, Buyers, and Stevenson (private communication). The relevant matrix elements between the ground state and the first excited state are listed in Table 7.

TABLE 6. As for Table 4 but for MnF_2: Co. The last two columns are the Ising model using two descriptions of the Co^{2+} wavefunction.

	MnF_2: Co		
	Experimental	Gladney (1966)	Martel *et al.*[a]
$A_{1g}(D)$	3.72[b]	3.72	3.72
$A_{1g}(D)+E_g$	5.08[c]	5.06	5.08
$A_{1g}(D)+B_{2g}$	5.02[c]	5.06	5.08
$A_{1g}(D)+B_{1u}$	5.10[d]	5.06	5.08
I_2'		0.104	0.100

[a] Martel, Cowley, Buyers, and Stevenson (private communication).
[b] Weber (1969).
[c] Parisot *et al.* (1970).
[d] Johnson and Weber (1971).

A substantial part of the difference between the energies of the ground and excited states arises because of the anisotropy introduced into the ground state doublet by the mixing of the higher excited states with the exchange field.

Using these values of the parameters, the exchange constant, I_2', can be deduced from the frequency of the $A_{1g}(D)$ mode. The results are shown in Table 6. The square root of the product of the exchange constants of MnF_2 and CoF_2 (Table 2) is 0.093 or about 10% less than the values in Table 6. The Ising model can also be used to calculate the frequencies of the pair modes, Table 6, which are in satisfactory agreement with the measured results. The mode associated with the neighbors ω_{N2} has a frequency in this model of 1.54 THz, within the band of pure MnF_2. The difficulties

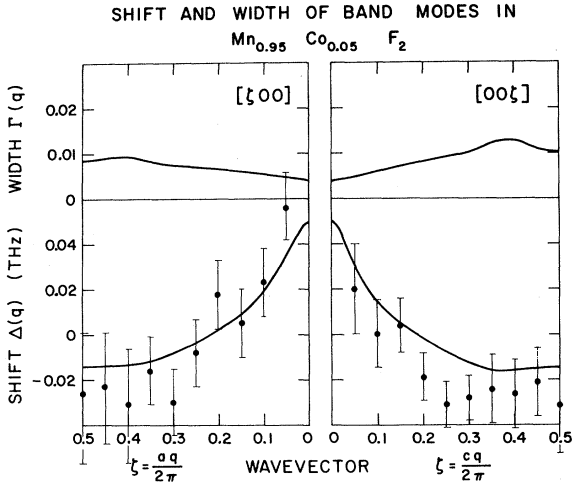

FIG. 27. Width and shift of the band modes in $Mn_{0.95}Co_{0.05}F_2$. The experimental shifts (full circles) are derived from the work of Buyers *et al.* (1968) and are compared with the theoretical calculations desdribed in the text (lines).

TABLE 7. The parameters of the ground state g and first excited state e for Co in the molecular field of MnF_2.

	Gladney (1966)	Martel *et al.*[a]
$\langle g \mid S_z \mid g \rangle$	1.34	1.30
$\langle e \mid S_z \mid e \rangle$	−0.04	+0.054
$\langle e \mid S_- \mid g \rangle$	1.61	1.66
$\langle e \mid S_+ \mid g \rangle$	−0.33	0.45
$\langle e \mid S_- + \frac{1}{2}L_- \mid g \rangle$	1.92	2.01
$\langle e \mid S_+ + \frac{1}{2}L_+ \mid g \rangle$	−0.64	−0.80
$E_e - E_g$	3.72	3.72

[a] Martel, Cowley, Buyers, and Stevenson (private communication).

arise from the presence of the nonzero matrix elements such as $\langle e \mid S_+ \mid g \rangle$, Table 7. This necessitates an extension to the cluster models described in Sec. III and also to the Green's function theories of Sec. V. In Fig. 28 we show calculations of the intensity of the localized mode as a function of wave vector transfer calculated with the cluster model which can be modified in a straightforward manner.

The modifications required to the Green's function formalism are more severe. The Green's functions G_1 and G_4 are now no longer zero if i and j belong to different sublattices. The matrix C, Eq. (5.9), has terms of the form $C_1(0j)$, when $j=A$. Despite these complications, the averaged Green's functions $\bar{G}_1$ and $\bar{G}_4$, Eq. (5.16), are still zero when i and j belong to different sublattices. This arises because terms from different sublattices cancel when the defect is permitted to be on either the up or down sublattice. Unfortunately the additional terms may not be neglected in calculating the parts of $\bar{G}_1$ and $\bar{G}_4$ that come from i and j on the same sublattice. Calculations have been made of the variation in the scattered neutron intensity from the localized mode, Fig. 28, and also of the shift and width of the band modes, Fig. 27. The theory is in very good agreement with the experimentally observed shift. The local mode structure factor shows the maximum at nonzero wave vector predicted by the theory. No Green's function calculations have been reported for the shape of the pair modes. The good agreement between theory and experiment shows that the use of a Heisenberg exchange interaction is surprisingly adequate to describe the results.

Parisot *et al.* (1970) have used a somewhat different description for the Co^{2+} ion in their cluster calculations. Their work is based on the model of Lines (1965). He uses an effective spin, $S=\frac{3}{2}$, model to describe the lowest four states of CoF_2. He then finds that they may be described by an effective spin Hamiltonian of the form

$$H=\gamma(S_x^2-S_y^2)+\delta S_z^2.$$

This approach has the defect that mixing can only be taken into account between the ground state and first excited state. The exchange parameter they deduce is then related to the effective spin and cannot be strictly compared with our results. They state that they are able to obtain agreement with the frequencies of the pair modes with the aid of this Hamiltonian and a cluster model.

8. MnF_2:Zn

This system has been studied by Misetich *et al.* (1968) using fluorescence measurements, and by Svensson *et al.* (1969b) using neutron scattering techniques. The former measurements gave a frequency of 1.3 THz, which was associated with the frequency of modes associated with Mn ions which were neighbors of a Zn defect. The latter were detailed measurements of the change in frequency and change in width of the neutron groups from MnF_2. The results shown in Fig. 29, exhibit a characteristic resonant form, a marked change in shift and increase in width, when the modes have a frequency of approximately 1.3 THz, which occurs for a reduced wave vector ζ equal to 0.35.

Theoretical calculations on this system are particularly attractive because the Zn ion is nonmagnetic and so does not interact with the Mn ions. There are then no unknown parameters. The Ising model predicts a frequency for the Mn neighbors of the Zn ions, $\omega_{N2}=1.39$ THz, which is somewhat larger than the frequency from either the fluorescence measurements or the resonance in the neutron scattering measurements.

Detailed Green's function calculations have been performed to compare with the results shown in Fig. 29. The calculations were performed as described in

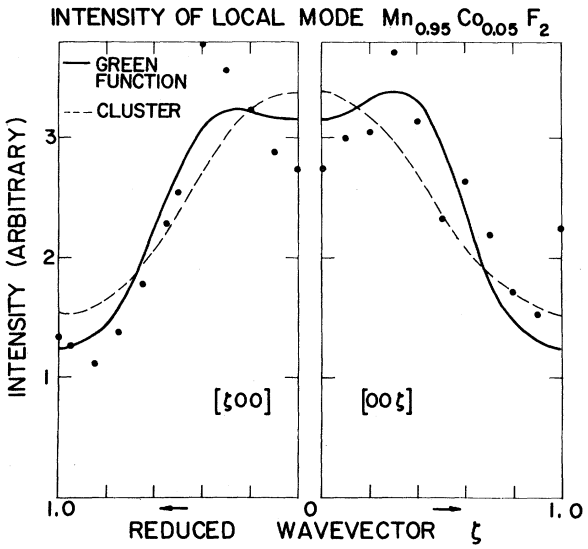

FIG. 28. Structure factor of the local mode in $Mn_{0.95}Co_{0.05}F_2$. The intensity of neutron scattering result observed by Buyers *et al.* (1968) has been divided by the form factor squared and the factor $(1+Q_z^2/Q^2)$ to obtain the experimental structure factor (points) for comparison with the theoretical lines. The experimental accuracy is approximately ±10%.

Sec. V. It was found to be necessary to be extremely careful about the treatment of the zinc ion to ensure that there was identically zero interaction with the lattice. The slightest amount of interaction introduced by errors in the numerical calculations (the P's) or in the treatment of the defect (neglect of I_1 or anisotropy) leads to a localized mode below the band which totally invalidates the calculations. The experimental resolution was folded with the results before comparing experiment and theory. In Fig. 29 we show the calculated form of the width and shift for the 5% specimen used in the experiments. The agreement is very satisfactory. Errors arising from the nonLorentzian form of the calculated curve as discussed in Sec. V have been avoided by convoluting the full line shape with the experimental resolution. The results for the line shape itself are shown for two groups in Fig. 30 and compared with the experimental results. The agreement with the Green's function theory is most satisfactory.

9. Other Magnetic Fluoride Systems

There are no measurements reported for low concentrations of defects for the systems described in this section. Although several calculations have been made, we shall not review them in detail but just point out the most salient features.

In the $KCoF_3$:Mn system both the host–host exchange constant (Buyers *et al.*, 1971a) and the impurity–host exchange constant (Svensson *et al.*, 1969) are known. Consequently we can calculate the frequencies of the modes associated with a Mn impurity in $KCoF_3$. When the Ising model is used, the calculation gives $\omega_D = 2.0$ THz which is within the band of pure

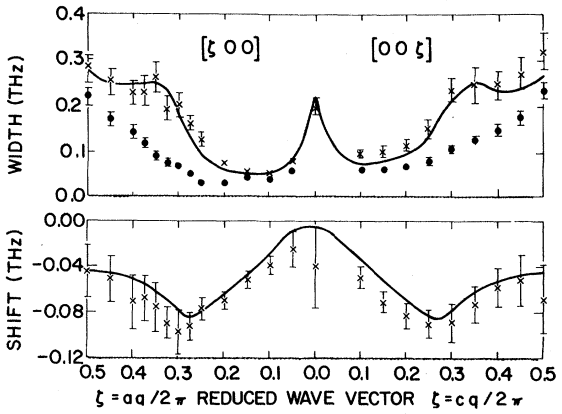

FIG. 29. The width and shift of magnons in $Mn_{0.95}Zn_{0.05}F_2$. The experimental results of Svensson *et al.* (1969b) are (crosses) the full width at half-height and frequency shift of the neutron groups in the doped specimen and also (full circles) the width obtained for pure MnF_2. The solid lines are the results of the Green's function theory described in the text and include the frequency dependence of the width and shift functions. For each wave vector the distribution observed for pure MnF_2 was folded with the full theoretical line shape to obtain widths that included instrumental resolution (Svensson, Cowley, Buyers, and Holden, private communication).

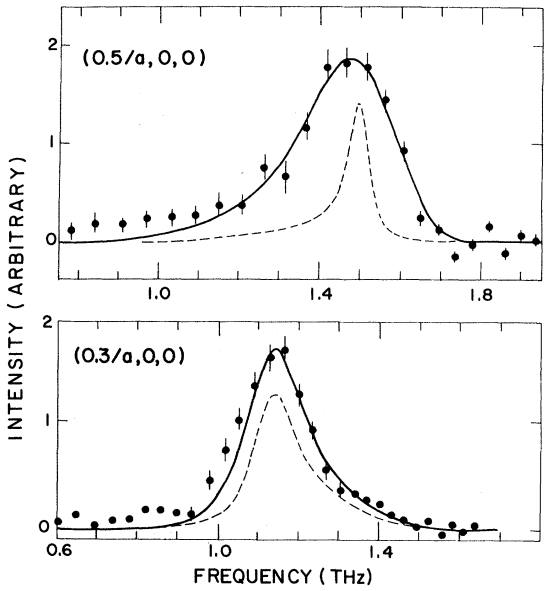

FIG. 30. Line shape of neutron groups in $Mn_{0.95}Zn_{0.05}F_2$. The theoretical curves (solid lines) were obtained by folding the theoretical line shape with frequency dependent width and shift functions (broken lines) with the instrumental resolution. The experimentally observed intensities (full circles) at two wave vectors are shown with some typical error bars.

$KCoF_3$, (Holden *et al.*, 1971b) and thus resonant behavior of the band modes would be expected. When, however, the Green's function method is used the calculation gives $\omega_D = 0.5$ THz which is well below the bottom of the band of $KCoF_3$, 1.1 THz, and consequently a localized mode is predicted. The marked difference in frequency arises because the Ising model treats all the host modes as having a frequency corresponding to the top of the $KCoF_3$ band. Instead the frequency of the localized mode is pushed down by a strong interaction with the relatively few modes of low frequency. Calculations have also been performed for the scattered neutron intensity of the localized mode and of the change in the frequency and width of the modes of $KCoF_3$ by introducing 5% of Mn impurities. The results are shown in Figs. 31 and 32. Note that although the theory predicts a constant frequency expected for a local mode the structure factor of Fig. 31 shows a large wave vector dependence. This is undoubtedly the result of the strong interaction with the modes at the bottom of the host band, and is possibly an indication that the mode is close to the boundary between localized and propagating behavior (see Sec. VIII). The frequency of the modes associated with the Co neighbors of a Mn ion, ω_N, is just below the top of the pure $KCoF_3$ band and so these modes do not give rise to any new localized modes.

In the CoF_2:Mn system a similar situation occurs. An Ising model calculation taking account of the mixing of the levels gives $\omega_D = 1.0$ THz which is just below the bottom of the band in pure CoF_2, 1.1 THz. (Martel

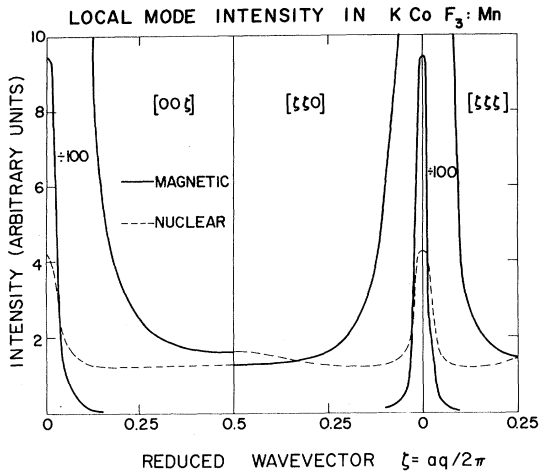

FIG. 31. Theoretical local mode structure factor in $KCo_{0.95}Mn_{0.05}F_3$ in magnetic and nuclear zones.

et al., 1968). A Green's function calculation again gives a lower frequency of 0.9 THz; this is well below the bottom of the band and thus a localized mode is expected. The modes associated with the Co neighbors of the Mn ions have a frequency on the Ising model, $\omega_N = 2.12$ THz, above the top of the band of frequencies of pure CoF_2 at 1.9 THz. In the Green's function calculation the frequencies of the eight different modes on the second nearest neighbors are split to give six modes classified by the irreducible representations of Eq. (3.8). The frequency of one of the modes, A_{1g}, is decreased to below the top of the pure CoF_2 band but the other modes have frequencies in THz of $\omega(E_u)=2.12$, $\omega(B_{2g})=2.18$, $\omega(A_{2u})=2.22$, $\omega(E_g)=2.26$, and $\omega(B_{1u})=2.27$. We therefore expect localized modes to occur at these frequencies.

These results must be considered as very tentative because they were obtained by assuming that the spin waves in the CoF_2 host are adequately represented by an effective spin $S=\frac{1}{2}$ Hamiltonian. Detailed calculations with this model have been made of the scattered neutron intensity from these localized modes and also of the shift and width of the band modes.

Similar conclusions may be arrived at by the study of the FeF_2:Mn system. The band of frequencies of pure FeF_2 lies between 1.58 and 2.37 THz (Hutchings *et al.*, 1970a). The Ising model predicts the frequency of excitations of a Mn ion as 1.80 THz, and of a Fe neighbor to the Mn ion as 2.45 THz. We have taken the Fe–Mn exchange identical to that found for Fe impurities in MnF_2. This system has been discussed using Green's function techniques by Tonegawa (1968). Using the appropriate ratios for $I'(2)/I(2)$, his calculations show that the mode localized mainly on the Mn ion has a frequency below the bottom of the FeF_2 band, while for the modes associated with the neighbors the A_{1g} mode has a frequency within the band, but the others are localized modes above the top of the FeF_2 band.

It is interesting to note that for these three systems there are marked discrepancies between the predictions of the Ising model and those of the Green's function model. In each case the Ising model predicts that the mode associated with the defect will give rise to either resonant or weakly localized behavior of the band modes, while the Green's function technique predicts a localized mode well below the band of the host crystal. It would be very interesting to perform an experiment to test these conclusions.

Although no localized modes below the band have been observed in materials of the type discussed here, measurements (Date *et al.*, 1965, 1968) of Fe^{3+} and Mn^{2+} in $FeCl_2$ by electron-spin resonance have found that these systems give localized modes below the bottom of the $FeCl_2$ band. It would however, take us too far away from our present subject to discuss these results in detail because $FeCl_2$ differs in crystal structure and magnetic properties from the fluorides discussed here. For similar reasons, the luminescence of Eu^{3+} ions in $KMnF_3$ which has exhibited the presence of a resonance mode within the band of the pure material (Hirano and Shionoya, 1970) will not be discussed.

VII. TEMPERATURE DEPENDENT EFFECTS

In the earlier sections we discussed the properties of magnetic defects at low temperatures. Considerable difficulties arise when we attempt to extend these theories to elevated temperatures. In part these difficulties arise because the theory of magnetic excitations at high temperatures is very difficult even for pure crystals and, despite a large amount of work, still not completely convincing. The greatest difficulties, however, arise in the treatment of the defects themselves even if the properties of the pure material are assumed to be known. In this section we shall be concerned, not with the pure crystal difficulties, but with the additional difficulties which arise in the defect crystal. In order to achieve this end we treat a very simple model in the first section, discuss the experimental results, and finally review more satisfactory theories.

1. A Simple Model

We consider a simple model of a linear chain of spins with nearest-neighbor Ising interactions, and solve the model within the molecular-field approximation.

The Hamiltonian of the pure system is

$$H=\sum_i IS_z(i)S_z(i+1), \tag{7.1}$$

where i is the index of the spin along the chain. The solution of this Hamiltonian within the molecular field approximation is given by the self-consistent equation

$$\langle S\rangle = B_S(2\beta I\langle S\rangle), \tag{7.2}$$

where the Brillouin function is

$$B_S(x)=\sum_{S_z} S_z \exp(xS_z)/\sum_{S_z}\exp(S_z) \qquad (7.3)$$

and $\beta=1/k_BT$.

Now suppose we introduce a spin S' into the chain at the origin and that it has an exchange interaction with its neighbors I'. The terms in the Hamiltonian involving the defect are

$$H_D=I'[S_z(-1)+S_z(1)]S_z'(0).$$

Within the molecular field approximation

$$\langle S_z(i)\rangle=B_S(\beta H_i), \qquad (7.4)$$

where

$$H_i=I[\langle S_z(i+1)\rangle+\langle S_z(i-1)\rangle] \qquad |i|>1$$
$$H_1=I\langle S_z(2)\rangle+I'\langle S_z(0)\rangle$$

and

$$H_0=2I'\langle S_z(1)\rangle.$$

Suppose the introduction of the defect causes a small perturbation in the expectation value of the spin so that

$$\langle S_Z(i)\rangle=\langle S\rangle+\Delta_i.$$

Treating Eq. (7.4) by perturbation theory yields

$$\Delta_{i+1}-\alpha\Delta_i+\Delta_{i-1}=0 \qquad |i|\geq 2 \qquad (7.5)$$

with

$$\alpha^{-1}=[\langle S^2\rangle-\langle S\rangle^2]I\beta.$$

Equation (7.5) is a standard recurrence relationship whose solution is given by

$$\Delta_i=A\lambda^{|i-1|} \qquad i\neq 0 \qquad (7.6)$$

with $\lambda=[\alpha\pm(\alpha^2-4)^{1/2}]/2$.

Since α is always greater than 2, the solution (7.6) is real; the positive sign corresponds to a value greater than one, and the negative sign to a number less than one. Since we are interested in a solution which decreases as the distance from the defect increases, the latter is the desired solution. The behavior of λ is shown in Fig. 33 as a function of temperature. A small value corresponds to a rapidly attenuated disturbance of the spin around the defect and a value near to one gives a disturbance extending a long way from the defect. Figure 33 shows that the disturbance is of longest range near the transition temperature. The coefficient A and the solution for $\langle S_z'(0)\rangle$ can be obtained by solving Eq. (7.4) explicitly to give

$$\langle S_z'(0)\rangle=B_{S'}[2\beta I'(A+\langle S\rangle)]$$
$$\langle S\rangle+A=B_S[\beta(I(\langle S\rangle+A\lambda)+I'\langle S_z'(0)\rangle)].$$

Once we have obtained the expectation values of the spins the excitation frequencies may be obtained directly

$$\omega_D=2I'\langle S_z(1)\rangle,$$
$$\omega_N=I'\langle S_z'(0)\rangle+I\langle S_z(2)\rangle,$$
$$\omega_i=I\langle S_z(i-1)\rangle+I\langle S_z(i+1)\rangle. \qquad |i|\geq 2.$$

In Figs. 34 and 35 we show the temperature dependence of $\langle S_z'(0)\rangle$, Δ_1 and Δ_2 as functions of temperature when $S=\frac{5}{2}$ for $S'=\frac{1}{2}$ and 2, respectively. The values of I' were chosen so that the frequency of the neighbors, ω_N, at low temperatures was: greater, A; equal to, B; or smaller than, C, the frequency of the host in the pure crystal at low temperatures. The results show that $\langle S_z'(0)\rangle$ is much less temperature dependent than the host spin $\langle S\rangle$ for all the cases where $S'=\frac{1}{2}$. This is because ω_D is much greater than $2I\langle S\rangle$ so that the probability of thermally produced excitations on the defect is much less than that of excitations on the host spins. The spin deviation of the neighbors increases with increasing temperature for A and B, but initially decreases for model C. This decrease is because

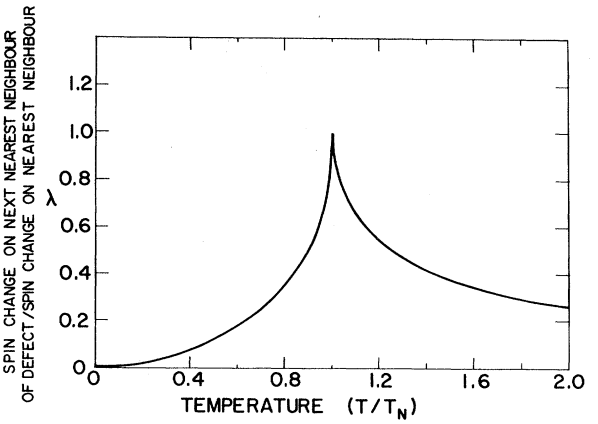

FIG. 33. Decay of spin distrubance round an impurity as a function of temperature. The perturbation in average spin decreases by the factor λ for every step made along the chain away from the defect.

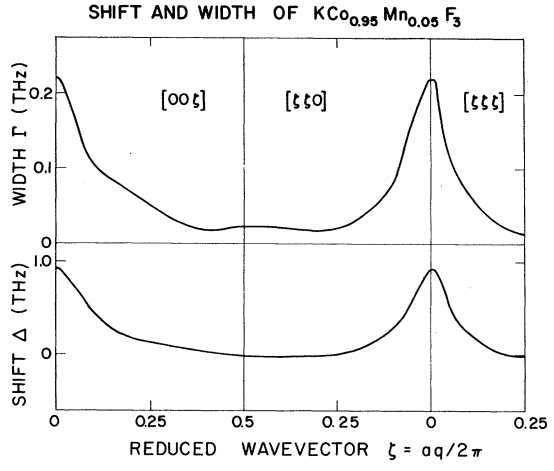

FIG. 32. Width and shift of band modes in $KCo_{0.95}Mn_{0.05}F_3$.

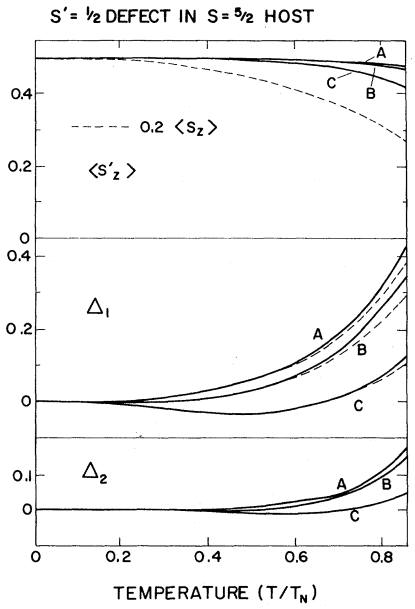

FIG. 34. Temperature dependence of the magnetization round a defect with $S'=\frac{1}{2}$ in a host having $S=\frac{5}{2}$. Results when the nearest neighbor frequency is greater than (A), equal to (B), or less than (C), the host frequency are shown. The two lower sections show the spin perturbation on nearest, Δ_1, and next nearest, Δ_2, neighbors of the defect (solid lines). The same quantity is shown in the middle section when the average spins on second and higher neighbors are constrained to be equal to the host magnetisation $\langle S_z\rangle$ (broken lines).

the frequency ω_N is less than $2I\langle S\rangle$ thus increasing the probability of spin deviations. At higher temperatures with $S'=\frac{1}{2}$, Δ_2 begins to increase because $\langle S_z'(0)\rangle$ is not decreasing with increasing temperature as fast as $\langle S\rangle$ and ω_N thus becomes greater than $2I\langle S\rangle$.

The calculations were also performed with $\lambda=0$ prohibiting the spin deviations on next nearest neighbors. The results for Δ_1 which are shown by the dotted curves are negligibly different from other curves for $T/T_N<0.6$. For any λ, Δ_2 is negligible for $T/T_N<0.5$.

Close to the phase transition, the results showed an interesting phenomenon illustrated in Fig. 36, for the case $S'=\frac{1}{2}$. The defect spin $\langle S_z'(0)\rangle$ decreased as T_N was approached, but at the transition there was a discontinuity in slope with both $\langle S_z'(0)\rangle$, $\langle S_z(1)\rangle$, and $\langle S_z(2)\rangle$ being constant until at some considerably higher temperature they fall to zero. This corresponds to the occurrence of stable clusters around each defect above T_N. The exchange is sufficiently strong near the impurity that it polarizes the neighboring ions so as to form a stable cluster. This cluster then breaks up at some higher temperature when the thermal entropy is sufficient. This higher temperature is dependent upon the exchange constants. The same effects occur for larger values of S', but the critical exchange, I'/I, for the clusters is then smaller.

One may speculate that in three dimensions the temperature range of stable clusters will be closer to T_N by an amount of the order of $2T_N/z$. It is not then surprising that no experimental evidence has yet been found to support the existence of these clusters.

2. Experimental Results

The temperature dependence of the excitation frequencies has been studied by both neutron and optical scattering techniques. The most straightforward results to analyze theoretically are those of the frequency of the localized mode associated with the defect. This has been measured with neutron scattering by Holden *et al.* (1969) in MnF_2:Co as shown in Fig. 37. It has also been obtained by Johnson and Weber (1971) in MnF_2:Fe. Both results show that the temperature dependence of the excitation is less than that of the sublattice magnetization of the pure crystal.

These results are consistent with the simple model calculations shown in Figs. 34 and 35. For both Co^{2+} and Fe^{2+} in MnF_2 the excitations on the neighbors have frequencies close to those of the pure crystal and therefore correspond to case B of the simple model. The excitation frequency on the defect is proportional to $\langle S_z(1)\rangle$ which is less temperature dependent than $\langle S\rangle$.

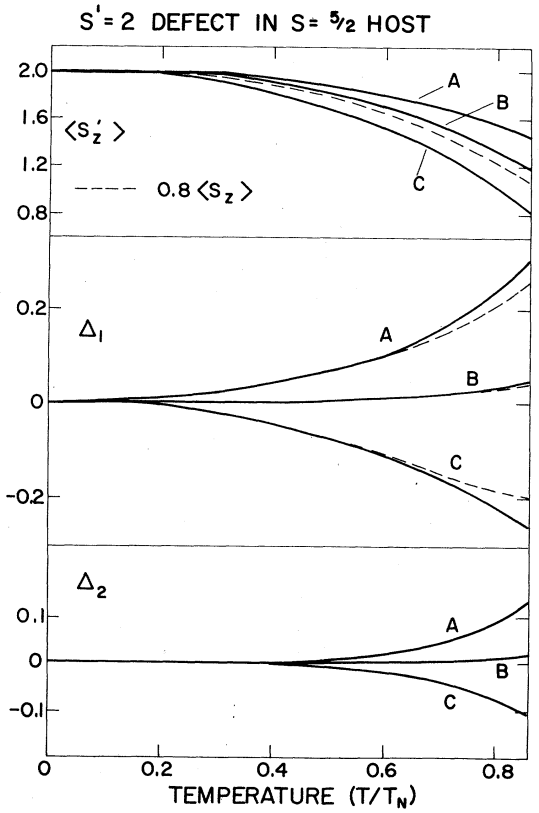

FIG. 35. The same as Fig. 34 but for a defect with $S'=2$ in a host having $S=\frac{5}{2}$.

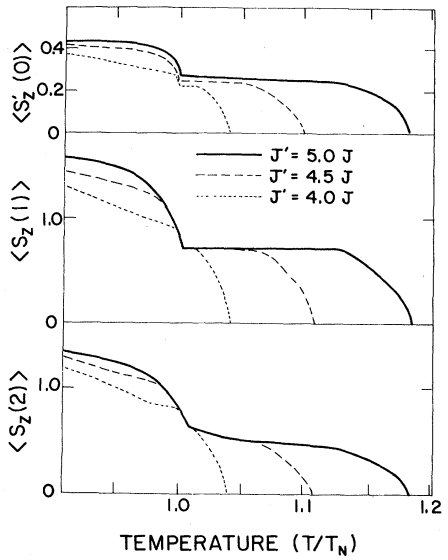

FIG. 36. The average spin near the Néel point on the defect and on its first two neighbors as a function of temperature for three ratios of exchange. Here $S=\frac{5}{2}$, $S'=\frac{1}{2}$, and $I=J$.

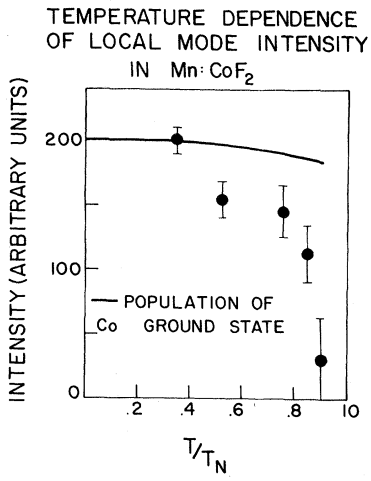

FIG. 38. Temperature dependence of the local mode intensity in $Mn_{0.95}Co_{0.05}F_2$ (full circles) measured by neutron scattering. The solid line is the population of the Co^{2+} ground state taking into account the variation of local mode frequency as measured in the experiment (Holden and Buyers, private communication).

The prediction of the model that the range parameter λ of the spin perturbation increases with temperature is borne out by the measured intensity of the local Co mode in MnF_2 (Holden and Buyers, private communication). Figure 38 shows that the intensity falls with temperature much faster than the population of the Co^{2+} ground state as might be expected for a mode which is becoming increasingly spread out with temperature.

Raman scattering measurements have been reported on the temperature dependence of pair modes in MnF_2:Ni (Oseroff and Pershan, 1968; Moch *et al.*, 1968) and in MnF_2:Fe (Oseroff and Pershan, 1968). The results show that the temperature dependence of the pair modes is less than either that of the sub-lattice magnetization or that of the pair modes in pure MnF_2, as shown in Fig. 39. This is to be expected for a pair mode where one member of the pair is localized above the band and therefore weakly temperature dependent. Similar results were obtained with infrared absorption

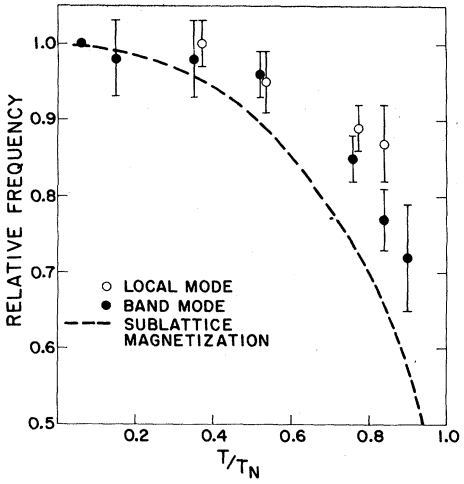

FIG. 37. The temperature dependence of the cobalt local mode frequency in $Mn_{0.95}Co_{0.05}F_2$ measured by Holden *et al.* (1969). The frequencies are normalized to the results at helium temperatures.

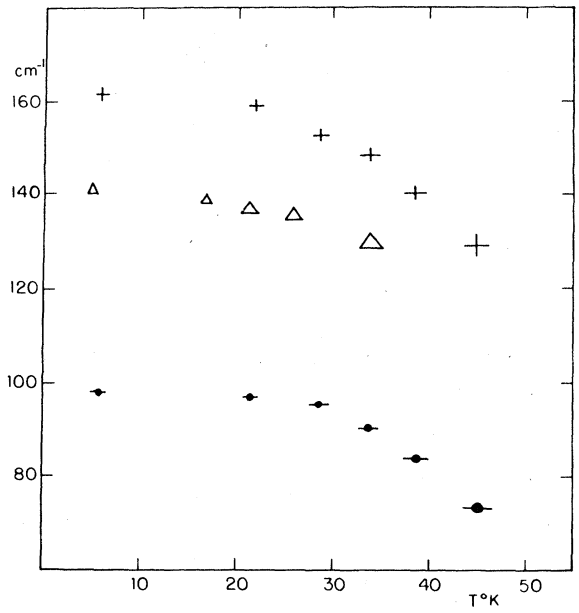

FIG. 39. Temperature dependence of pair modes observed in Raman scattering (Oseroff and Pershan, 1968). The results for MnF_2:Ni (crosses), and MnF_2:Fe (triangles) fall more slowly with temperature than the pair modes of pure MnF_2 (full circles).

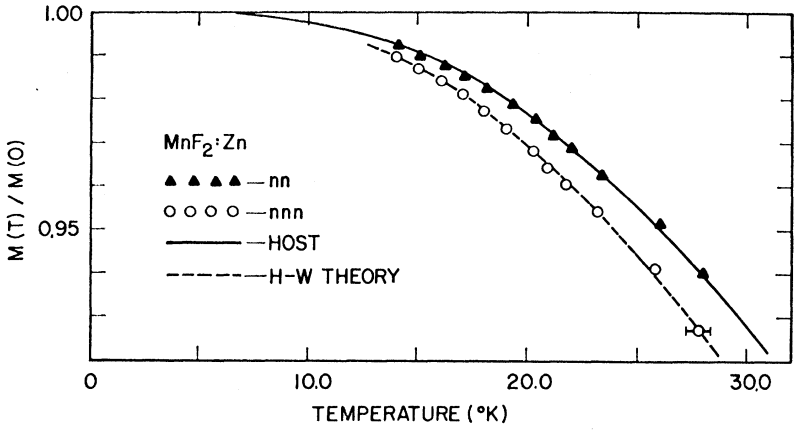

FIG. 40. Temperature dependence of the normalized magnetization on sites that are nearest neighbors (nn) and next-nearest neighbors (nnn) to a defect in MnF_2:Zn measured by NMR (Butler *et al.*, 1970). The host magnetization and the results of the theory of Hone and Walker (1971) are also shown.

for the pair mode $A_{1g}(D)+T_{1u}$ in MnF_2:Fe (Johnson and Weber 1971). These latter results are especially interesting in that they show that the pair mode is less strongly temperature dependent than the local mode.

One of the techniques which gives the most detailed information about the temperature dependence of defect systems is NMR. Butler *et al.* (1970) have studied the F^{19} resonance in MnF_2:X with X=V, Fe, Co, Ni, and Zn, and have analyzed their data to obtain the magnetization of the defect and its nearest and next nearest neighbors. Their measurements were all taken at temperatures below $0.5T_N$, and were interpreted assuming that the magnetization of those neighbors further away from the defect than second nearest neighbors was identical with that of the pure host. This approximation is, as we have seen in Sec. VII.1, in principle inadequate but the results of Figs. 34 and 35 suggest that the error is small. At 50% of T_N, Δ_2 is no more than 0.01. With the aid of this approximation they were able to obtain the magnetization of the defect and its two nearest neighbors as functions of temperature. Their results for MnF_2:Zn are shown in Fig. 40 and for MnF_2:Ni, and MnF_2:Fe in Fig. 41. The magnetization on the Fe site in MnF_2:Fe shown in Fig. 41 is taken from Mössbauer measurements of Fe^{57} by Wertheim *et al.* (1969). The results show that the magnetization of the defect is considerably less temperature dependent than that of the host, while that of the neighbors may be either more or less temperature dependent than the host. This is again in qualitative agreement with the behavior predicted in Sec. VII.1.

Butler *et al.* (1970) interpret their results in more detail. In MnF_2:Zn, the magnetization of the nearest ferromagnetic neighbors, Fig. 40, is identical with that of the pure host, whereas that of the next nearest antiferromagnetic neighbors is considerably more temperature dependent. They interpret this result as evidence that the deviation in magnetization is very localized near the defect, and furthermore is only significant if there is a strong direct interaction between the defect and the neighbor. Noting that for pure MnF_2 $|I_1| \ll |I_2|$, this interpretation leads them to conclude that the deviations of the magnetizations of the nearest neighbors in MnF_2:Ni and MnF_2:Fe result from large antiferromagnetic and ferromagnetic I_1' couplings in these materials.

This result is clearly of interest considering the analysis of theory and experiment presented in Sec. VI. In that section we showed that the low temperature

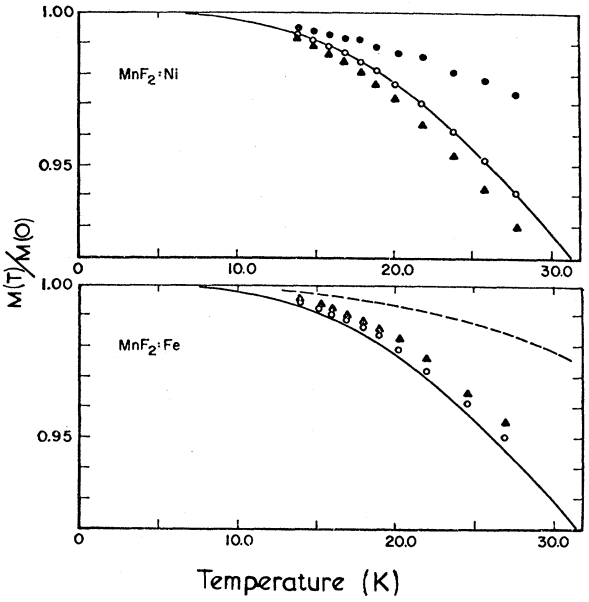

FIG. 41. Temperature dependence of the normalised magnetization on atoms on and near the defect in MnF_2:Ni and MnF_2:Fe (Butler *et al.*, 1970). The NMR results for the defect are shown as full circles, for the nearest neighbors as triangles and for the next nearest neighbors as open circles. The magnetization on the Fe site in MnF_2:Fe (broken line) is taken from the Mössbauer study of Wertheim *et al.* (1969). The solid line is the host magnetization.

experiments could be interpreted in terms of I_2' alone, and concluded that the small discrepancies could well be due to inadequacies in the theory. In terms of the simple model (Sec. VII.1) the analysis of Butler *et al.* (1970) can be shown, for the case, B, in which the low temperature defect and host frequency are the same, to be equivalent to setting $A=0$ (no spin change on the neighbors) at all temperatures. At $0.5T_N$, this gives an error in $(\langle S_z'(1)\rangle/S)$ of 0.012 for $S'=\frac{1}{2}$ and 0.004 for $S'=2$. Since the deviations in magnetization between one neighbor and another found by Butler *et al.* (1970) are about 0.005, their interpretation is open to doubt. On the other hand, our model of necessity gives $|\Delta_2| < |\Delta_1|$ whereas they find $|\Delta_2| > |\Delta_1|$ for both MnF_2:Ni and MnF_2:Fe. The present authors therefore feel that I_1' is likely important in these systems but that its magnitude is probably considerably smaller than has been suggested. Further work is needed to find the value of I_1' which is consistent with experiment when the spin deviations occurring around the defect are derived self-consistently.

3. Theoretical Calculations

There have been only a few attempts to calculate the temperature dependence of magnetic defect systems. Holden *et al.* (1969) used a cluster model, solved the self-consistent equations with the molecular field theory and found fair agreement (Fig. 42) with experiment for the frequency of the $A_{1g}(D)$ mode of Co in MnF_2. This model is a generalization of the model of Sec. 1 to three dimensions but with the added assumption that the magnetization is that of the pure crystal for atoms beyond third nearest neighbors of the defect. The ordinate in Fig. 42 corresponds to $(1+\Delta_1)/\langle S\rangle$ of Sec. VII.1. Johnson and Weber (1971) applied the model of Holden *et al.* (1969) to Fe in MnF_2 and found good agreement for the temperature dependence of the $A_{1g}(D)$ mode, but too large a dependence for the $A_{1g}(D)+T_{1u}$ pair modes. In view of the present failure of theory to explain the temperature dependence of pair modes in pure crystals (Fleury, 1970), this latter failure is perhaps not surprising. It seems probable, however, that as the local mode becomes more spread out with increasing temperature, the attractive interaction between the $A_{1g}(D)$ mode and T_{1u} mode decreases. The small temperature dependence may therefore be partially a result of the decrease in the binding as suggested by Fleury (1970) for pair modes in pure crystals.

A more precise theory could be obtained if it were possible to solve the Green's function theory of Sec. V at finite temperatures. Unfortunately even in pure crystals this problem has not been solved but some progress has been made. In Sec. V the Green's functions were decoupled so as to give

$$G[S_+(k)S_z(i), S_-(j);\omega]=\langle S_z(i)\rangle G[S_+(k), S_-(j);\omega].$$

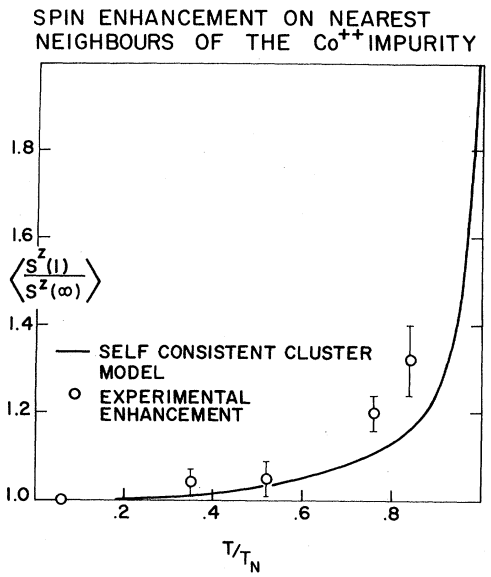

FIG. 42. The spin enhancement on the nearest antiferromagnetic neighbors of the Co impurity in MnF_2:Co (Holden *et al.*, 1969).

In a pure material, $\langle S_z(i)\rangle$ has the same value $\langle S(T)\rangle$ or $-\langle S(T)\rangle$ for all ions. The equations for the Green's functions can then be obtained in the same way as Eq. (5.3) except that in the expressions for $\mathbf{D}(ik)$, $\langle S(T)\rangle$ replaces S. The Green's functions are then dependent upon $\langle S(T)\rangle$, which must itself be calculated by the theory. This can be achieved by considering the definition of the Green's functions from which it is seen that

$$\langle S_z(i)\rangle = S\int_{-\infty}^{\infty} \mathrm{Im}\,\{G[S_+(i), S_-(i);\omega]\}d\omega. \quad (7.7)$$

The solution for the Green's functions must then be obtained self-consistently in that the value of $\langle S_z(i)\rangle$ obtained from Eq. (7.7) must be the same as that used to calculate the Green's functions in the first place.

In practice it is somewhat easier to obtain $\langle S_z(i)\rangle$ from an equation obtained by Callen and Shtrikman (1965) but we need not discuss this in detail. The expression involves an integral over the same Green's function so that the self-consistency problem is unchanged.

The same theory may be applied to the defect crystal. The main difficulty arises in the form of the defect matrix on the right-hand side of Eq. (5.9). Since the introduction of a defect alters not only the exchange interactions but also the expectation values of the spins of, in principle, every site in the crystal, the defect matrix is of infinite order because it contains the expectation value of the spin on every site in the crystal. It is clearly impossible to solve the complete self-consistency problem or to obtain a solution to the single-

defect problem even if the N spins were given. Solutions have only been obtained by assuming that far enough away from the defect $\langle S_z(i)\rangle = \langle S(T)\rangle$. This reduces the defect matrix, C, to a tractable size and reduces the number of self-consistency conditions. Watarai and Kawasaki (1970) have used a severe form of this type of approximation to describe the excitation frequencies of MnF_2:Ni as a function of temperature. In their model they replace $\langle S_z(i)\rangle$ by their values in the unperturbed system for all i except the defect for which it is assumed that $\langle S_z'(0)\rangle/\langle S(T)\rangle = S'/S$. These approximations remove the self-consistency problem altogether. The results must, however, be regarded as only tentative because the temperature dependence of the magnetization on and near the defect is known (Figs. 40 and 41) to be different from that of the pure host.

To date the only attempt at a self-consistent solution has been made by Hone, Callen, and Walker (1966) for the Heisenberg ferromagnet. They performed calculations in which they treated the magnetization $\langle S_z'(0)\rangle$ of the defect correctly and that of the nearest neighbor approximately. Hone and Walker (1971) have performed similar calculations for MnF_2:Zn using a model with only nearest antiferromagnetic neighbors for MnF_2 and allowing for the deviation of the magnetization of the nearest neighbors. The result for the magnetization on these neighbors are compared with experiment in Fig. 40; the agreement is very satsifactory.

Despite this undoubted success it is difficult to extend the theory to higher temperatures. At higher temperatures the range of the spin correlations becomes longer and the problem more difficult to solve with these techniques. It seems as if there is still further scope for use of simple cluster models to understand the range of the spin deviations further before embarking on more detailed calculations.

No theoretical work has been reported on the temperature dependence of the frequencies for pairs of excitations. This is not surprising in view of the failure as yet of the theory to describe the temperature dependence of two-magnon processes in pure crystals.

VIII. FINITE CONCENTRATIONS

1. Experiments

Since the magnetic fluorides we have been discussing have very similar chemical properties, it is possible to obtain single crystals with large concentrations of both constituents. They therefore provide excellent systems on which to study the properties of crystals containing large numbers of defects.

Unfortunately it is very difficult to obtain optical measurements on high concentration systems. Parisot *et al.* (1971) have studied the concentration dependence of the frequency ω_A of the host pair modes, and the frequency ω_B of the $A_{1g}(D)+E_g$ pair modes in Ni-doped $KMnF_3$ and $RbMnF_3$. They found considerable difficulty in extending the results beyond 2% of Ni, but found that for $RbMnF_3$:Ni the frequencies varied linearly with concentration in that range;

$$\partial\omega_A/\partial c = 0.069 \text{ THz}/\% \qquad \partial\omega_B/\partial c = 0.132 \text{ THz}/\%.$$

Hughes (1971) studied the antiferromagnetic resonance of Co in MnO by infrared absorption, but the line became too broad to follow beyond 6%. For fluorescence studies, the concentration limit is even lower, of the order of 10^{-4}, because of broadening of the exciton lines by crystal field effects.

Neutron scattering results are available for large concentrations in the CoF_2/MnF_2 and $KCoF_3/KMnF_3$ systems (Buyers *et al.*, 1971b). The results, Figs. 43 and 44, for the crystals of $Co_{0.7}Mn_{0.3}F_2$ and $KCo_{0.71}Mn_{0.28}F_3$ are of particular interest in that they show two branches both of which have a significant bandwidth; the frequencies change significantly with wave vector. Furthermore, the experimental results showed that both of these branches were well defined excitations in that their width was much less than their frequency although significant width was observed in the upper branch of $Co_{0.7}Mn_{0.3}F_2$. Both of the Mn/Co systems therefore show qualitatively similar behavior. The introduction of a small amount of Co into the Mn salt gives rise to a local mode well above the band of the pure host excitations. At least in the case of $KMnF_3$:Co, this local mode exhibits a negligible bandwidth even when the concentration of Co ions is 0.20. However at some concentration as yet unknown, the bandwidth of the Co modes begins to increase, while the bandwidth of the Mn excitations decreases. If we accept the theoretical results of Sec. VI, at some concentration less than 29% of Mn ions the lower branch exhibits negligible bandwidth, and becomes a localized branch below the bottom of the Co band. Further work is, however, needed to establish the critical concentration at which the modes become nonlocalized. Presumably this arises when the localized modes overlap with one another sufficiently. This is expected to be at a much higher concentration for Co ions for which the local mode is of small spatial extent, than for Mn ions, for which the localized mode is spread over many neighbors.

2. Cluster Models

As always in this subject, the simplest model is a cluster model. In the case of crystals containing a large concentration of defects, this model may be solved within the single atom or Ising approximation. In this section, it is convenient to modify our notation, because with crystals containing many defects it is not advantageous to treat one as host and the other as a defect. We shall now consider a system conposed of two spins; a concentration c of S_A, and $(1-c)$ of S_B. These spins interact only with their nearest neighbors with exchange constants I_A, I_B, and I_{AB} representing the interactions between pairs of A spins, pairs of B spins,

and an A and a B spin. The form of the interaction is taken to be of the Ising form. The calculation of the spectrum of elementary excitations at low temperatures then proceeds by considering the probability that a given spin has certain numbers of A and B neighbors. The excitation frequency is then given by the molecular field approximation. For example, the probability that an atom has r A neighbors and $z-r$ B neighbors is

$$p\binom{r}{z}=\frac{z!}{r!(z-r)!}c^r(1-c)^{z-r}.$$

For an A spin, the excitation frequency for this configuration is

$$rI_{\mathrm{A}}S_{\mathrm{A}}+(z-r)I_{\mathrm{AB}}S_{\mathrm{AB}} \tag{8.1}$$

and for a B spin is

$$rI_{\mathrm{AB}}S_{\mathrm{A}}+(z-r)I_{\mathrm{B}}S_{\mathrm{B}}. \tag{8.2}$$

The scattering cross section may then be calculated as a series of delta functions at these excitation frequencies with the intensities given by

$$cb^2_{\mathrm{A}}p\binom{r}{z}$$

if the A spin is considered or

$$(1-c)b^2_{\mathrm{B}}p\binom{r}{z}$$

for the B spin. For b_{A} or b_{B}, we substitute the scattering length of the A or B spins for the appropriate probe

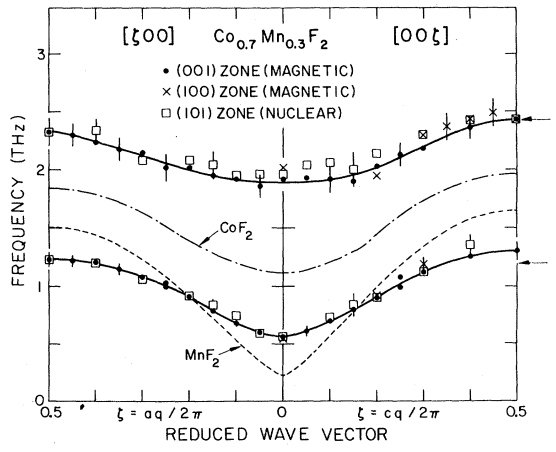

FIG. 43. Frequencies corresponding to the peaks in the neutron scattering from magnetic excitations in $Co_{0.7}Mn_{0.3}F_2$ (Buyers *et al.*, 1971b). The arrows show the predictions of the Ising model for the Mn^{2+} frequency (lower arrow) and cobalt frequency (upper arrow).

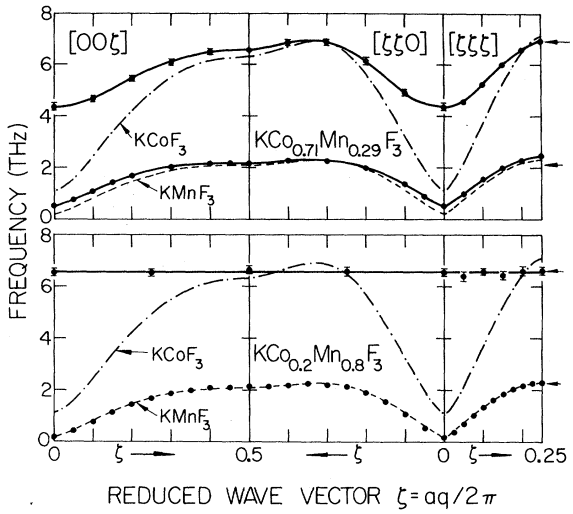

FIG. 44. Frequencies corresponding to the peaks in the neutron scattering from magnetic excitations in $KCo_{1-c}Mn_cF_3$ for $c=0.29$ and $c=0.80$. The broken lines show the dispersion relations of the pure crystals.

which for neutrons is the square of the matrix element of $(L_+ + 2S_+)$ between the ground and first excited state.

Calculations of this form have been made (Buyers *et al.*, 1971b) for the Co/Mn systems discussed in Sec. VIII.1 with the use of exchange constants known from work on the pure materials or from crystals containing only a few defects. For Co^{2+} modes, the variation of exchange mixing with configuration is accurately approximated by rewriting Eqs. (8.1) and (8.2) in the form

$$\nu(\mathrm{Mn})=\nu(\mathrm{Mn}:z\mathrm{Mn})r/z+\nu(\mathrm{Mn}:z\mathrm{Co})(z-r)/z \tag{8.3}$$

and

$$\nu(\mathrm{Co})=\nu(\mathrm{Co}:z\mathrm{Mn})r/z+\nu(\mathrm{Co}:z\mathrm{Co})(z-r)/z. \tag{8.4}$$

The $\nu(\mathrm{A}:z\mathrm{B})$ are the excitation frequencies of atoms A surrounded by a full complement z of neighbors B and are as given in Sec. VI by the Ising model when proper account is taken of the mixing. The results are shown in Figs. 43 and 44 by arrows and the cluster spectrum is shown in Fig. 45. A surprisingly good account of the scattering observed at zone boundaries is obtained, including the larger width of the upper mode in $Co_{0.7}Mn_{0.3}F_2$. The model does not include any wave vector dependence so it fails quite badly at the zone centers. It is remarkable that such a simple model seems to account for the results obtained at zone boundaries in both pure and very concentrated defect systems.

The same techniques may also be applied to pair modes. The average molecular field on the spin A is

$$H_{\mathrm{A}}=z(cI_{\mathrm{A}}S_{\mathrm{A}}+(1-c)I_{\mathrm{AB}}S_{\mathrm{B}})$$

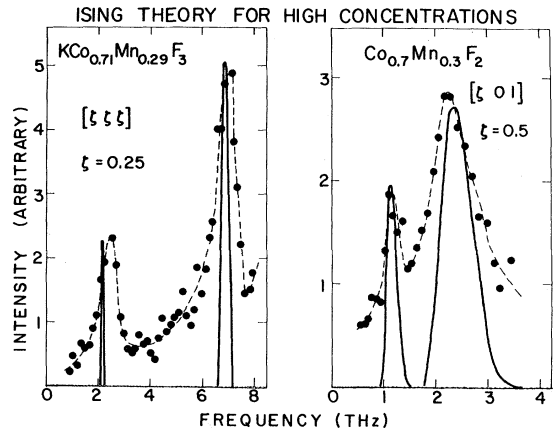

FIG. 45. Neutron scattering at zone boundaries in $KCo_{0.71}Mn_{0.29}F_3$ and $Co_{0.7}Mn_{0.3}F_2$. The experimental results of Buyers *et al.* (1971) (broken lines and full circles) are compared with the results of the Ising theory (solid lines). The solid lines have been drawn smoothly through the results of the Ising theory which predicts a series of discrete frequencies for each atom.

and on the spin B is

$$H_B = z(cI_{AB}S_A + (1-c)I_BS_B).$$

Now consider a pair mode in which two neighboring B spins are altered. On a simple spin model the frequency is given by

$$\omega_{B+B} = 2(z-1)(cI_{AB}S_A + (1-c)I_BS_B) + I_B(2S_B - 1).$$

If a pair mode consists of neighboring A and B spins, then we have

$$\omega_{A+B} = (z-1)[c(I_A+I_{AB})S_A + (1-c)(I_{AB}+I_B)S_B] + I_{AB}(S_A+S_B-1).$$

Using these results we can calculate that

$$\partial\omega_{B+B}/\partial c = 2(z-1)(I_{AB}S_A - I_BS_B),$$

while

$$\partial\omega_{A+B}/\partial c = (z-1)[(I_A+I_{AB})S_A - (I_{AB}+I_B)S_B].$$

For Ni in $RbMnF_3$, these results yield 0.013 THz/% and 0.055 THz/%, much less than the observed values of 0.069 THz/% and 0.132 THz/% (Parisot *et al.*, 1971). Presumably the discrepancy arises because the modes on the near neighbors of a defect have frequencies very close to those of the propagating band modes. Thus they spread out significantly and are not well described by an Ising model. They are therefore disturbed by defects which are much further away than those included in our simple model. Parisot *et al.* (1971) have carried out a similar calculation for $\partial\omega/\partial c$ and obtain better agreement with experiment than we have. The present authors, however, cannot reproduce their expressions in detail and prefer the expressions given above. The above theory for pair modes further shows that many different modes can occur whose frequencies depend upon whether both spins are of type A, or type B, or a mixture, and upon the configuration of the surrounding spins. It would be interesting to look for these additional modes with optical techniques.

3. Green's Function Theories

The application of Green's function theories to systems containing large numbers of defects has been discussed by many authors. Most of the work has been concerned with the application of these techniques to the analogous phonon and electron problems in which it is assumed that either the mass or one-electron energies vary from site to site while the force constants or electron hopping probabilities are independent of the type of atoms involved. In this section, we shall take over their work to our situation but point out the places at which difficulties are likely to occur.

The analysis begins by further study of the exact equation for the Green's functions in the crystal, Eq. (5.14), which is shown schematically in Fig. 46(a). In Sec. V we showed that it was essential to discuss the scattering from infinite-order perturbation theory in order to be able to obtain the results from even a single defect correctly. We therefore in Eq. (5.15) made a partial summation to incorporate the scattering at a single site, as shown in Fig. 46(b). The result is unsatisfactory for two reasons: First, it permits the successive defects to be the same even though we have summed all the multiple scattering at a single

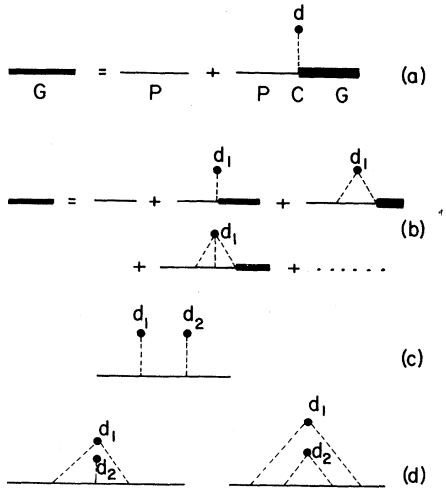

FIG. 46. Diagrams corresponding to the equations for the Green's function in a crystal containing defects. The exact equation for G is shown in (a) in terms of the perfect crystal Green's function P, and the defect matrix C caused by the interaction (broken line) with defects d. An approximation that includes multiple scattering at a single defect is shown in (b). In the term shown in multiple scattering (c) the summation over d_2 should be restricted to values not equal to d_1. Terms corresponding to scattering that occurs between different multiple scatterings from d_1 are shown in (d).

defect; in the term shown in Fig. 46(c) the summation over d_2 should be restricted to only those values not equal to d_1, whereas Eq. (5.15) does not have this restriction. This difficulty was discussed by Elliott and Taylor (1967) who showed that inclusion of the terms $d_2=d_1$ adds additional terms to the right-hand side of Eq. (5.14), the first of which is schematically

$$c^2\mathsf{C}(d)\mathsf{P}(d)\mathsf{C}(d).$$

These terms may be incorporated to give a result accurate to c^2, if in Eq. (5.12) for $\mathsf{X}(d)$ the matrix M is given by

$$\mathsf{M}(ij,\omega)=[\mathsf{I}\delta_{ij}-(1-c)\sum_k \mathsf{P}(ik,\omega)\mathsf{KC}(kj)]. \quad (8.5)$$

The second approximation in Fig. 46(b) is the neglect of scattering occurring between the different multiple scatterings at a single defect as shown by the terms of Fig. 46(d). These additional terms may be incorporated by replacing the unperturbed propagator in Eq. (8.5) by the appropriate propagator in the perturbed crystal which we shall write as $\mathsf{G}^H(ik,\omega)$. The simplest approximation for $\mathsf{G}^H(ik,\omega)$ was used by Davies and Langer (1963) and is to put it equal to the total perturbed propagator $\bar{\mathsf{G}}(ik,\omega)$. This theory is also unsatisfactory because $\bar{\mathsf{G}}(ik,\omega)$ includes the scattering from all the defects, whereas $\mathsf{G}^H(ik,\omega)$ should include the scattering from all the defects except the one being considered. This problem was considered by Leath and Goodman (1966), Leath (1968), and Aiyer *et al.* (1969). The solution is most readily obtained by noting that G^H is the Green's function obtained omitting the scattering at the site. It therefore treats the site as if it were a host atom rather than a defect site. Using the definition of a defect Green's function G^D, we obtain the result that

$$\mathsf{G}^H=\mathsf{G}-\mathsf{G}^D,$$

$$\mathsf{G}^H(ij,\omega)=\sum_k[\delta_{ik}\mathsf{I}-c\mathsf{L}^D(ik,\omega)]\bar{\mathsf{G}}(kj,\omega), \quad (8.6)$$

where $\mathsf{L}^D(ik,\omega)$ is the matrix inverse of $\mathsf{M}(ik,\omega)$ of Eq. (8.5), but with G^H replacing P. Since $\mathsf{G}^H(ik,\omega)$ depends on $\mathsf{M}(ik,\omega)$ which further depends on $\mathsf{G}^H(ik,\omega)$, the solution must be obtained self-consistently. This solution is then equivalent to the self-consistent theories of Taylor (1967) for the lattice dynamical problem, and Soven (1967) and Yonezawa (1968) for the electron problem. In the theory, the single-site scattering is included self-consistently, but the theory still fails to include the scattering by pairs and larger clusters, although the theory might be developed along the lines taken by Aiyer *et al.* (1969).

As yet, little progress has been made in applying the theory to magnetic systems. Calculations have been made using Eq. (8.5) for $\mathsf{M}(ij,\omega)$ for several systems. In the case of $KCoF_3$:Mn the results are shown in Fig. 47; they surprisingly accurately reproduce the behavior of the upper band of excitations but totally fail to describe the lower band. In the model the lower band is split into two with the upper part very weak. This is possibly because the model describes the behavior well within the band of the host frequencies but fails outside at large concentrations. In the other two systems to which the theory has been applied, the results are far less satisfactory. In CoF_2:Mn the upper band shown in Fig. 43 is outside the band of frequencies of pure CoF_2. The model cannot then predict either its behavior or that of the lower band correctly. The model was also applied to MnF_2:Zn containing only 5% of zinc. In this case inclusion of the $(1-c)$ factor in the expression for $\mathsf{M}(ij,\omega)$ alters the frequency of excitations, so that the pole of $\mathsf{M}(ij,\omega)^{-1}$ at $\omega=0$ appears at a finite frequency. Since the zinc is nonmagnetic, this result is entirely nonphysical and spurious. We conclude therefore that Eq. (8.1) provides little advantage for calculations over Eq. (5.13). It possibly enhances the agreement for the change in the frequencies of band modes, but the changes produced in the frequencies of localized modes may well be spurious.

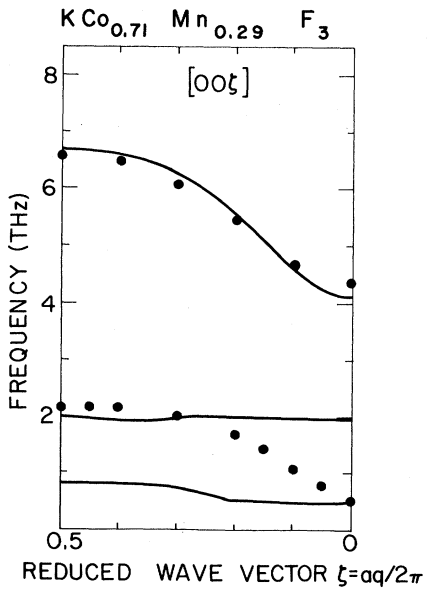

FIG. 47. The theory to order c^2 for magnetic excitations in $KCo_{0.71}Mn_{0.29}F_3$ (solid lines), and the experimental results of Buyers *et al.* (1971b) (full circles).

There are several considerable difficulties which arise when one attempts to apply the more general formulae to magnetic systems. Both of the simple models used extensively in phonon and electron problems have a 1×1 defect matrix. There is then only a simple function of frequency which needs to be made self-consistent. In our problem the defect matrix is 14×14 or larger, so that the self-consistency problem is far more serious.

This difficulty brings up yet another complexity. The analysis we have been describing so far assumes that each defect is surrounded by only host spins. At

finite concentrations this is not the case as emphasized in the cluster model of Sec. VIII.2. It is therefore not adequate to apply the self-consistent theory in the simple way we have been describing. A more satisfactory approach would be to calculate the defect matrix **C** for each possible cluster and then to average them all by the probability of their occurrence. The self-consistency problem would then require an enormous amount of work. Elliott (private communication) has suggested that the problem might be simplified sufficiently to be tractable if only the Ising part of the self-energy were treated in this way and the difference in the transverse part of the exchange neglected.

The special symmetry of the Green's functions and self-energy for a two sublattice antiferromagnet, namely,

$$\Sigma_4(-\omega) = -\Sigma_1(\omega)$$

then reduces the self-consistency condition to a scalar equation with real and imaginary parts. Preliminary results of Buyers, Pepper, and Elliott (private communication) indicate that the theory correctly predicts two branches of excitations both with significant band width at high concentration. The results are in reasonable agreement with experiment.

4. Localization at High Concentration

Even in the case of the simpler phonon and electron problems there is evidence to suggest that the single site scattering approximation may not be adequate to discuss problems of localization (Thouless, 1970). In our case, we would expect a single site approximation to be even more suspect because the Ising energy at one atom depends on the configuration of neighbors. The Ising energies on pairs of neighboring atoms are therefore intrinsically correlated. We must expect the single site self-consistent theories, if we could solve them, to fail especially in the neighborhood of the concentrations where localization begins to occur.

Anderson (1958) first discussed in a general way the conditions for excitations in alloys to be localized or propagating. For quasibinary alloys such as the materials of Sec. VIII.1, the probability of propagation increases as the transverse exchange energy (hopping integral for electronic alloys) becomes comparable with the difference in single site energies of the two types of atom. A form of the criterion for localization suggested by Buyers *et al.* (1971b) for antiferromagnets is

$$\chi(\omega) = \frac{2\,|\,\omega-\omega_A\,|^c\,|\,\omega-\omega_B\,|^{1-c}}{W_A(1-c)+cW_B} > 1,$$

where W_A, W_B are the bandwidths of the pure materials and ω_A, ω_B are the centers of the bands. This is clearly an oversimplification as it does not make allowance for the fact that the molecular field single site energy for an antiferromagnet is close to the zone boundary energy rather than to the center of the band, and further the dependence of Ising energy on the neighbors, as we have said, is not explicitly included. Nevertheless, in the $(Co, Mn)F_2$ and $K(Co, Mn)F_3$, system, this criterion is surprisingly accurate in predicting for the crystals studied to date whether a branch is localized or propagating. For the upper branch in $Co_{0.7}Mn_{0.3}F_2$, however, localized character is predicted. It is to be noted that for this branch the character of the branch is not unambiguously determined by the measurements since the variation of frequency with wave vector is less than the width of the excitation. These modes may in fact be local in agreement with the criterion, and possibly consist of a random structure of discrete poles as described by Anderson (1970).

IX. CONCLUSIONS

The properties of magnetic defects have been described with particular emphasis on mixed crystals of the transition metal fluorides. These systems provide particularly clean examples of the defect phenomena through which experiment and theory may be compared in a more complete way than is possible with many other systems. The primary reason for this is that it is possible to perform very detailed experiments on the nature of the excitations in these systems with optical and neutron spectroscopy. Far less detailed information is available for the analogous electron problem. Furthermore, since all of the transition metal ions have very similar sizes and chemical properties, the mixed crystals show little tendency to order, and may be grown as large single crystals with large concentrations of both constituents. Since the magnetic properties are not directly correlated with the atomic sizes, large magnetic defects may be introduced without appreciably straining the crystals as so often happens with mass defects. Experimentally therefore they provide an excellent system to study defect properties.

Theoretically there are advantages and disadvantages of antiferromagnetic systems. The disadvantages result largely from a change in spin altering the excitation frequencies on all of the neighboring ions so that a single defect causes a perturbation at several sites, unlike the simple mass defect problem. In part, these additional complexities are purely of a computa-

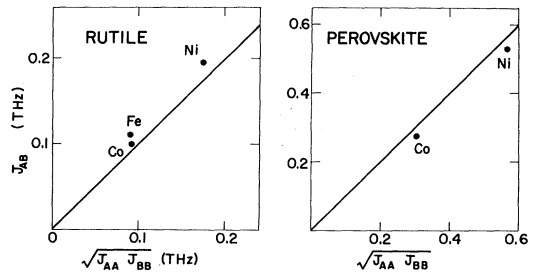

FIG. 48. Heisenberg exchange constants ($J=I$) in units of THz for transition metal fluorides of the rutile and perovskite structure. The host is always the manganese salt.

tional nature but as such they seem to prohibit any attempt at self-consistency in a way which is tractable in simpler models. However, these additional complexities may also give rise to more localized modes and resonant effects than occur in the simple models. The main advantage of magnetic systems is that the exchange constants between constituents may be determined from low-concentration experiments, and expected to be valid for all compositions because of the small strain.

Experiments and theory have now demonstrated many of the features of low-concentration systems. The frequencies and spatial extent of localized modes, the frequencies and widths of pairs of excitations, and the perturbation of the excitations of the host have all been studied and the results found to be in reasonable accord with theoretical calculations. From these results the effective exchange constant for various different interactions has been deduced and it is found, as shown in Fig. 48, to be similar to that given by the square root of the product of exchange constants of the pure materials. This is to be expected from the simple theory of superexchange (Anderson, 1950) but is rather surprising for the ions containing unpaired orbital angular momentum for which the exchange is expected to be more complicated (Elliott and Thorpe, 1968).

One aspect of this work which needs further clarification is the magnitude of the exchange between the ferromagnetically aligned nearest neighbors in the rutile structure. There are indications in the analysis of optical measurements and NMR measurements that these interactions are much stronger in defect crystals than in pure crystals. However, both of these interpretations are based on approximate theories and are needed to explain data very precisely, so that further work is required to confirm these results.

The present theories enable a large number of predictions to be made about systems containing only a few defects. It is to be expected that over the next few years many of these predictions will be worked out theoretically in detail and tested experimentally. Of particular interest is the prediction of localized modes below the band of Co host frequencies when Mn impurities are introduced.

Further developments will probably include theoretical and experimental work on the temperature dependence of the excitations and also on the effects occurring at large concentrations. The theory for both of these is very much more difficult than that of low-temperature dilute systems, but promises to be very rewarding. The work at high temperatures may provide insight into suitable ways of discussing the temperature dependence of spin waves in pure materials, while of even more interest is the possibility of testing the theory of excitations in disordered systems in detail. This latter study may well help to answer the difficult questions posed by the theories of localization in the treatment of the conductivity of alloys.

ACKNOWLEDGMENTS

Thanks are due to E. C. Svensson and T. M. Holden who made several unpublished results available and who provided much useful advice and encouragement. During part of this work one of the authors (R.A.C.) was at Atomic Energy of Canada, Ltd. The provision of facilities by the Department of Theoretical Physics, Oxford University, is gratefully acknowledged by one of the authors (W.J.L.B.). We are grateful to the reviewers for bringing some errors in the typescript to our attention, and to our colleagues for constructive criticism.

REFERENCES

Aiyer, R. N., R. J. Elliott, J. A. Krumhansl, and P. L. Leath, 1969, Phys. Rev. **181,** 1006.
Anderson, P. W., 1950, Phys. Rev. **79,** 350.
Anderson, P. W., 1958, Phys. Rev. **109,** 1492.
Anderson, P. W., 1970, Comments Solid State Phys. **2,** 193.
Baumann, F. C., J. P. Harrison, R. O. Pohl, and W. D. Seward, 1967, Phys. Rev. **159,** 691.
Born, M., and K. Huang, 1954, Dynamical Theory of Crystal Lattices, (Oxford U. P.).
Brinkman, W. F., and R. J. Elliott, 1966, Proc. Roy. Soc. **A294,** 343.
Butler, M., U. Jaccarino, N. Kaplan, and H. J. Guggenheim, 1970, Phys. Rev. **B1,** 3058.
Buyers, W. J. L., R. A. Cowley, T. M. Holden, and R. W. H. Stevenson, 1968, J. Appl. Phys. **39,** 1118.
Buyers, W. J. L., T. M. Holden, E. C. Svensson, R. A. Cowley, and M. T. Hutchings, 1971a, J. Phys. C **4,** 2139.
Buyers, W. J. L., T. M. Holden, E. C. Svensson, R. A. Cowley, and R. W. H. Stevenson, 1971b, Phys. Rev. Letters **27,** 1442.
Callen, H. B., and S. Shtrikman, 1965, Solid State Commun. **3,** 5.
Chinn, S. R., H. J. Zeiger, and J. R. O'Connor, 1970, J. Appl. Phys. **41,** 894.
Date, M. and M. Motokawa, 1965, J. Phys. Soc. Japan **20,** 465.
Date, M. and M. Motokawa, 1968, J. Phys. Soc. Japan **24,** 41.
Davies, R. W., and J. S. Langer, 1963, Phys. Rev. **131,** 163.
Dietz, R. E., G. Parisot, A. E. Meixner, and H. J. Guggenheim, 1970, J. Appl. Phys. **41,** 888.
Elliott, R. J., and D. W. Taylor, 1967, Proc. Roy. Soc. (London) **296,** 161.
Elliott, R. J., and M. F. Thorpe, 1968, J. Appl. Phys. **39,** 802.
Elliott, R. J., M. F. Thorpe, G. Imbusch, R. Loudon, and J. B. Parkinson, 1968, Phys. Rev. Letters **21,** 147.
Elliott, R. J. and M. F. Thorpe, 1969, J. Phys. C **2,** 1630.
Fleury, P., 1968, Phys. Rev. Letters **21,** 151.
Fleury, P., 1970, J. Appl. Phys. **41,** 886.
Fleury, P., and R. Loudon, 1968, Phys. Rev. **166,** 514.
Gladney, H. M., 1966, Phys. Rev. **146,** 253.
Griffith, J. S., 1961, The Theory of Transition Metal Ions (Cambridge U. P., Cambridge).
Heeger, A. J., A. M. Portis, D. T. Teaney, and G. Witt, 1961, Phys. Rev. Letters **7,** 307.
Heine, V., 1960, Group Theory in Quantum Mechanics, (Pergamon, Oxford).
Hirano, M. and S. Shionoya, 1970, J. Phys. Soc. Japan **28,** 926.
Holden, T. M., W. J. L. Buyers, and R. W. H. Stevenson, 1969, J. Appl. Phys. **40,** 991.
Holden, T. M., R. A. Cowley, W. J. L. Buyers, E. C. Svensson, and R. W. H. Stevenson, 1971a, J. de Physique **32,** C1–1184.
Holden, T. M., W. J. L. Buyers, E. C. Svensson, R. A. Cowley, M. T. Hutchings, D. Hukin, and R. W. H. Stevenson, 1971b, J. Phys. C **4,** 2127.
Hone, P., H. B. Callen, and L. R. Walker, 1966, Phys. Rev. **144,** 283.
Hone, D., and L. R. Walker, 1971, as reported by Butler *et al.* (1970).
Hughes, A. E., 1971, Phys. Rev. B1 **3,** 877.
Hutchings, M. T., 1964, Solid State Physics **16,** 227.

Hutchings, M. T., B. D. Rainford, and H. J. Guggenheim, 1970a, J. Phys. C **3,** 307.
Hutchings, M. T., M. F. Thorpe, R. J. Birgeneau, H. J. Guggenheim, and P. A. Fleury, 1970b, Phys. Rev. B **2,** 1362.
Izyumov, Y. A., 1965, Advances in Physics **14,** 569.
Johnson, L. F., R. E. Dietz, and H. J. Guggenheim, 1966, Phys. Rev. Letters **17,** 13.
Johnson, K., and R. Weber, 1971, Journal de Physique **32,** C 1-1070.
Kirby, R. D., I. G. Nolt, R. W. Alexander, and A. J. Sievers, 1968, Phys. Rev. **168,** 1057.
Kittel, C., 1963, *Quantum Theory of Solids* (Wiley, New York).
Leath, P. L., and B. Goodman, 1966, Phys. Rev. **148,** 968.
Leath, P. L., 1968, Phys. Rev. **175,** 963.
Lifshitz, J. M., 1943, J. Phys. USSR **7,** 215.
Lines, M. E., 1964, Phys. Rev. **A135,** 1336.
Lines, M. E., 1965, Phys. Rev. **A137,** 982.
Lloyd, P., 1969, J. Phys. C **2,** 1717.
Lovesey, S. W., 1968, J. Phys. C **1,** 102.
Low, W., 1960, Solid State Physics, Suppl. 2.
Martel, P., R. A. Cowley, and R. W. H. Stevenson, 1968, Candian J. Phys. **46,** 1355.
Misetich, A., and R. E. Dietz, 1966, Phys. Rev. Letters **17,** 13.
Misetich, A., R. E. Dietz, and H. J. Guggenheim, 1968, in *Localized Excitations in Solids*, edited by Wallis, R. F. (Plenum, New York) p. 379.
Moch, P., G. Parisot, R. E. Dietz, H. J. Guggenheim, 1968, Phys. Rev. Letters **21,** 1596.
Moch, P., G. Parisot, R. E. Dietz, and H. J. Guggenheim, unpublished, referred to by Thorpe (1970).
Moch, P., R. Moyal, C. Dugautier, and H. J. Guggenheim, 1971, Journal de Physique **32,** C1-806.
Mott, N. F., 1967, Advances in Physics **16,** 49.
Nagai, M., and A. Yoshimori, 1961, Prog. Theor. Phys. **25,** 595.
Nicklow, R. M., P. R. Vijayaraghavan, H. Smith, and M. K. Wilkinson, 1968, Phys. Rev. Letters **20,** 1245.
Nikotin, O., P. A. Lindgard, and O. W. Dietrich, 1969, J. Phys. C. **2,** 1168.
Oguchi, T., 1960, Phys. Rev. **117,** 117.
Okazaki, A., K. C. Turberfield, and R. W. H. Stevenson, 1964, Phys. Letters **8,** 9.
Oseroff, A., and P. S. Pershan, 1968, Phys. Rev. Letters **21,** 1593.
Oseroff, A., P. S. Pershan, and M. Kestigian, 1969, Phys. Rev. **188,** 1046.
Parisot, G., S. J. Allen, R. E. Dietz, H. J. Guggenheim, R. Moyal, P. Moch, and C. Dugautier, 1970, J. Appl. Phys., **41,** 890.
Parisot, G., R. E. Dietz, H. J. Guggenheim, P. Moch, and C. Dugautier, 1971, Journal de Physique **32,** C1–803.
Parkinson, J. B., 1969, J. Phys. C **2,** 2003.
Peter, M., and J. B. Moch, 1960, Phys. Rev. **118,** 137.
Pickart, S. J., M. J. Collins, and C. G. Windsor, 1966, J. Appl. Phys. **37,** 1054.
Richards, P. L., 1963, J. Appl. Phys. **34,** 1237.
Schäfer, G., (1960), J. Phys. Chem. Solids **12,** 233.
Schwinger, J., Phys. Rev. **51,** 584.
Shiles, E. and D. Hone, 1970, J. Phys. Soc. Japan **28,** 51.
Soven, P., 1967, Phys. Rev. **156,** 809.
Svensson, E. C., B. N. Brockhouse, and J. M. Rowe, 1965, Solid State Commun. **3,** 245.
Svensson, E. C., W. J. L. Buyers, T. M. Holden, R. A. Cowley, and R. W. H. Stevenson, 1969a, Canadian J. Phys., **47,** 1983.
Svensson, E. C., T. M. Holden, W. J. L. Buyers, R. A. Cowley, and R. W. H. Stevenson, 1969b, Solid State Commun. **7,** 1693.
Stout, J. W., M. I. Steinfield, and M. Yuzuri, 1968, J. Appl. Phys. **39,** 1141.
Takeno, S., 1963, Progress of Theor. Phys. **30,** 565 and 731.
Tanabe, Y., T. Moriya, and S. Sugano, 1965, Phys. Rev. Letters **15,** 1023.
Taylor, D. W., 1967, Phys. Rev. **156,** 1017.
Thorpe, M. F., 1969, Phys. Rev. Letters **23,** 472.
Thorpe, M. F., 1970, Phys. Rev. B, **2,** 2690.
Thouless, D. J., 1970, J. Phys. C **3,** 1559.
Tinkham, M., 1956, Proc. Roy. Soc. (London) **A236,** 535.
Tonegawa, T. and J. Kanamori, 1966, Phys. Letters **21,** 130.
Tonegawa, T., 1968, Prog. Theor. Phys. **40,** 1195.
Tonegawa, T., 1969, Prog. Theor. Phys. **41,** 1.
Tyablikov, S. V., 1959, Ukr. Mat. Zh. 11, 287. See also S. V. Tyablikov, *Methods in Quantum Theory of Magnetism* (Plenum, New York, 1967).
Walker, L. R., 1963, *Magnetism*, edited by G. T. Rado and H. Suhl (Academic, New York) Vol. I, p. 299.
Watarai, S., and T. Kawasaki, 1970, Solid State Commun. **8,** 2177.
Weber, R., 1968, Phys. Rev. Letters **21,** 1260.
Weber, R., 1969, J. Appl. Phys. **40,** 995.
Wertheim, G. K., H. J. Guggenheim, and D. N. E. Buchanan, 1969, J. Appl. Phys. **40,** 1319.
Wolfram, T., and J. Callaway, 1963, Phys. Rev. **130,** 2207.
Yonezawa, F., 1968, Progr. Theor. Phys. **40,** 734.
Ziman, J. M., 1968a, J. Phys. C **1,** 1532.
Ziman, J. M., 1968b, J. Phys. C **2,** 1230, 1704.
Zubarev, D. N., 1960, Usp. Fiz. Nauk., **71,** 71 (Soviet Phys.–Usp. **3,** 320).

ANNOUNCEMENT

The Review of Particle Properties will appear this year in the April issue of Physics Letters B.